MARSHALL

A Study of Space Station Contamination Effects

ANALYTIC
(HB)
IN-CAT 88-
147142

*Proceedings of a workshop held at
Hilton Head Island
South Carolina
October 29–30, 1987*

NASA

A Study of Space Station Contamination Effects

Edited by
M. R. Torr
J. F. Spann
and T. W. Moorehead
NASA George C. Marshall Space Flight Center
Marshall Space Flight Center, Alabama

NASA

National Aeronautics
and Space Administration

Scientific and Technical
Information Division

1988

SUMMARY

On October 29-30, 1987, a workshop was convened with the specific objective of reviewing the status of contamination around the Space Station, the extent to which contamination in various categories can be predicted at the present time, and the extent to which the predicted levels might limit scientific investigations from Space Station. The workshop was held under the general sponsorship of F. von Bun of the Office of Space Science and Applications and was chaired by M. R. Torr of the Marshall Space Flight Center. The participants in the workshop were scientists representing a range of disciplines and whose collective expertise allowed the coupled areas of induced atmosphere and particulates, together with optical, plasma, surface, and gas phase processes, to be addressed.

Each participant was asked to address the anticipated levels of contamination in his area of specialization. Since relatively little data are available at present, each was asked to identify the fundamental parameters driving the uncertainties on the estimates. The estimated range of uncertainty for each area lay between 10 and 100. This range is sufficiently large that some of the conclusions may change as parameters are quantified. The papers presented by the participants are contained in this document. The major conclusions were, briefly, as follows:

Because of the lack of data on the induced gas abundance around the Space Station, both the abundances and the composition mix of the major species are based on models. The results of such models are dependent on a number of poorly known parameters, including: outgassing and vent rates, vent locations, RCS and docking rates, and the decay times for such events. In addition, such models are very dependent on the elastic scattering cross sections (and the angular dependence of these cross sections), together with the role of the surface in establishing the velocity of the reemitted species. Further analysis of vehicle sources, sensitivity studies of the model, and laboratory measurements of elastic scattering cross sections are considered to be the most important tasks to be conducted in this area.

The neutral abundances (modeled), in turn, drive the estimates of induced emissions and elements of the plasma environment. However, in the case of the emissions (UV, VIS, IR) it is not only the neutral abundances and major species composition that are important, but also the abundance of species in excited electronic, vibrational, or rotational states. Both elastic and inelastic (ionization, excitation) cross sections and atomic and molecular parameters (transition probabilities, Franck Condon factors) are needed. The excitation mechanisms for some vehicle-induced glows are not understood and so scaling parameters with height are needed. With present estimates of these missing parameters, the Space Station environment would meet the stated emission requirements in the UV and VIS (with the exception of specific lines and bands) for station altitudes above 420 km at solar maximum (2×10^8 cm^{-3} ambient density). However, significant contamination is anticipated in the infrared. To allow more useful estimates, laboratory measurements of gas phase and gas-surface collision products and cross sections, together with shuttle measurements of induced emissions, are considered

PRECEDING PAGE BLANK NOT FILMED

most important. At the present time, there is no requirement for the level of induced discrete emissions. Following further study, it may be desirable to establish one.

Surface deposition is potentially significant. In this area the quantification of the parameters already discussed above would be most valuable. It is anticipated that controls on the payload will be needed.

The requirements on particulates as currently specified will be difficult to meet without stringent controls on hardware and operations. Laboratory studies of surface erosion, together with further analysis of existing shuttle data bases, and measurements from shuttle of release velocities and drag effects are needed in this area.

The plasma environment is dealt with more fully by another working group. However, the ion products and rate of ionization of the induced neutral environment should be carefully tracked.

A further summary of the conclusions is presented in Table 1.

Over the next 2 years, a fundamental improvement can be made in our ability to assess the extent of contamination in the Space Station environment if the following studies can be conducted: sensitivity assessment of the neutral abundance model to uncertainty ranges on input parameters; laboratory measurements of differential cross sections of O (5 eV) and N_2 (10 eV) on N_2 and H_2O; laboratory measurements of the products of O, N, and N_2 on surfaces such as Al_2O_3 or SiO_2; laboratory measurements of ionization cross sections; and further analysis of neutral and particulate data acquired from shuttle. Beyond this, the next step would be a few well focussed investigations from the space shuttle.

M. R. Torr
Chairman

Table 1. Summary of Conclusions Resulting from Space Station Contamination Workshop

Area	Anticipated Contamination	Range of Uncertainty	Major Parameter	Leak Rates	Outgassing Rates	Surface Materials	Vent Rates	Vent Locations	Vent Design/ Species	RCS/Resistojet Rates	Docking Rates	Elastic Cross Sections	Excitation Cross Sections	Ionization Cross Sections	Sticking Coefficient	Reemitted Velocities	Surface Chemistry	Gas Phase Processes	Surface Erosion	Studies Needed	Space Station Requirements/Comments
Neutral Abundances																					
Major Species	Some Viewing Directions Exceed JSC 30426 Column Concentration	10-20	—	X	X	X	X	X	X	X	X	X			X	X	X	X	X	• Analysis of Vehicle Sources • Lab Measurements of Differential Cross Sections • Measurements of Outgassing Rates • Sensitivity Tests on Model	• Review Requirements After Further Studies • Earth Pointing Requirements Definition • JSC 30426 Update
Excited State Species	No Specifications	100	Major Abundances	X	X	X	X	X	X	X	X		X	X	X	X	X	X			
Deposition	Potentially Limiting	100		X	X	X	X	X	X	X	X	X			X	X	X	X	X	• Measure Backscattering Cross Sections • Condensation Coefficients • Source Characteristics	• Need Payload Controls • Exterior of Space Station Must Be Clean ~<10^{-13} gm/cm²s Outgassing is Required for All Surfaces • JSC 30426 Update
Emissions																					
UV	Marginally Meets Requirements at 450 km (Except for Discrete Emissions)	10	Neutral Abundances			X			X			X	X	X	X	X	X	X	X	• Lab Measurements and Theoretical Determination of Elastic and Inelastic Cross Sections and Atomic/Molecular Parameters • Lab Measurements of 5 eV 0 on Typical Surfaces • Shuttle Measurements of Emissions and Abundances	• Review Requirements After Further Studies • May Need to Introduce Discrete Emission Requirement • Need to Set Requirements for $\lambda > 200\mu m$ • All Proposed Vented Species Should be Screened for Fluorescence, Dissociation/Ionization Products • JSC 30426 Update
VIS						X			X			X	X	X	X	X	X	X	X		
IR	Significant Induced Levels	100	Surface Effects			X			X			X	X	X	X	X	X	X	X		
Particulates	Requirements as Stated may not be Achievable	10-100				X										X			X	• Further Analysis of Existing Shuttle Data • Shuttle Measurements of Velocities, Drag Effects • Lab Measurements of Erosion • Theoretical Model of Impact Sources, and Examination of Retrieved Surfaces	• $\Delta I \cdot \Delta t$ May be More Useful than I for IR Spec. • Need to Track and Record (Centrally) all SS and Payload Activities Such as Instrument Movement, Gas Release • JSC 30426 Update
Electromagnetic	Potentially Significant Induced Noise and Magnetic Field	10-100	• Neutral Abundances • Motional emf • Power Line Leakage • Arcs • Pick-up Ion Current											X						• Theoretical Studies and Modeling	• Add Ionization Requirement to JSC 30426 • Establish Requirements for Structure Resistance, Conductivity, Current Collecting Area, Leakage

Key Parameters Needing Quantification — Station Sources; Atomic and Molecular Parameters

TABLE OF CONTENTS

Page

NEUTRAL ENVIRONMENT

PLASMA ELECTROMAGNETIC ENVIRONMENT

OPTICAL ENVIRONMENT

PARTICULATE ENVIRONMENT

SPACECRAFT CONTAMINATION

TABLE OF CONTENTS (Concluded)

NEUTRAL ENVIRONMENT FOR SPACE STATION

R. O. Rantanen

Science and Engineering Associates, Inc.
6535 S. Dayton St., Suite 2100
Englewood, CO 80111

Abstract. The molecular number column densities along specific experiment lines-of-sight on the Space Station cross boom generally meet JSC 30426 requirements. The deposition of contaminants on payload surfaces exceeds the JSC 30426 requirements. These model predictions require updating because of the impact on background brightness predictions. An increase of a factor of 2 to 10 in column densities would result in an unacceptable optical background.

Introduction

The results presented in this brief position paper are a result of studies initiated by OSSA to determine the contamination compatibility of the cross boom and dual keel Space Station configurations with attached payloads. Details of this study are available in Space Station Contamination Assessment Summary, dated November 16, 1987.

Approach

The approach was to define the three-dimensional configuration of the Space Station and calculate surface-to-surface view factors and solid angles between surfaces and points in an extensive point matrix around the Space Station via a modified TRASYS model (Jensen and Goble, 1983).

Figure 1 shows the two levels of detail used for the geometry. One was a 145 node model for gas collision sources and interactions and the other a 350 node higher fidelity model for surface-to-surface deposition calculations.

The sources used for the operational period are shown in Table 2. In addition the RCS engines firing along z positioned at x = -750, y = $\pm$2000, and Z = -250 cm and the resistojet positioned at x = -3385, y = 0, and Z = -255 cm were included as sources for non-operational periods.

The surfaces of the modules and the service facility outgas at a rate of 6.1×10^{10} molecules $cm^{-2} s^{-1}$ (1×10^{-11} g $cm^{-2} s^{-1}$). The solar panels, thermal radiators, and power radiators outgas at a higher rate, 3.1×10^{12} molecules $cm^{-2} s^{-1}$ (5×10^{-10} g $cm^{-2} s^{-1}$). Outgassing molecules are considered to be emitted in a Lambertian distribution.

The criterion for leakage from Space Station modules is a total of 2,270 g day^{-1} (5 lb day^{-1}). This total leak rate was partitioned among the modules as follows. Seals were divided into three major categories according to increasing propensity for leakage: factory installed seals such as at fixed viewing ports (called "Inactive Seals Installed in Factory"), on-orbit installed seals such as those between modules and nodes that are not made and broken repeatedly (called "Inactive Seals Installed On-Orbit"), and active seals that are made and broken repeatedly on-orbit (called "Active Seals"). Inactive seals installed in factory were considered leakfree. Inactive seals installed on-orbit and active seals were represented by short cylinders or
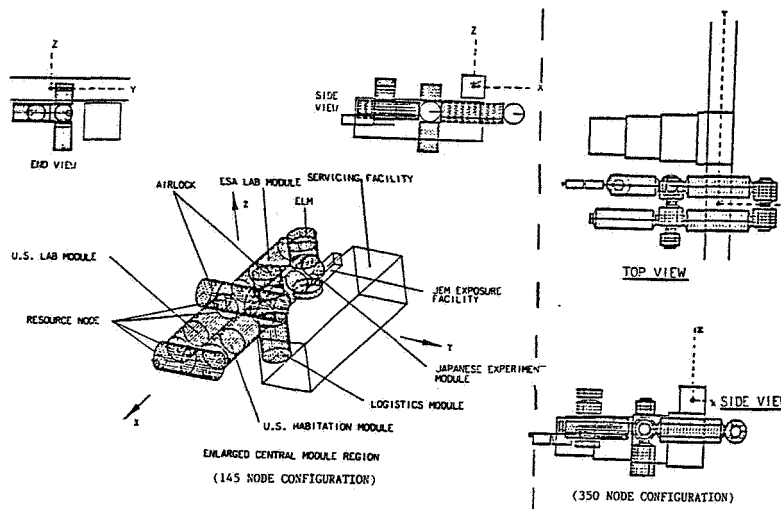
Fig. 1. Modeled configurations.

Table 1. Molecular Sources-Quiescent Period

SOURCE	TYPE	CONSTITUENTS	RATE
MODULE/SERVICE FACILITY SURFACES	OUTGASSING	MEAN MOL. WT. = 100	6.1×10^{10} MOLECULES/CM^2/SEC
SOLAR PANELS	OUTGASSING	MEAN MOL. WT. = 100	3.1×10^{12} MOLECULES/CM^2/SEC
THERMAL RADIATORS	OUTGASSING	MEAN MOL. WT. = 100	3.1×10^{12} MOLECULES/CM^2/SEC
POWER RADIATORS	OUTGASSING	MEAN MOL. WT. = 100	3.1×10^{12} MOLECULES/CM^2/SEC
INACTIVE SEALS INSTALLED ON ORBIT--TYPE 1 (RING)	LEAKAGE	75% N_2, 22% O_2, 2% H_2O, 1% CO_2	1.3×10^{15} MOLECULES/CM^2/SEC
INACTIVE SEALS INSTALLED ON ORBIT--TYPE 2 (RING)	LEAKAGE	75% N_2, 22% O_2, 2% H_2O, 1% CO_2	1.6×10^{15} MOLECULES/CM^2/SEC
INACTIVE SEALS INSTALLED ON ORBIT--TYPE 3 (RING)	LEAKAGE	2270 GM/DAY (5 LB_M/ DAY) TOTAL	75% N_2, 22% O_2, 2% H_2O, 1% CO_2	1.7×10^{15} MOLECULES/CM^2/SEC
ACTIVE SEAL (RING)	LEAKAGE		75% N_2, 22% O_2, 2% H_2O, 1% CO_2	4.0×10^{15} MOLECULES/CM^2/SEC
AIR LOCK (DISK)	LEAKAGE	75% N_2, 22% O_2, 2% H_2O, 1% CO_2	3.6×10^{14} MOLECULES/CM^2/SEC
DOCKING RING (DISK)	LEAKAGE	75% N_2, 22% O_2, 2% H_2O, 1% CO_2	4.8×10^{15} MOLECULES/CM^2/SEC
VENT (LOCATED AT X=0, Y=-325 CM, Z=-831 CM, POINTING IN -Y DIRECTION)	VENT	0.1 GM/SEC	75% N_2, 22% O_2, 2% H_2O, 1% CO_2	1.0×10^{21} MOLECULES/SEC

"rings" in the Space Station model. "Type 1" (three seals) and "Type 2" rings
(eight seals) were assigned a leak rate of 1.3 x 10^{15} and 1.6 x 10^{15}

molecules cm^{-2} s^{-1}, respectively (see Table 2), corresponding to a flow
rate of 90.7 g day^{-1} (0.2 lb day^{-1}) for each seal. The difference in
molecular flux for type 1 and type 2 rings was a result of different surface
areas of the rings. "Type 3" rings (two seals) were assigned a leak rate of
1.7 x 10^{15} molecules cm^{-2} s^{-1}, corresponding to a flow rate of 75.7 g
day^{-1} (0.167 lb day^{-1}) each. One active seal was considered at the
attachment of the logistics module. This major ring source was assigned a
leak rate of 4.0 x 10^{15} molecules cm^{-2} s^{-1}, corresponding to a flow rate
of 227 g day^{-1} (0.5 lb day^{-1}). The remaining major leakage sources, the
air locks and docking rings, were also assigned a leak rate corresponding to a
flow rate of 227 g day^{-1} (0.5 lb day^{-1}). The specific molecular leak
rates depended on the area of the sources, which in these cases were disks
(see table). Leakage is considered to be emitted in a Lambertian
distribution.

The vent passed an average flow rate of half the total average rate of 0.1
g s^{-1}. The other half was passed through an identical vent facing in the +y
direction in order to give zero net thrust. The latter vent was not included
in the model since it was entirely shadowed from the region of interest (above
the modules). The vent was considered as a point source producing a density
distribution given by

$$N(\text{molecules cm}^{-3}) = 5.7 \times 10^{15} \cos^2 \{0.94\ \theta\}/r^2$$

where r is the distance in cm from the source and θ is the angle from plume
centerline.

Results

Cross Boom

Densities of the molecular sources were calculated at every point around
the Space Station and the type of molecule and its source were tracked. A
total of 30 different molecules or source state of the molecules was used.
These included ambient, surface reemitted ambient, outgassing, leakage, and
vent plus the scattered component of each of these.

Lines-of-sight were calculated at three positions along the boom. One
position was at the center of the boom and the others 15 meters from the
center. At the boom center the total number column density ranged from 2.4 x
10^{12} to 9.6 x 10^{11} molecules cm^{-2}. By species the surface reemitted
atomic oxygen ranged from 7.7 x 10^{11} to 4.5 x 10^{11} atoms cm^{-2}, the
surface reemitted N_2 ranged from 1.2 x 10^{12} to 2.3 x 10^{11} molecules
cm^{-2}, O_2 ranged from 3.4 x 10^{11} to 3.9 x 10^{10} molecules cm^{-2}, and
H_2O ranged from 7.3 x 10^{10} to 2.7 x 10^9 molecules cm^{-2}. At y = 15
meters from the center the total density ranged from 4.7 x 10^{12} to 9.0 x
10^{11} molecules cm^{-2}. Water was the only species that exceeded require-
ments at a level of 7.5 x 10^{11} molecules cm^{-2} for one line-of-sight. The
results for y = -15 meters ranged from 6.5 x 10^{12} to 1.1 x 10^{12} molecules
cm^{-2} for total number column densities. Water reached a peak of 7.3 x
10^{11} molecules cm^{-2} for one line-of-sight. These results are summarized
in Figure 2.

Direct flux deposition levels on surfaces at the three points along the
cross boom reached rates of 5 x 10^{-12} to 1.8 x 10^{-11} g cm^{-2} s^{-1} and
depended on solar array position. These values were for a flat surface facing
forward, aft, left/right and upward along Z. For surfaces with a limited

	TOTAL NCD RANGE MOLECULES/CM²	O ATOMS/CM²	N₂ MOLECULES/CM²	O₂ MOLECULES/CM²	H₂O MOLECULES/CM²
BOOM CENTER Y=0	2.4×10^{12} TO 9.6×10^{11}	7.7×10^{11} TO 4.5×10^{11}	1.2×10^{12} TO 2.3×10^{11}	3.4×10^{11} TO 3.9×10^{10}	7.3×10^{10} 2.7×40^{9}
Y=15M	4.6×19^{12} TO 9.0×10^{11}	–	–	–	UP TO 7.5×10^{11}
Y=-15M	6.5×10^{12} TO 1.1×10^{12}				UP TO 7.3×10^{11}

*DURING NONOPERATIONAL PERIODS THE COLUMN DENSITIES RANGED FROM 5.6×10^{12} TO 5.6×10^{15} MOLECULES/CM²

Fig. 2. Number columnm density ranges cross boom – quiescent period.

	DEPOSITION GM/CM²/s
o DIRECT FLUX - CROSS BOOM - DUAL KEEL	5×10^{-12} 3.0×10^{-14} 2.2×10^{-12}
o RETURN FLUX - CROSS BOOM	2.8×10^{-14} 2.3×10^{-13}

Fig. 3. Deposition ranges at payload positions on flat surfaces.

field-of-view the direct flux did not deposit. The return flux of contaminants via scattering interaction with the ambient ranged from 2.3 x 10^{-13} to 2.8 x 10^{-14} g cm^{-2} s^{-1} on flat surfaces. Limited fields-of-view of 0.1 steradians only received significant deposition when viewing along the direction of motion. These levels on the +x facing surfaces ranged from 1.2 x 10^{-12} to 3.9 x 10^{-13} g cm^{-2} s^{-1}. The deposition results are summarized in Figure 4.

Dual Keel

The number column densities for the dual keel lines-of-sight were 1 to 2 orders of magnitude less than the cross boom and should be acceptable for payload viewing.

The direct flux deposition levels on flat surfaces at the three points along the keel ranged from 2.2 x 10^{-12} to 3.0 x 10^{-14} g cm^{-2} s^{-1}.

Non-Operational Periods

The RCS engines firing along the +Z axis (upward) were evaluated for contributions to number column densities along the cross boom. The water content ranged from 5.6 x 10^{15} to 2 x 10^{13} molecules cm^{-2}. Since the effluent of the engines is H_2O it clearly replaced the other sources as the predominant contaminant. The resistojet with only one jet operating produced number column densities of water that ranged from 5 x 10^{13} to 1 x 10^{11} molecules cm^{-2} for H_2O. Multiple resistojets would cause the same increase in the column densities.

Figures 4, 5, and 6 show the types of graphic data that are presented in "Space Station Contamination Assessment Summary." Figure 4 shows the iso density contours in the X-Z plane. The numbers on the contours correspond to multiples of the ambient density which was 1.3 x 10^{8} molecule cm^{-3} for this study. Figure 5 shows lines-of-sight integrated for the contour shown in Figure 4. Figure 6 is the same as Figure 5 except that the densities at each
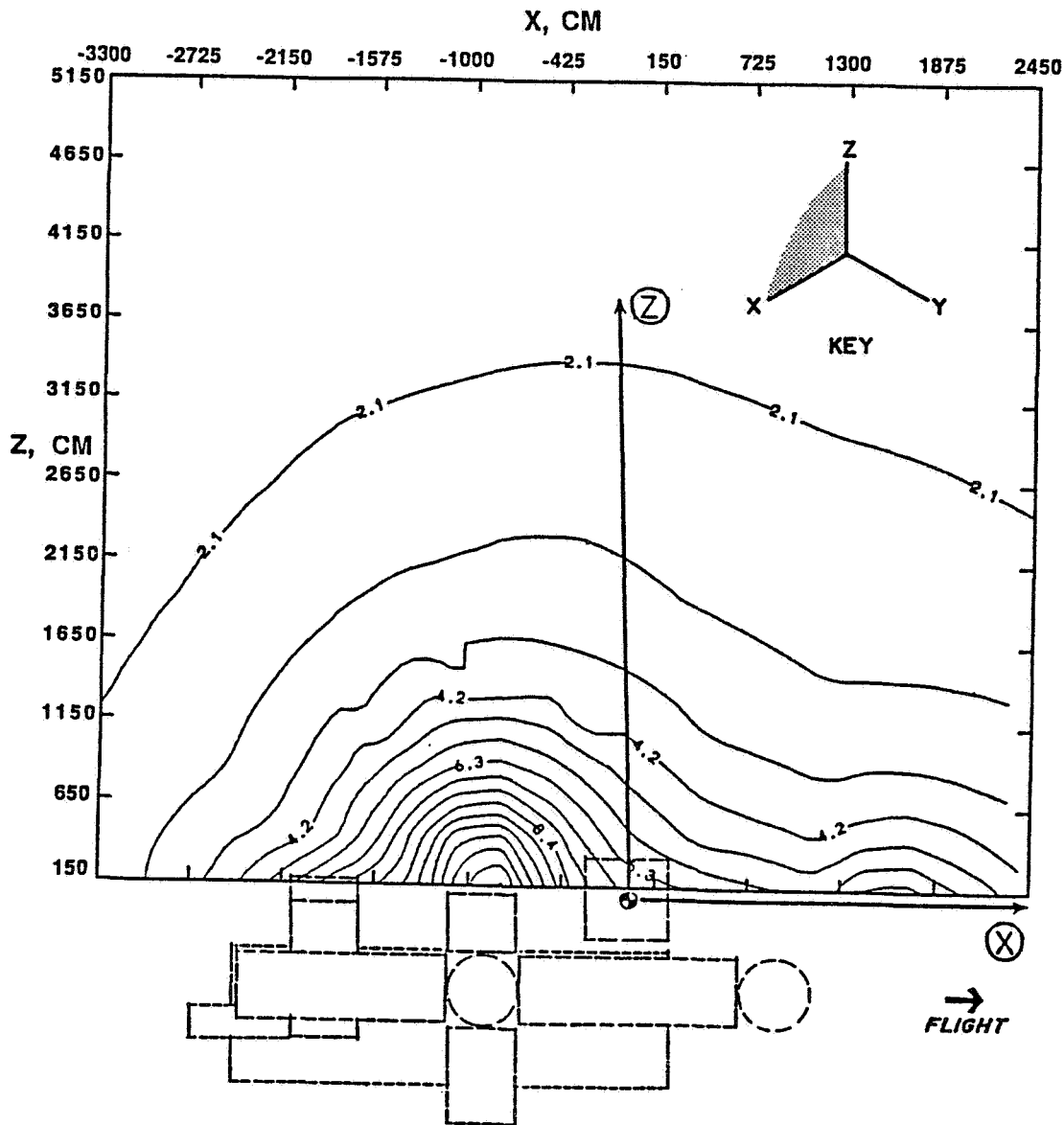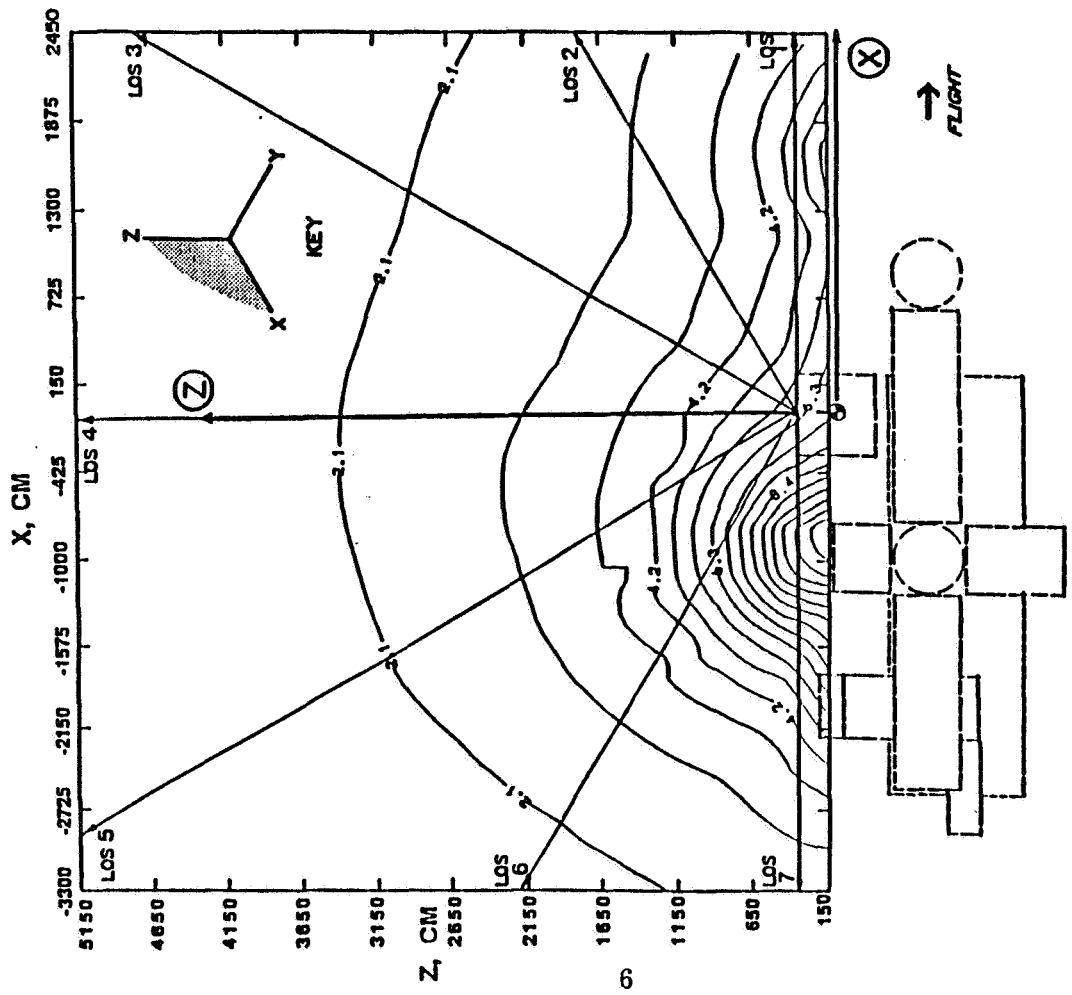
4

Fig. 4. Total density in X–Z plane at Y = 0.

point in the plane are shown so that users of the data can perform their own integration or use the densities directly for plasma analysis. The numbers are multiples of the ambient density.

Conclusions

Based on the assumptions for the sources only a few lines-of-sight on the cross boom exceed the JSC 30426 number column density requirements. It is not clear if these meet the zodiacal background requirements also in JSC 30426.

The dual keel configuration meets all column density requirements. For the dual keel the major contamination problems will result from the attached payloads creating local contaminant conditions that may be unacceptable.

5

LOS	TOTAL NCD w/o FREESTREAM AMBIENT	SPECIES NCD w/o FREESTREAM AMBIENT
LOS 1	1.7E+12	0 = 5.7E+11, N2 = 8.1E+11, O2 = 2.3E+11, H2O = 1.6E+10
LOS 2	1.4E+12	0 = 7.7E+11, N2 = 4.3E+11, O2 = 1.1E+11, H2O = 7.5E+9
LOS 3	1.3E+12	0 = 6.3E+11, N2 = 4.4E+11, O2 = 1.2E+11, H2O = 8.1E+9
LOS 4	1.4E+12	0 = 6.2E+11, N2 = 5.1E+11, O2 = 1.4E+11, H2O = 9.4E+9
LOS 5	1.3E+12	0 = 5.5E+11, N2 = 4.9E+11, O2 = 1.3E+11, H2O = 9.1E+9
LOS 6	1.3E+12	0 = 5.3E+11, N2 = 4.8E+11, O2 = 1.3E+11, H2O = 9.1E+9
LOS 7	1.1E+12	0 = 4.5E+11, N2 = 3.9E+11, O2 = 1.1E+11, H2O = 7.3E+9

ALL VALUES MEET REQUIREMENTS

Fig. 5. Total density in X-Z plane at $Y = 0$ and NCDs for coplanar lines-of-sight with origin at $X = 0$, $Y = 0$, $Z = 250$.
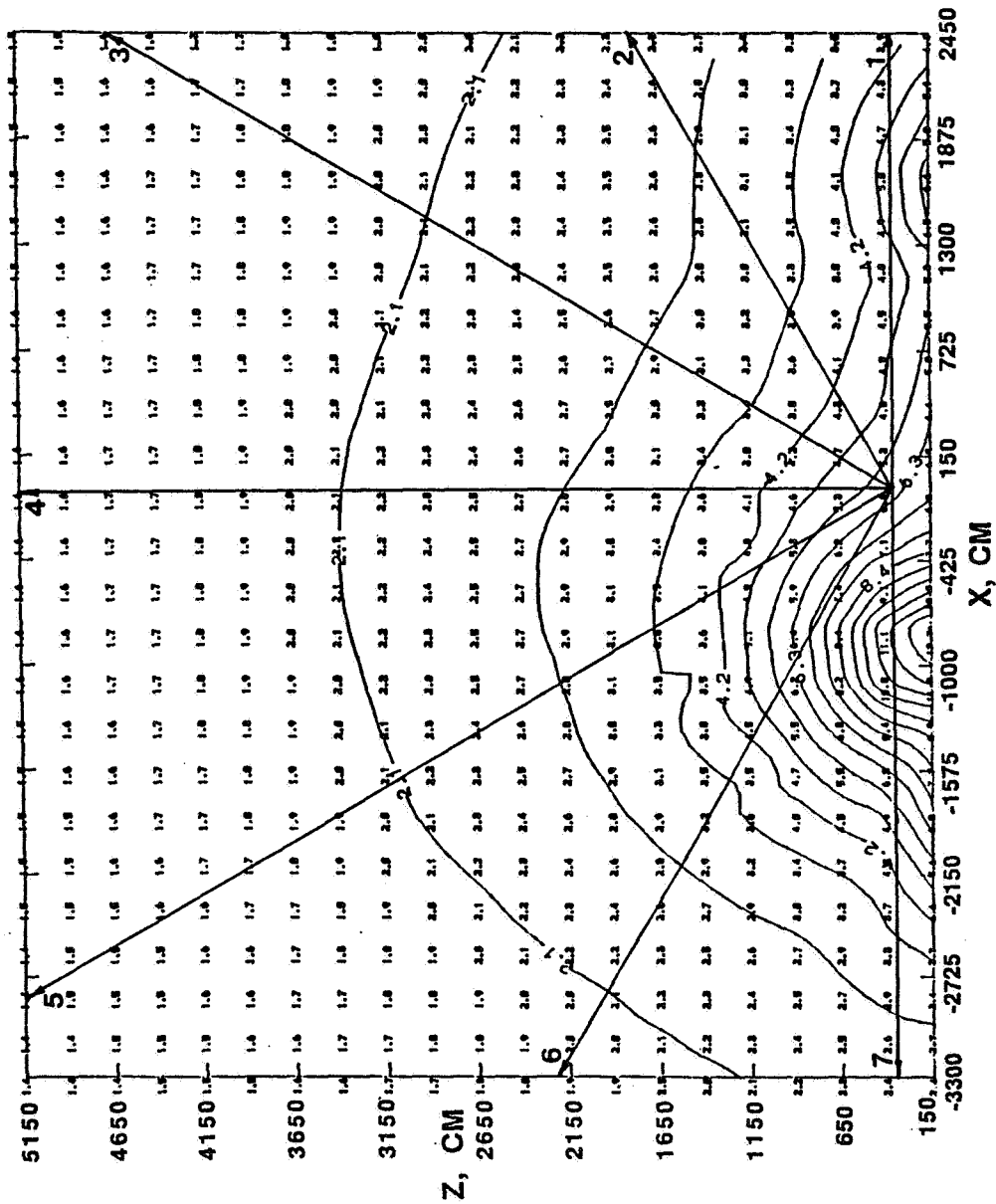
Fig. 6. Total density plot of Figure 5 with point values.

LOS	TOTAL NCD w/o FREESTREAM AMBIENT	SPECIES NCD w/o FREESTREAM AMBIENT
LOS 1	1.7E+12	O — 5.7E+11 N2 — 8.1E+11 O2 — 2.3E+11 H2O — 1.6E+10
LOS 2	1.4E+12	O — 7.7E+11 N2 — 4.3E+11 O2 — 1.1E+11 H2O — 7.5E+9
LOS 3	1.3E+12	O — 6.3E+11 N2 — 4.4E+11 O2 — 1.2E+11 H2O — 8.1E+9
LOS 4	1.4E+12	O — 6.2E+11 N2 — 5.1E+11 O2 — 1.4E+11 H2O — 9.4E+9
LOS 5	1.3E+12	O — 5.5E+11 N2 — 4.9E+11 O2 — 1.3E+11 H2O — 9.1E+9
LOS 6	1.3E+12	O — 5.3E+11 N2 — 4.8E+11 O2 — 1.3E+11 H2O — 9.1E+9
LOS 7	1.1E+12	O — 4.5E+11 N2 — 3.9E+11 O2 — 1.1E+11 H2O — 7.3E+9

Deposition levels on both the cross boom and the dual keel exceed the requirements on a flat surface at the payload positions. The dual keel levels are 1 to 2 orders of magnitude less than the cross boom. Limited field-of-view surfaces meet the deposition requirements except when viewing along the direction of motion.

The total leakage rate of 2270 gm day^{-1} (5 lb day) has not been demonstrated as an engineering feasibility. A change of a factor of 2 would cause more lines-of-sight to have column densities that exceed the criteria.

Any sources other than leakage and outgassing from the European and Japanese module have not been included.

The experiment volume pumpdown vent location used in this study minimizes its effluent impact on upper hemisphere viewing but does cause a potential problem for Earth pointing systems. This location has not been approved or shown to be the best location for engineering purposes. The flow rate used was an average during volume pumpdown. Higher values will occur initially. No gas emissions other than cabin air were analyzed.

Experiments with surfaces within 2 or 3 meters of each other must have outgassing rates less than 1×10^{-13} g cm^{-2} s^{-1} in order to meet the deposition requirements on nearby payloads.

The operation of the RCS engines and the resistojets creates number column densities that exceed requirements.

Recommendations

The following recommendations are made because of their potential impact on Space Station and the attached payloads.

1. Update Contamination Model/Perform Sensitivity Study
    Include Phase I extra solar arrays and remove service facility. Perform trades on collision cross section, scattering distribution, and surface emissions.

2. Experiment Vent Optimization
    Determine optimum vent location taking into account, engineering requirements, attached payload needs, venting needs, gases used, densities near solar panels, microgravity needs, etc.

3. Update JSC 30426 Requirements
    Based on spectral brightness versus column density upgrade requirements. Also, revisit other updates that may be required for deposition, particulates, etc.

4. International Module Sources
    Determine other contaminant sources that may exist from the European and Japanese modules. Input to the contamination model for evaluation.

5. Shuttle/Hermes Visits Docked
    Determine molecular deposition and particulate source impact of the Shuttle docked to the Space Station and for visits by the European Space plane (Hermes).

6. Update Outgassing Sources
    Determine levels of outgassing that may exist for sources or determine what is allowed based on analysis.

7. Spectral Brightness
   Continue modeling by D.G. Torr, UAH, to allow brightness predictions to be incorporated into number column density predictions. Support this study with update neutral gas density predictions.

8. Flight Experiments
   Flight experiments at several altitudes to measure spectral brightness emissions of known sources are required to obtain necessary excitation data for predictions. Also gas density/direction measurements are required at several altitudes to verify/update contamination model predictions.

9. Detection Sensors
   A combination of sensors to verify the contaminant environment are required to be placed on the Space Station at multiple locations. These should be decided upon, built, flight tested, and finally packaged for Space Station.

10. Surface Effects
    Determine the surface phenomena that exist for excitation of adsorbed species and their subsequent remission.

11. Payload to Payload Contamination
    Model the payloads on the boom to see what column densities may exist for near neighbors and the deposition requirements for close proximity payloads.

12. Earth Pointing Requirements
    Develop a set of contamination number column density and spectral background brightness requirements for Earth pointing systems. This may allow vent location to be better located for upper hemisphere viewing.

13. Model Verification Shuttle Data
    Revisit Shuttle data that has not been reduced for correlation to contamination predictions. Include IECM, SPAS, IR measurements, and any other data that are useful.

Reference

Jensen, C.L., and Goble, R.G., Thermal Radiation Analysis System, MCR-73-105 (Rev. 5), June 1983.

SPACE STATION NEUTRAL EXTERNAL ENVIRONMENT

H. Ehlers and L. Leger

NASA Johnson Space Center, Houston, TX

Abstract.   Molecular contamination levels arising from the external induced neutral environment of the Space Station (Phase I configuration) have been calculated using the MOLFLUX model. Predicted molecular column densities and deposition rates generally meet the Space Station contamination requirements. In the doubtful cases of deposition due to material outgassing, proper material selection, generally excluding organic products exposed to the external environment, must be considered to meet contamination requirements. It is important that the Space Station configuration, once defined, is not significantly modified to avoid introducing new unacceptable contamination sources if the contamination requirements are to be met.

Introduction

Deposition of harmful molecular layers on Space Station elements and scientific instruments leading to performance degradation as well as the deterioration of electromagnetic signals from stellar objects due to induced contamination of the environment are a serious concern. They must be assessed as early as possible as part of the Space Station design/development process. The only means to accomplish this is through the use of mathematical models that relate certain Space Station characteristics such as material usage and presence of concentrated gas sources in all locations to their effect on critical instrument/equipment performance. The MOLFLUX program is such a model. If the contamination analysis indicates that a particular Space Station configuration and operating mode leads to "excessive" contamination levels, then design changes must be made (where possible under given circumstances) to reduce this level. On the other hand, once the Space Station configuration is well defined and in all respects acceptable, it should not be significantly modified to avoid introduction of new unacceptable contamination sources. The model predictions discussed in this paper have been produced to provide a preliminary understanding of the effects which the Space Station design may have on meeting its objective.' The conclusions reached should play a significant part in the development phase of the Space Station.

Space Station Configuration

The basis for this assessment of the neutral external Space Station environment is the Space Station Phase I configuration. For analysis purposes, the Space Station (solar panels normal to flight direction) is divided into about 300 surface nodes (without the truss) and about 700 nodes including the truss. These as well as a number of "point" nodes represent the potential sources of contamination such as module leakage, gas vents, thrusters, other vehicles (e.g., the Space Shuttle orbiter), outgassing, etc., and receivers of contamination. This system also allows for an assessment of the Space Station interaction with the ambient atmosphere.

Model Description

The MOLFLUX program was developed as an analytical tool to predict the flow

of molecules in the vicinity of vehicles in the space environment. Program output parameters were chosen to address the requirements set by various NASA/contractor contamination working groups including the Space Station External Contamination Working Group (CWG). Program input parameters were selected primarily on the basis that they are fairly easily measurable or at least reasonably predictable. The key to the program itself is a solid scientific foundation. It is based on a numerical integration of the Bhatnagar, Gross, Krook (BGK) model approximation of the Boltzmann kinetic equation for a mixture of gases (Robertson, 1976).

An evaluation of the molecular flow conditions surrounding the Space Station shows that the mean free path of molecules immediately in front of the surface of the large solar panels under ram conditions is on the order of 250 meters. This value, which is based on the assumption of a constant ambient density of approximately 2.1×10^8 molecules cm^{-3} is large compared with the width of these panels (approximately 10 meters). Therefore a free molecular flow condition exists, with the mean free path increasing rapidly with the distance from the surface. Material outgassing also leads to free molecular flow. At Space Shuttle orbits, where the ambient density is about 10 times as high, the mean free path is about 25 meters, or comparable with the mean orbiter cross section, indicating near free molecular flow conditions. Evaluations such as this one lead to the conclusion that, with few exceptions, either free or "near free" molecular flow exists around spacecraft such as the Space Station in Earth orbit and farther out in space. This conclusion is valid also for thruster plumes with the exception of a small plume volume of viscous and transition flow close to the nozzles or for extremely long firing times.

Accordingly, a model of nearly free molecular flow appears to be adequate to deal with most space-related applications. MOLFLUX has been developed with these thoughts in mind. The distribution function for all species is, therefore, a small perturbation (due to molecular collisions) from the free molecular flow case and allows for backscattering return flux and attenuation calculations. The result is a program of reasonable size and accuracy with maximum flexibility. In general the treatment of data is kept in line with their accuracy, since any model is only as good as the input data used. The capability to introduce input data as well as to evaluate output data is left very general and adaptable to the needs of the user. The model describes the molecular environment in terms of parameters such as local density, column density, direct flux, and return flux (including deposition). The predictions depend on geometric configuration, contamination source characteristics, trajectory/attitude, ambient environment, instrument field-of-view, etc. Predicted direct fluxes involving "points in space," as well as surfaces, are based on line-of-sight (LOS) view factor, distance, and direction calculation techniques. Density and column density are derived from direct flux predictions. One surface reflection (no deposition) was permitted to derive the predicted data in this paper. The model is designed to maximize prediction accuracy specifically in areas where it counts most, i.e., data regarding instrument LOS and instrument field-of-view. The number and location of "space" points are chosen accordingly. Model accuracy is consistent with available input data accuracy as outlined in detail below.

Prediction uncertainties of contamination models are mainly the results of uncertainties of input data.

Part of the molecular deposition on surfaces is caused by backscattering return flux resulting from collisions of contamination molecules with ambient molecules. Elastic molecular collision frequencies and cross sections strongly depend on the velocity distribution of the various molecules involved. Molecular velocities range from thermal velocities all the way up to about 8 km

s^{-1} and more. Present cross section estimates are based on values determined from viscosity measurements since no in situ flight measurements have been performed to date. The MOLFLUX program considers only collisions of high-speed (7.7 km s^{-1}) ambient molecules with local contamination species due to the fact that only these contribute significantly to the backscattered return flux at Space Station altitudes. Under these conditions, the cross section error is estimated to be on the order of a factor 2. Cross section errors of molecules colliding at velocities ranging from thermal to some 10 km s^{-1}, if considered, would be much larger, on the order of a factor 6, increasing the error of return flux predictions accordingly. Since return flux rates are proportional to collision frequencies, the cross section errors translate directly into return flux errors and corresponding deposition rate errors.

Inelastic molecular collisions involving chemical reactions, creation of excited molecules, release of different kind of molecules, etc., do take place, particularly during interaction of ambient high velocity molecules such as atomic oxygen with surfaces (ram cases), modifying the results due to surface reflections and emissions significantly. Unfortunately no quantitative experimental data useful for model inputs are available. Therefore, considerable prediction errors are introduced affecting column density, return flux deposition, and ram cases. Errors due to undefined chemical reactions can amount to some 25%; those due to creation of excited molecules may be significantly larger. The molecular composition of the atmosphere is time- and location- dependent causing an error in return flux and deposition predictions estimated to be about up to a factor of 10 depending on the specific situation.

Surface deposition of molecules is the result of complex processes involving the formation of an equilibrium between impinging molecules and (re-)emitted molecules. This equilibrium is affected by parameters such as surface material and temperature, velocity and kind of impinging molecules, solar radiation, atomic oxygen impact, etc., and therefore, very time dependent. No formula describing adequately the result as a function of all these parameters exists. Accordingly, each case must be analyzed in detail and this has not been done individually for the Space Station. All of the present predictions are the result of very rough estimates based on impinging molecular fluxes. Such predictions may have errors of the order(s) of magnitude(s).

Material outgassing rates depend on material characteristics and the environmental conditions to which the material is exposed including temperature, material history, and exposure history. Such rates have not been adequately formulated to date. Each case must be treated on an individual basis. Current predictions are based on short-term Skylab and Space Shuttle experience generally featuring different materials and may, therefore, vary by orders of magnitude (depending on who is estimating), impacting severely predictions of column densities and molecular deposition rates.

Module leak locations and rates are impossible to adequately define, particularly over long periods of time in thermal and high vacuum environments. Point sources, ring-shaped sources, and area sources have been modeled and basically all lead to very similar results. Presently the Space Station module design leak rate totals 5 lb day^{-1} for practical reasons. There is no proof that the actual leak rate will be smaller or larger than this, particularly over a period of years. An error of a factor 2 may be a reasonable assumption.

Laboratory gas venting is a necessity which can be in conflict with requirements for astronomical observations. The present goal is to design vents and venting procedures which meet both the requirements for adequate venting and astronomy. Preliminary assessments are very encouraging. However, it is too early for a valid error analysis except as discussed in other sections.

The Space Station thruster system design is not well enough defined at this time to permit an acceptable assessment and error analysis. Predictions based on substitute designs may carry significant errors (order of magnitudes).

Since exact solutions to the common gas flow equations such as those named after Boltzmann have not been yet found for general application, analysts are forced to use approximations. Today's prediction techniques, although far from being perfect, however, when applied correctly produce approximation errors which are small compared with the errors introduced by the lack of valid experimental input data.

Predicted Data

Column Density

Module leakage at a total rate of 5 lb day^{-1} has been modeled using several different methods: point sources, ring sources, and area sources. The not so surprising result is that, for any of these, in the worst case, the column density along the module periphery (at about 5 m diameter) is about 3×10^{11} for H_2O, 2×10^{11} for CO_2, and 1 to 2×10^{13} for all gases combined. At reasonable distance of payloads from the modules (leaks), such as 10 m (e.g., locations above the boom) these column densities rapidly drop by a factor 10.

Column densities produced by the whole Space Station (above the contributions from the undisturbed atmosphere) including the effects of module leakage (5 lb day^{-1}), material outgassing (1 x 10^{-11} g cm^{-2} s^{-1}), and ambient gas impingement (ram at ambient of 2×10^8 cm^{-3}) have been calculated for various LOS's originating from a prime measurement point (PMP) located centrally 5 m above the center line of the transverse boom. A typical result (for the LOS in +x direction, direction of flight) is the following: outgassing (M = 100): 0.7×10^{10} molecules cm^{-2}, H_2O: 0.2×10^{11} molecules cm^{-2}; CO_2: 0.1×10^{11} molecules cm^{-2}, and total (all species): 0.6×10^{13} molecules cm^{-2}. The docked Space Shuttle adds approximately 25% and the truss itself less than 10% to the total value. The column densities for LOS's in the upper hemisphere are: outgassing: $<0.1 \times 10^{11}$, H_2O: $<0.2 \times 10^{11}$, CO_2: $<0.2 \times 10^{11}$, and total: $<0.6 \times 10^{13}$, all in molecules cm^{-2}, unless the LOS passes near surfaces such as solar panels, payloads, etc.

Column densities of LOS's passing directly in front of solar panels with normals pointing into ram at ambient density of 2×10^8 cm^{-3} are between 1 and 2×10^{13} molecules cm^{-2} (induced atmosphere only!).

Column densities produced by small gas vents can be acceptable except for LOS's with points located in the immediate vicinity of the vent(s).

Deposition

Return fluxes due to ambient elastic scattering corresponding to the Space Station column densities defined above for the +x direction and for a field-of-view of $10°$ (half angle) are as follows: outgassing: 0.5×10^{-13}, H_2O: 0.4×10^{-14}, CO_2: 0.7×10^{-14}, and total: 0.2×10^{-11}, all in g cm^{-2} s^{-1}. Return fluxes for LOS's on the wake side of the upper hemisphere have values which are two to three decades lower.

Direct fluxes from the Space Station to a flat surface with its normal in +z direction (vector away from the center of the Earth), at the same PMP, are as follows: outgassing: 0.4×10^{-14}, H_2O: 0.8×10^{-16}, CO_2: 0.8×10^{-16}, and total: 0.1×10^{-11}, all in g cm^{-2} s^{-1}. The sources considered here are material outgassing, module leakage and ram condition. These low values are due to the fact that few surfaces are in the field-of-view. Direct fluxes to

the surface with its normal vertical to the +z direction have values in the low 10^{-12} g cm^{-2} s^{-1} range for each of the following species: outgassing, H_2O, CO_2. Direct flux from Space Station surfaces exposed to the ambient atmosphere to a flat plate with its normal in the -x direction (same PMP) totals 0.4 x 10^{-9} g cm^{-2} s^{-1}.

Actual deposition, based on these rates, depends on surface temperature, surface material, etc. Only a fraction of the outgassing molecules sticks to a surface at ambient temperature.

Molecular deposition on various Space Station elements during Space Shuttle approaches due to thruster firings have been calculated for a great variety of cases involving system engineering simulator (SES) approaches. The results may be summarized as follows: Some of these approaches have produced deposition levels as low as a few Å in thickness on payloads mounted to the transverse boom. The results are very preliminary due to the assumptions made that about 1% of the impinging fluxes remains on the surface and forms a layer of 1 g cm^{-3} density. The deposition levels can be significantly higher if the best available techniques for the Space Shuttle approach are not applied.

Comparison With Requirements

This comparison of predicted data and corresponding requirements is based on the specific assumptions made concerning the values of input parameters and the requirements as defined at this time in JSC 30426. Some of these requirements are briefly summarized below.

Molecular Column Density: For IR active species, such as H_2O, CO_2, etc., 1 x 10^{11} molecules cm^{-2} each (max. 3 x 10^{11} total). For non-IR active species, such as O_2, N_2, H_2, noble gases, etc., 1 x 10^{13} molecules cm^{-2} each (max. 5 x 10^{13} total).

Molecular Deposition: For 300K surface, 2π sr field-of-view, 1 x 10^{-14} g cm^{-2} s^{-1}; for 300K surface, 0.1 sr field-of-view, 1 x 10^{-16} g cm^{-2} s^{-1}; for 5K surface, 0.1 sr field-of-view, 2 x 10^{-13} g cm^{-2} s^{-1}.

Comparison of molecular column densities indicates that, in all practical situations, the predicted values are well within the requirements. In some extreme cases the predicted values are near the requirement limit. These cases involve rather unrealistic extreme LOS locations/directions such as those directly along "long" surfaces (e.g., near modules and solar panels). In cases where a LOS passes through a local high density gas volume created by leaks or vents, the column density may exceed requirements. However, these cases are easily avoidable.

Comparison of molecular deposition data, assuming "reasonable sticking factors," show that, for the most part, the requirements are met. In the doubtful cases of deposition due to material outgassing resulting from return flux as well as direct surface to surface flux, proper material selection, generally excluding organic products which are exposed to the external environment, is necessary in order to meet contamination requirements. In addition, it appears possible that deposition requirements may be met for the case of Space Shuttle proximity operations, provided that the utmost care is taken to minimize the impingement of contamination fluxes on the Station elements from the Space Shuttle thrusters through optimization of maneuvering procedures.

This data comparison raises concern for possible unacceptable contamination effects, particularly, due to material outgassing. The uncertainty of source

rates and sticking factors as well as of the effects of the layers themselves aggravates this point. The only way to arrive at a fair comparison of predictions and requirements in these questionable cases is to improve the quality of the model input data as discussed later. In addition, it is advisable to compare various model predictions in order to verify significant conclusions and eliminate possible prediction errors.

Affected Space Station Experiments

Certain Space Station experiments may be affected by the induced environment and/or by the interaction with the ambient environment. For instance, measurement of the undisturbed neutral and plasma environment is precluded. Certain measurements may not be possible due to an excessive background. These must be defined through a thorough analysis of sufficient detail and accuracy involving the specific instrument and the predicted environment. The question, "why and to what degree does the particular measurement deteriorate with the presence of a specific amount of a specific species of molecule?" must be clearly answered. At the present time only general categories of measurements may be flagged for potential impacts and further detail study. Operating time of some instruments may be affected by "nonquiescent" periods. Requirements by different types of scientific activity may be in conflict with each other, e.g., venting of gases resulting from processing of materials or stemming from He release by instruments themselves may limit times of astronomical observations and vice versa.

Quantification of Input Data

Presently prediction accuracy limits of contamination models are set by the input data, not the modeling techniques. In order to significantly improve the accuracy of predictions coming from today's contamination flow models, a number of molecular reaction processes and their results must be much better understood. The following are examples of the more important areas:

o Molecular collision frequencies (or cross sections) in the molecular velocity range from thermal to 10 km s^{-1}, particularly near 8 km s^{-1}, must be measured for various specie combinations and excited states. Facilities needed to do this are slowly becoming available.

o Emission and absorption cross sections of molecules must be better known to properly correlate optical effects and molecular column densities. Accommodation coefficients for gases and Space Station surface materials and distribution functions of emitted and reflected molecules must be better defined through measurement.

o Measurement of outgassing rates, particularly long-term, of materials actually used on the Space Station is a necessary goal.

o Knowledge of precise deposition/re-evaporation rates determined in the actual environment (sunlight, atomic oxygen atoms, physical/chemical changes) is mandatory.

o Measurement and definition of processes leading to an accurate understanding of molecular "glow" (ram effect, thruster plumes, etc.) are indispensable.

While all these measurements are necessary, one has to keep in mind, however, that even much improved and highly accurate model predictions are of little value if the actual sensitivity and resulting performance degradation due to the presence of each specific contamination species is not precisely known for comparison. This requires a very active participation of principal investigators (PI's) in the contamination assessment process.

What can be done now? Most, if not all, of these measurements can be performed now, either in the laboratory or on the Space Shuttle.

Conclusion

Molecular column densities and deposition rates predicted by the MOLFLUX model generally meet Space Station contamination requirements. Proper materials, generally excluding organic products exposed to the external environment, must be selected in order to meet contamination deposition requirements. Special sealing considerations must be applied to assure acceptable leakage rates for modules, pressure vessels, fluid containers and associated connections, etc. Molecular deposition due to Space Shuttle proximity operations (thruster firings) can be within requirement limits, provided the maneuvering procedures are optimized.

Reference

Robertson, S. J., Spacecraft Self-Contamination Due to Back-Scattering of Outgas Products, LMSC-HREC TR D496676, Lockheed Missiles and Space Company, Huntsville, Alabama, 1976.

CONTAMINANT IONS AND WAVES IN THE SPACE STATION ENVIRONMENT

G. B. Murphy

Department of Physics and Astronomy
The University of Iowa
Iowa City, IA 52242

Introduction

It is a difficult task to estimate, with any degree of certainty, the probable environment of any large space structure or system given that the system has not been firmly defined. This environment is a product of the natural environment and its interactions with that structure and system. We shall distinguish between the so-called induced environment, the molecular, particulate, photon and wave environment which results from the disturbing effects of a large object flying at orbital speeds through the ionosphere, and the contaminant environment which is produced when solids, liquids or gases are released from the system and interact with the induced environment in an array of chemical and physical processes. Our task is made particularly difficult by two important unknowns: a firm definition of the system and its contaminants; incomplete knowledge of the chemical and physical processes which can take place. In this paper we will address the probable plasma environment of Space Station. That is, we will discuss the particles (ions and electrons) and waves which will likely exist in the vicinity of the Space Station and how these may affect the operation of proposed experiments. Differences between quiescent operational periods (as defined by JSC 30426) and non-operational periods as well as probable effects from Shuttle operations will also be discussed. Areas which need further work are identified and a course of action suggested.

Background

Much of our knowledge about the interactions between large bodies and the ionospheric plasma had, until the time before Shuttle flights, been obtained from observations aboard small scientific satellites and various scaled laboratory investigations. The recent era of Spacelab-type payloads aboard the Shuttle orbiter has provided a wealth of heretofore unobtainable information. The Shuttle is not only the largest body flown to date but, as was discovered over a period of time, carries with it a large gas cloud. The discovery of "Shuttle glow" (Banks et al., 1983), broadband electrostatic noise (Shawhan et al., 1984a), heated electron populations (McMahan et al., 1983), a modified ion environment (Hunton and Carlo, 1985), and contaminant ions in the wake (Grebowsky et al., 1987) have begun to fill in pieces in what appears to be a complex puzzle associated with the large body induced environment and contaminant interactions. Recent studies of the neutral and ion population during thruster operations (Wulf and Von Zahn, 1986; Narcisi et al., 1983; Shawhan et al., 1984b), modification of the plasma during FES

operations and H_2O dumps (Pickett et al., 1985), the discovery of pick-up ions consistent with chemistry of the H_2O, O^+ interaction (Paterson, 1987), as well as observations by neutral mass spectrometers (Wulf and Von Zahn, 1986; Miller, 1983), have helped to sort out the differences between interactions which are of the induced variety and those which result from release of contaminants by the orbiter. Observations by IR, optical, and UV instruments on board the orbiter (Torr, 1983; Torr and Torr, 1985; Koch et al., 1987), and by IR on the ground (Witteborn et al., 1987) have provided insight into the effects of both absorption and emission by this contaminant population. It is now clear as a result of these pathfinder experiments that in order to conduct experiments in plasma physics, provide long-term monitoring and a data base for the ionosphere, observe astronomical targets over a broad range of wavelengths, and provide sensitive remote sensing capability, the Space Station environment must be cleaner than that of the orbiter in many respects. Much work has already been done in assessing just how clean that environment must be in order to meet the minimum science requirements (Space Station Payload Contamination Compatibility Workshop, 1987). It will be the purpose of this paper to assess what the particle and wave environment might be and whether the current specifications are adequate in this regard. This assessment will be based on current contamination control requirements, knowledge of proposed space station configuration, and our best guess about the scaling laws for certain plasma interactions.

Particle Environment

A number of investigators have studied the composition of the Shuttle ion environment and compared it to that which was expected of the natural environment at the orbiter altitude (Grebowsky et al., 1987; Siskind et al., 1984; Reasoner et al., 1986). The studies observe large amounts of H_2O^+ which results from the rapid charge exchange reaction

$$H_2O + O^+ \rightarrow H_2O^+ + O$$
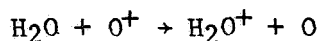
as well as smaller amounts of H_3O^+.

$$H_2O^+ + H_2O \rightarrow H_3O^+ + OH$$
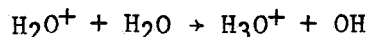
The amount of H_2O^+ (and H_3O^+) observed appears to be directly proportional to the surface temperature leading to the conclusion that most of this observed water is offgassed from Shuttle tiles or other porous surfaces (Narcisi et al., 1983). The amount of water can be estimated by neutral mass spectrometers but caution must be taken since frequently these instruments can only observe molecules which are scattered back toward the orbiter either by collisions with ambient molecules or the cloud itself. Several attempts have been made to estimate water density or by observing the ion population and then doing a kinetic analysis. This has been done with observations obtained within the orbiter bay (Narcisi, 1983) and with data which were obtained during the PDP free-flight on Spacelab 2 (Paterson, 1987). Other estimates have been obtained by observing the infrared signature and then estimating column densities (Koch et al., 1987). The remarkable thing about all of these methods is that although they have shown some decay in the amount of water during the lifetime of the mission and variation among missions, the neutral

observations, ion observations, and IR observations give a consistent picture which can be modeled within the accuracy of the known cross sections for the charge exchange reaction. The significance of this is that if we know one of the above parameters accurately, e.g., column density from IR observations, we can predict another, e.g., contaminant ion population, through a modeling of the chemistry and kinetics of the gas cloud. Several authors have developed models of this "gas-cloud" interaction; notably Patterson (1987) has modeled a steady state cloud and shown the production of H_2O^+ to scale with background O^+ density and Hastings et al. (1987a) have developed time-dependent models of clouds which would be associated with a brief gas release, such as the opening of a gas relief valve or a thruster operation.

This contaminant ion population can be a source of several problems.

(1) These ions create an additional wake which trails the object in a sense which is perpendicular to the magnetic field line instead of parallel to the velocity vector.

(2) Depending on the nature of the ions they may result in a deposition problem on some surfaces facing the ram direction.

(3) Depending on the excitation state of the ions, they may add to the IR, optical or UV spectrum which is sensed by a particular instrument.

(4) The current created by these pick-up ions is believed to be responsible for plasma instabilities which enhance the background wave environment.

(5) Molecules which have low ionization potential may be susceptible to the critical ionization velocity (CIV) process causing enhanced plasma density, production of wave turbulence, and possible photon emission.

Let us look at the above possibilities in light of Space Station operations. Although much of our shuttle experience has been gained by observing the H_2O/O^+ interaction, any process such as charge exchange, photoionization, ionization by CIV, etc., will produce the pick-up ion cloud and present a similar set of problems to experiments or the Space Station.

Figure 1 presents a cartoon of the composite nature of the Shuttle environment to illustrate the first point above. Superimposed on the induced environment (i.e., the neutral and plasma wake) is the wake produced by the pick-up ions. Generated in the orbiter rest frame they will appear to move past the vehicle perpendicular to field lines. Any experiment expecting to be in the neutral or plasma wake may in fact be in a location dominated by these contaminant ions. As mentioned in point 2, it is clear that these ions could interact with or stick to surfaces when they were presumed to be part of a freely expanding cloud. Possible surface degradation could result from the fact that they can strike the ram surfaces with near orbital velocity (their energy is dependent on the reaction that creates them as well as their mass). This implies chemistry which takes place in front of ram surfaces (e.g., glow) and that which takes place on surfaces must take these ions into account.

Regarding point 3, since these ions form an asymmetric distribution about the vehicle and since their column density is greatest in the wake direction, it is important to evaluate not only the atomic physics associated with the neutral molecule but its ionized and possibly excited state as well. If the

ionized species has a particular emission line which is undesirable optically, this may be particularly noticeable in the wake direction.

We will discuss in more detail the effects described by points 4 and 5 in the next section. Let us first, however, summarize the primary contributors to the ion environment.

Molecular contaminants resulting from outgassed or vented products can interact with the ambient population through several processes creating an ionized cloud which will trail behind the Space Station much like the tail of a comet. If the ionizable contaminants are held to levels well below that of the Shuttle (how much below will be discussed in the next section), the ion environment during operational periods should be acceptable to most experimenters. However, a very important gap exists in our knowledge. A study of the OSSA Space Station waste inventory (Bosley et al., 1986) reveals a large number of possible waste gas and liquid products. Although interactions of simple molecules like H_2O, N_2, and CO_2 with the O^+ plasma are reasonably well understood, the chemistry of this large possible "soup" of waste products involves many unknowns. It would seem prudent to assess the possible interaction of some of these waste gases by realistic laboratory experiments before deciding that they are allowable vent gases.

Wave Environment

It will be difficult to assess whether the wave environment described in JSC 30420 and JSC 30237 can be met in its entirety. Analysis of the wave environment aboard the orbiter based on PDP data from OSS 1 and Spacelab 2 have led to the emerging picture, again depicted by the cartoon of Figure 1, that the broadband noise environment may be dominated not by the induced environment associated with the large body interaction as was originally believed, but by production of waves by the gas cloud itself. If this is the case it may be possible to correlate the general level of this background noise to the density of the water cloud. In Figure 2, we present data that have been compiled from the published literature (Pickett et al., 1985). The level of noise at 1 kHz (chosen as typical of the broadband noise spectra for these data) is plotted for three different cases of "small" gas cloud releases. The level of uncertainty in the measurement of H_2O density is represented by the vertical error bars. The three cases chosen represent almost 3 orders of magnitude in gas quantity. In all cases the dominant gas is H_2O. The first is the H_2O vapor cloud associated with the orbiter outgassing per se, the second an operation of the Flash Evaporator System (FES), and the third a typical operation of a VRCS thruster. In all cases the releases were on the dayside and in an ambient density of O^+ plasma of ~10^5 cm^{-3}. Note that the data indicate that the noise is linearly proportional to the density of gas released. The best fit to the data is that the intensity (at 1 kHz) of electrostatic noise is proportional to the product of H_2O and O^+ density. The constant of proportionality is such that at a 1 g s^{-1} release rate the measured electric field anywhere within the general interaction region will be ~1 mV m^{-1} in a 150 Hz bandwidth. (150 Hz is the approximate bandwidth at which these measurements were made.) This law is certainly not absolute but leads the author to believe that most of the observed noise can be tied to this contaminant release. Further examination of turbulence measured by the Langmuir probe and electrostatic waves observed near the orbiter wake by the PDP on Spacelab 2 leads one to speculate that the wake
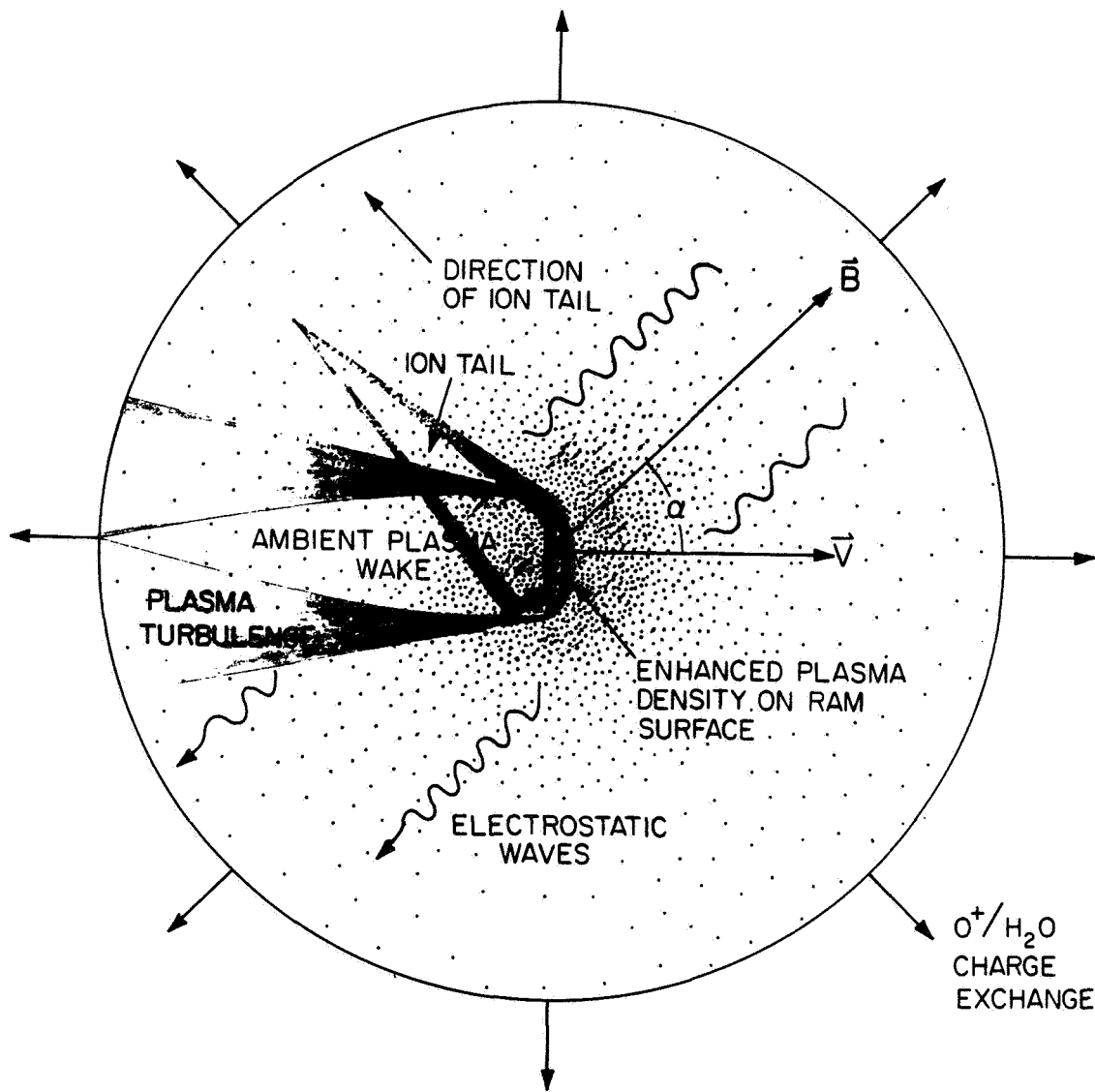
Fig. 1. The neutral cloud of gas which expands from the orbiter undergoes chemical interactions such as change exchange which results in an ion tail and creates plasma waves presumed to be driven by the ion currents.

noise is dominant only in a region confined to the wake and wake boundaries and most wake noise observed elsewhere is dominated by the production of noise associated with instabilities resulting from ion pick-up current generated by the contaminant water cloud.

In order to properly scale this phenomena we must establish more firmly the instability that causes the wave growth and the process that saturates the

ELECTROSTATIC NOISE
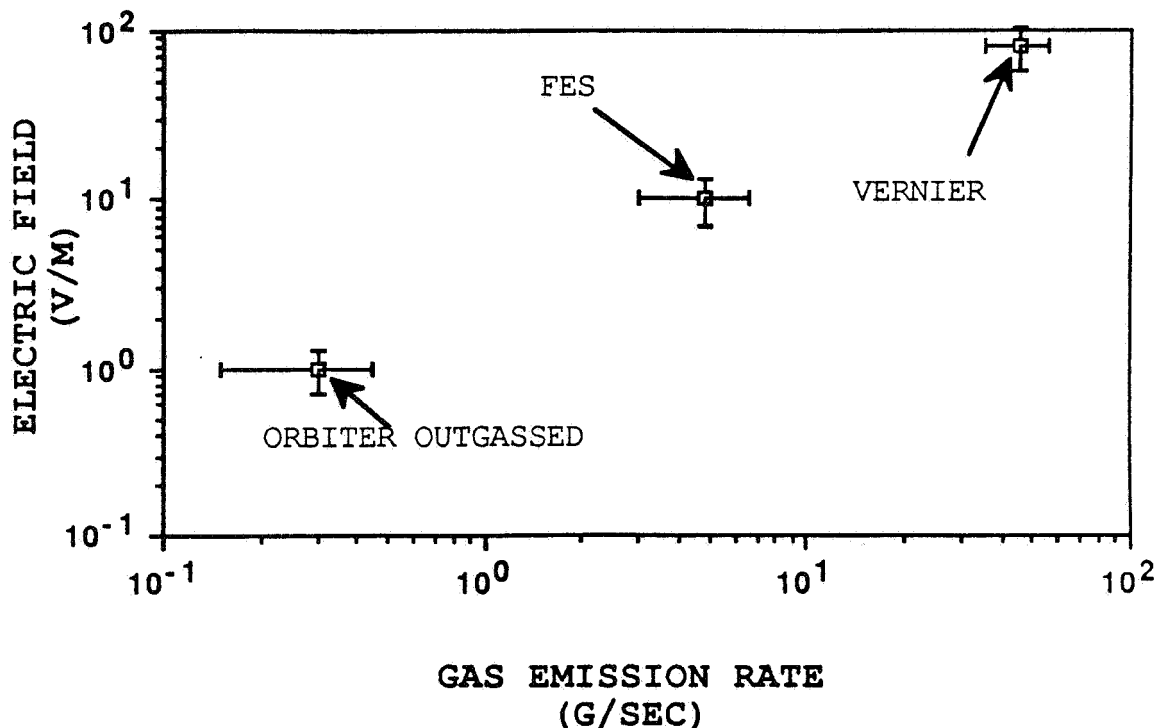
Fig. 2. Gas releases of three different magnitudes and the measured electrostatic noise show roughly a linear correlation. Estimates of outgassing rates for the first data point are a consensus of observations of inferred column density from IR and measurements of both ion and neutral densities. Emission rates of FES and VRCS are well defined.

instability. CIV may play a role in this process (Papadopoulos, 1984) but will again be very dependent on the gas composition. More experiments are required before we can definitely say that the above scaling law applies to molecules other than water, since the importance of a particular instability or CIV varies with molecular species.

Extrapolating this insight into the Space Station environment we are again led to conclude that the plasma environment will be acceptable and the JSC requirements met only during periods where ionizing components of the contaminant gases are minimized. Although the large modules and solar arrays may be a source of plasma noise generated by turbulence in their wake, at points midway along the transverse boom or on the upper or lower keel, this noise may be at an acceptable level at least for some geometric configurations of the velocity vector and magnetic field. Other sources of noise, currents carried by the structure to complete the $\vec{V} \times \vec{B}$ current loop (Hastings and Wang, 1987), radiation of noise by the cable trays or solar arrays or currents

(Hastings et al., 1987b), conduction of noise by sheath waves, etc. must be solved by appropriate design and are not within the scope of this discussion.

What numerical limits must be placed on the ionizing contaminants in order to meet the JSC 30237 specification and provide an environment free of this source of noise? Examining JSC 30237 for the spec on broadband emission for systems at standard locations, we find that at 1 kHz we must be less than 103 dB μV m^{-1} MHz^{-1}. Scaling to the 150 Hz bandwidth of the measurements taken in compiling Figure 2, we find that these emissions must be less than $\sim$0.02 mV m^{-1} which, using the linear scaling law of Figure 2, implies an emission rate of water of $<$20 mg s^{-1}. This should be manageable for a structure like the Space Station which will not be covered with a material that continually outgasses water. The mass release rate of other ionizable molecules could be scaled appropriately depending on their cross section for ionization. The sum total of all of these easily ionizable molecules would then have to be such that their emissions are below JSC 30237 specifications. This compares favorably with recommendations from the Space Station Payload Contamination Compatibility Workshop which recommended lower column densities of most species.

In January 1987 the OSSA contamination compatibility workshop recommended several changes in JSC 30426, which included lowering total acceptable column densities of O_2, N_2, and H_2, as well as noble gases and other UV and non-IR active molecules. A further specification should be included which defines ionizable gases and the acceptable release rates for them. Furthermore, it is very important that we gain a detailed understanding of the chemistry and physics of reactions which occur between the ambient environment and the large shopping list of molecules which may be released during the non-operational periods to insure that experiments and the Space Station hardware are not subjected to effects described earlier.

Non-Quiescent Environment

JSC 30426 states that the Space Station be capable of supporting quiescent operation periods of up to 14 days. This period of minimum perturbation is essential for many science investigations and any disturbances during this period, however minor, must be noted. It is not clear that the requirement to record such disturbances is fully satisfied. Section 5.0 simply states that "...monitoring of the environment to a limited extent will be required." Since the IOC phase Space Station will not be gravity gradient stable, some fine tuning of attitude will be required. Whether it is accomplished with jets only or some combination of jets and gyros is unclear. It is clear, however, that during the long "quiescent" periods there will undoubtedly be some disturbances whether they be occasional jet firings, experiment vents, purges, or relief valve operations, EVA crew activity, etc. A clear requirement to monitor specific critical aspects of the environment must be in place. Space Station elements must have a way of "notifying the system" of an impending disturbance. Some monitoring can and should be real time and some may only be required after the fact. Whether PIMS or some other monitoring package is responsible is yet to be determined but the requirement must be a system responsibility with data accessable to all.

Non-quiescent periods, such as Shuttle docking, will provide significant disturbances. It is the concensus of a number of independent observations that the Shuttle orbiter carries with it a large amount of contaminant material, particularly water. Column densities near the orbiter of 10^{12} to

10^{13} should be expected. There is some disagreement over the decay time of the associated cloud. IECM observations (STS-2, STS-3, STS-4) indicated an initial decay time of ~10 hours. However, Narcisi et al. (1983) has observed wide variations in the water density cloud with some overall decrease in H_2O density with time, but a much stronger correlation between density and surface temperature. Raitt (private communication, 1987) reports that an ion signature, characteristic of H_2O^+ in his retarding potential analyzer, practically disappeared by the end of mission 51F. (51F spent a lot of time in a hot attitude due to a several day long solar observation cycle.)

The conclusion that may be reached from all of this is that the amount of contamination that will be carried into the space station environment by the orbiter may be reduced by simply waiting some minimum period of time ($\gtrsim 24$ hours) in a relatively hot attitude behind the station, then going to a cool attitude for several hours before beginning the approach and docking. Clearly it will not be possible to operate some experiments while the orbiter is in rendezvous phase, both because of the outgassed cloud and thruster plume impingement. Docking procedures which minimize plume impingement and thruster activity will be preferred. Operation of experiments while the orbiter is present may be possible and is dependent on the type of experiment.

Other disturbances to the environment, such as EVA activity, should be scheduled as much as is practical for the non-quiescent periods since gaseous products associated with the EVA suit can provide significant disturbances.

Summary

The developing requirements for Space Station must be responsive to the needs of the user and in line with the reality of Space Station logistics. They must also be internally consistent, be carried out to as full an extent as possible, and be "living documents" which can incorporate new knowledge as it becomes available. The PWWG (Particle and Waves Working Group) has been responsive to the user's needs in writing requirements and assuring that the proper tools are in place to implement them. The definition and control of the particle, plasma, and wave environment has incorporated specific needs from a wide range of potential users. The Contamination Working Group has likewise been responsive and JSC 30426 reflects the panel's concern for the cleanliness of the Space Station environment for the user, the Station safety and longevity, and for the preservation of the delicate natural chemical balance of the ionosphere. It is not clear whether some oversight group such as the CWG will be responsible for continual evaluation and enforcement of the requirements. Some mechanism will be required to do this.

Only minor modifications to the documents may be required, but the importance of these modifications cannot be over emphasized. Let us first deal with recommendations to changes in JSC 30426:

(1) Incorporate specific requirements relating to easily ionizable molecules which contribute to the plasma environment. This should be stated in $g \cdot s^{-1}$ emission instead of column density; e.g. total water emission should be less than ~1 mg s^{-1} for adequate margin. Other common gases which contribute to this environment are N_2, CO_2, and H_2, e.g.:

$$N_2 + O^+ \rightarrow N_2^+ + O$$

$$N_2 + O^+ \rightarrow NO^+ + N$$
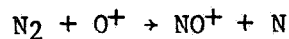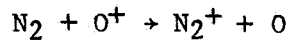
(2) Analysis of proposed vented products during non-operational periods must be performed to determine if the proposed contaminants are acceptable.

(3) More specific requirements for monitoring the environment should be in place. These should include real time or "warn" flags for certain releases which must be accounted for in data analysis or known about ahead of time.

JSC 30252, the Plasma Effects Control Process Requirements Document, must be consistent with the expected contamination levels and reflect the difference between operational and non-operational periods. Further recommendations in regards to operational considerations are the following:

(1) The orbiter should be allowed to outgas for $\gtrsim 24$ hours before docking with the Station (the orbiter should be behind the Station).

(2) Procedures minimizing thruster activity and plume impingement should be implemented for docking activity.

(3) Any plan which includes continuous thrusting for reboost should be eliminated for environmental considerations.

(4) Brief gaseous releases, either by Station hardware or other equipment, must be minimized, documented, and made available in a common data base.

(5) EVA activity should be confined to non-quiescent periods whenever possible.

(6) It may be appropriate to include a section on operational guidelines in the JSC 30426 document.

Last of all, several recommendations regarding uncertainties about the physical processes involved are appropriate:

(1) The cross sections for charge exchange reactions of a broad range of molecules are not well known for O^+ at 5 eV.

(2) The susceptability of certain molecules to CIV at Space Station altitudes is unknown. Laboratory and Shuttle experiments are appropriate.

(3) The precise cause of "Shuttle glow" must be determined.

(4) Models which predict line-of-sight emissions and absorption must take into account possible ionized species that are present. In order to do this, accurate models of cross sections for reactions are required.

(5) The mechanism for production of broadband instabilities must be better understood so scaling laws can be used with more assurance.

All of the above physical considerations may also be applied to co-orbiting platforms. The environmental constraints may be similar or tighter depending on experiment complements.

References

Banks, P. M., P. R. Williamson, and W. J. Raitt, Space Shuttle glow observations, Geophys. Res. Lett., 10, 118, 1983.

Bosley, J. and G. Curran, OSSA Space Station Waste Inventory, NASA/Ames Research Center, SS Projects Office, November 1986.

Grebowsky, J. M., H. A. Taylor, Jr., M. U. Pharo, III, and N. Reese, Thermal ion perturbations observed in the vicinity of the Space Shuttle, Planet. Space Sci., in press, 1987.

Hastings, D. E. and J. Wang, Induced emission of radiation from a large Space Station-like structure in the ionosphere, J. Spacecraft & Roc, submitted, 1987.

Hastings, D. E., N. A. Gatsonis, and T. Mogstad, A simple model for the initial phase of a water plasma cloud about a large structure in space, J. Geophys. Res., in press, 1987a.

Hastings, D. E., A. Barnett, and S. Olbert, Radiation from large space structures in low earth orbit with induced AC currents, J. Spacecraft & Roc, submitted, 1987b.

Hunton, D. E. and J. M. Calo, Low energy ions in the Shuttle environment: Evidence for strong ambient-contaminant interactions, Planet. Space Sci., 33, 8, 1985.

Koch, D. G., et al., Infrared observation of contamination from Shuttle flight 51F, Adv. Space Res., in press, 1987.

McMahan, W., R. Salter, R. Hills, and D. Delorey, Measured electron contribution to Shuttle plasma enviornment, AIAA-83-2598, AIAA Shuttle Environment and Operations Meeting, October 31-November 3, 1983.

Miller, E. R. (ed.), STS-2, -3, -4 Induced Environment Contamination Monitor (IECM) Summary Report, NASA TM-82524, 1983.

Narcisi, R. S., R. E. Trzcinski, G. Federico, L. Wlodyka, and D. Delorey, The gaseous and plasma environment around the Space Shuttle, paper #83-2659 AIAA Conference on Shuttle Environment and Operations, Washington, D.C., 1983.

Narcisi, R. S., Quantitative determination of the outgassing water vapor concentrations surrounding space vehicles from ion mass spectrometer measurements, Adv. Space Res., 2, 10, 1983.

Papadopoulos, K., On the Shuttle glow (the plasma alternative), Radio Science, 19, 2, 1984.

Paterson, W. R., Ion plasmas in the vicinity of the Orbiter: Observations and modeling, M.S. Thesis, University of Iowa, July 1987.

Pickett, J. S., G. B. Murphy, W. S. Kurth, and C. K. Goertz, Effects of chemical releases by the STS-3 orbiter on the ionosphere, J. Geophys. Res., 90, 3487-3497, 1985.

Reasoner, D. L., S. D. Shawhan, and G. B. Murphy, Plasma Diagnostics Package measurements of ionospheric ions and Shuttle-induced perturbations, J. Geophys. Res., 91, 13,463-13,471 1986.

Shawhan, S. D., G. B. Murphy, and D. L. Fortna, Measurements of electromagnetic interference on OV102 Columbia using the Plasma Diagnostic Package, J. Spacecraft & Roc, 21, 4, 1984a.

Shawhan, S. D., G. B. Murphy, and J. S. Pickett, Plasma Diagnostics Package initial assessment of the Shuttle orbiter plasma environment, J. Spacecraft & Roc, 21, 387, 1984b.

Siskind, D. E., W. J. Raitt, P. M. Banks, and P. R. Williamson, Interactions between the orbiting Space Shuttle and the ionosphere, Planet. Space Sci., 32, 7, 1984.

Space Station Payload Contamination Compatibility Workshop: Final Report, NASA, OSSA Washington, D.C., June 1987.

Torr, M. R., Optical emissions induced by spacecraft-atmosphere interactions, Geophys. Res. Lett., 10, 114, 1983.

Torr, M. R. and D. G. Torr, A preliminary spectroscopic assessment of the Spacelab 1/Shuttle optical environment, J. Geophys. Res., 90, 1683, 1985.

Witteborn, F., L. J. Caroff, D. M. Rank, and G. Ashley, Nighttime spectroscopic and photometric observations of Spacelab-2 and other satellites, Geophys. Res. Lett., submitted, 1987.

Wulf, E. and U. Von Zahn, The Shuttle Environment: Effects of thruster firings on gas density and composition in the payload bay, J. Geophys. Res., 91, 3270-3278, 1986.

SPACE STATION INDUCED ELECTROMAGNETIC EFFECTS

N. Singh

Department of Electrical and Computer Engineering
University of Alabama in Huntsville
Huntsville, AL 35899

Abstract. We have identified several mechanisms which can cause electric (E) and magnetic (B) field contaminations of the Space Station environment. The level of E and B fields generated by some of them such as the motion of the vehicle across the ambient magnetic field B_0 and the 20–kHz leakage currents and charges can be controlled by proper design considerations. On the other hand, there are some mechanisms which are inherent to the interaction of large vehicles with the plasma and probably their contributions to E and B fields cannot be controlled; these include plasma waves in the wake and ram directions and the effects of the volume current generated by the ionization of the neutrals. The interaction of high–voltage, solar cell arrays with plasma is yet another rich source of E and B fields and it is probably uncontrollable. Wherever possible, quantitative estimates of E and B are given. A set of recommendations is included for further study in areas where we seriously lack an indepth knowledge.

1. Introduction

Space Station is likely to affect the electromagnetic environment in several ways, some of which are discussed here. A summary of various possible causes of generating electromagnetic fields in the immediate neighborhood of the Space Station is as follows.

(1)   Radiation of EM waves by the currents induced in the structure by $V_s \times B_0 \cdot L$, where V_s is the Space Station velocity, B_0 is the geomagnetic field, and L is an appropriate dimension of the spacecraft.

(2)   Currents and charges induced on the structure due to the 20 kHz power line leakage.

(3)   Leakage of the 20–kHz power to the metallic interconnects in the solar cell arrays.

(4)   Wake as a source of plasma waves; both the strong density gradients and the nonthermal charge particle velocity distributions are likely to induce enhanced levels of electric and magnetic fields.

(5)   Interaction of the contaminant cloud with the ambient plasma in the ram direction.

(6)   Ionization of the contaminant neutrals (such as H_2O) produces a volume current (pick–up current) which can modify the ambient magnetic field and also can cause plasma instabilities.

(7)   Solar cell arrays as a source of EM noise.

In the following discussion we describe our present state of the understanding of the above mechanisms for generating EM effects. Wherever it is possible, we attempt to provide quantitative estimates for the electric and magnetic fields generated by the mechanisms. At the very outset we emphasize that the estimates are not sacrosanct as they are based on physical arguments and not on rigorous mathematical treatments of the individual problems. The estimates on the electric and magnetic fields are compared with the available specifications for the Space Station.

We note that the EM fields generated by the mechanisms (1), (2), and (3) can be controlled to some extent by proper design considerations for the Space Station structure, power distribution system, and ac to dc conversion. On the other hand, the EM fields generated by mechanisms (4) to (6) are inherent to the plasma environment of the Space Station. Since very little is known about the noise generation by high—voltage, solar cell arrays, it is immature to comment about its controlability.

2. Radiation of EM Waves by Currents Induced in the Structure by the Motional EMF (Figure 1).

The motional EMF in a moving conductor at the altitudes of the Space Station can be as large as 0.3 V m^{-1}. Assuming a length of about 100 m (as that of the keel), an estimate of the maximum possible EMF is about 30 volts. The induced EMF can drive a current through the structure, but the current drawn is critically controlled by the ambient plasma and its contact with the structure. These are difficult unsolved problems. However, the current collection at the positive end involves the collection of electrons, while at the negative end the collection of ions. Since the ion thermal current density in the ambient plasma is considerably smaller than the electron current density, the ions are likely to dictate the current in the structure. If the ion current collecting area at the negative end is S_i, the current flow through the structure is approximated by

$$I = J_i S_i \,, \quad N_o e \, V_{ti} < J_i < N_o e \, V_s \tag{1}$$
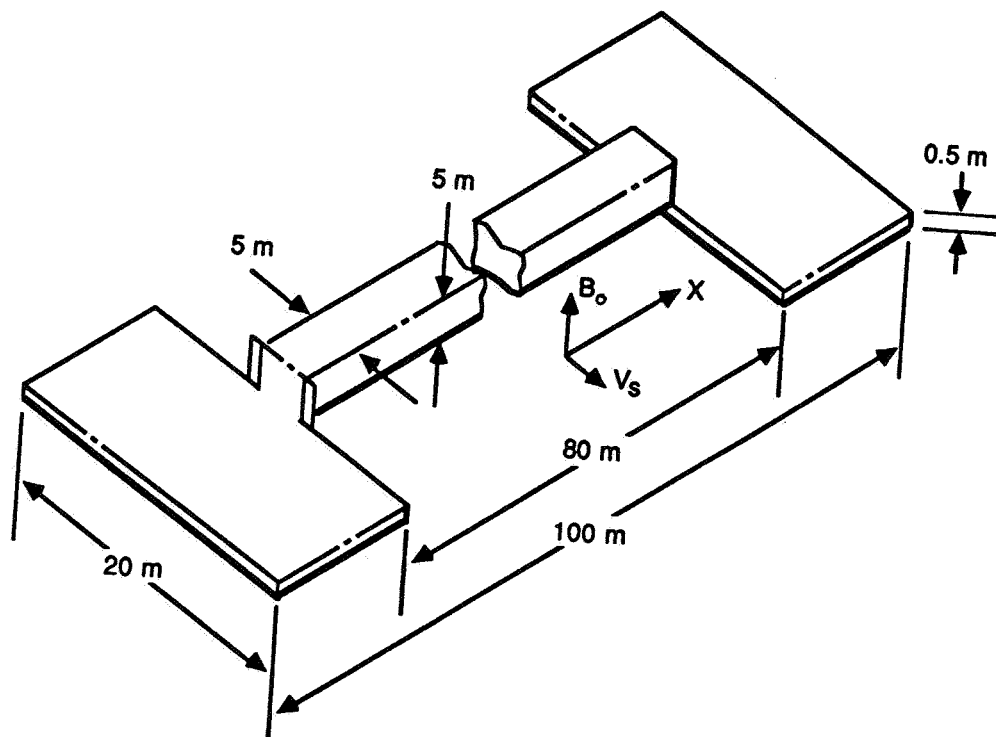
Fig. 1.   Schematic diagram showing motion of a space station like structure across the geomagnetic field B_o.

32

where V_{ti} is the ion thermal velocity, N_0 is the ambient plasma density, and e is the magnitude of the electronic charge. The upper limit on the ion current density J_i is determined by the ram current while the lower limit by the ion thermal motion. Thus, the maximum possible power available for radiation is given by

$$P = V_s BL J_i S_i \qquad (2)$$

The ion current density with the ambient plasma density $N_0 = 10^5$ cm^{-3} and ion temperature of 0.3 eV is found to be in the range 10^{-4} A m^{-2} > J_i > 3 × 10^{-5} A m^{-2}. Thus, the radiated power is found to be

$$9 \times 10^{-4} S_i < P < 3.3 \times 10^{-3} S_i \text{ watts} \qquad (3)$$

Assuming S_i to be about 500 m^2, the radiated power lies in the range 0.45 watts < P < 1.65 watts. This estimate of power, based on intuitive arguments, is approximately the same as obtained by more rigorous calculations (Hastings et al., 1987; Chlouber, 1987).

Now let us consider the frequency range over which the power will be distributed. The radiation occurs at frequencies given by

$$f = \underline{k} \cdot V_s / 2\pi \text{ Hz} \qquad (4)$$

where $\underline{k}$ is the wave vector of the radiation. Since maximum possible value of k in a plasma is roughly λ_d^{-1}, the highest radiated frequency is given by

$$f \simeq \frac{1}{2\pi} \frac{V_s}{\lambda_d} \simeq f_{pe} \frac{V_s}{V_{te}} = f_{pi} \frac{V_s}{V_{ti}} \qquad (5)$$

where f_{pi} and f_{pe} are the ion and electron plasma frequencies and V_{ti} and V_{te} are the ion and electron thermal velocities.

At the altitudes of Space Station $f_{pi} \simeq 23.4$ kHz and $f_{\ell h} \simeq 5.4$ kHz. Thus, a variety of wave modes are likely to be excited; these include Alfvén waves, electromagnetic ion–cyclotron mode, ion–acoustic mode, ion Bernstein waves, and lower hybrid waves.

Whether a given wave mode is radiated or not also depends on the wavelength spectrum of the current source in the structure. If some wavelengths are not in the source, they are not radiated even if the plasma allows such a radiation.

The component of $\underline{k}$ parallel to the velocity of the structure is relevant here. Thus, if the dimension of the structure in the direction of the motion is L_v, the typical radiated wave number spectrum is given by

$$k_v < L_v^{-1} \qquad (6)$$

and the radiated frequency

$$f_o < \frac{1}{2\pi} V_s / L_v \qquad (7)$$

Since $V_s \simeq 7.3$ km s^{-1} and $L_v \approx 5$ m, $f_o < 230$ Hz. Thus, the Space Station structure is likely to curtail the radiation in frequencies higher than about 230 Hz. This frequency is lower than H$^+$ cyclotron frequency, but several times larger than 0$^+$ and $(H_2 0)^+$ cyclotron frequencies. Thus, the possible wave modes are the Alfvén waves, electromagnetic

ion—cyclotron waves, ion—acoustic waves, and 0^+ Bernstein modes. The latter two waves are warm plasma effects.

The warm plasma effects on the radiation from structures in space have not been investigated at all. Longitudinal plasma waves may have some important ramifications as they heat the plasma near the source. Heating involves Landau damping and/or ion—cyclotron damping.

Since the plasma waves are likely to be damped near the structure, the radiated power away from it will be primarily in the form of Alfvén waves. The electric field strength of the Alfvén waves is approximately

$$E \simeq (\mu_0 V_a \frac{P_a}{S})^{1/2} \quad V \ m^{-1} \tag{8}$$

where V_a is the Alfvén velocity, S is cross section of the Space Station perpendicular to the ambient magnetic field, $\mu_0 = 4\pi \times 10^{-7}$ H m^{-1} and P_a is the power in Alfvén waves. Assuming, $P_a = 1$ watt and $S - 10^3$ m^2, $V_A = 200$ km s^{-1}

$$E \simeq 16 \ mV \ m^{-1} \ and \ B = 80 \ nT \tag{9}$$

The electric field strength given above is roughly comparable to the requirement given in Figure 3.1—3 of JSC 30420. But the corresponding B field specifications are much lower than the estimate given above.

Recommendation: Very close to the structure, the electrostatic waves arising because of the warm plasma effects may play an important role in determining the electric field fluctuation level and also the extent of plasma heating which may have some ramifications for the chemical reactions near the Space Station surface. Thus, it is important to develop a quantitative understanding of these effects. A more unified theory including warm plasma effects and the calculations of the current patterns on complex structures in space is needed to fully understand the problem of radiation because of the motion of the Space Station

3. 20 kHz Power Line Radiation

It is decided that the power system on Space Station will operate at 20 kHz. This frequency falls in a frequency band, which is very important for natural plasmas; it is the band in which whistler and VLF waves propagate in the ionosphere. Assuming a plasma density $N_0 = 10^5$ cm^{-3} and magnetic field $B_0 = 0.31$ Gauss near the Space Station, the various characteristic frequencies are

$$f_{pe} = 2.8 \ MHz, \quad f_{pi} = 16.3 \ kHz, \quad f_{ce} = 0.87 \ MHz,$$
$$f_{ci} = 29.6 \ Hz, \quad f_{\ell h} = 3.2 \ kHz$$

Thus, the 20 kHz falls in the range $f_{\ell h} < f < f_{ce}$

The sources in this frequency band radiate EM and plasma waves within a cone aligned with the magnetic field with the cone apex at the source (Singh and Gould, 1971). The half cone angle for $f \ll f_{ce}$ is given by (Figure 2)
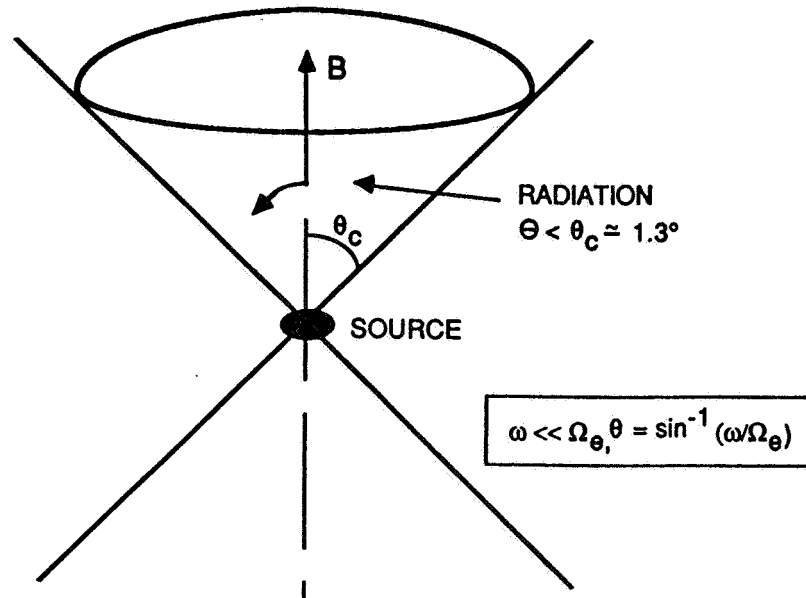
$$\theta_c = \sin^{-1}(f/f_{ce}) \simeq 1.3^\circ$$

Fig. 2.   Radiation cone of 20–kHz power from Space Station power systems. In the figure cone angle is exagerated; the half–cone angle is only about 1.3° implying highly magnetic field–aligned radiation.

Thus, the radiation of 20 kHz will be primarily focussed along the B field.

The estimation of the power and radiated fields requires some knowledge of the magnitude and distribution of the leakage currents and charges on the Space Station structure. Unfortunately, this exercise has not been carried out and without such an exercise, I feel that an estimation analysis is primarily academic.

Recommendations: A complete analysis of the power distribution system is needed to predict how much and where on the structure it is likely to have leakage currents and charges. Cable connectors, where fringing fields are likely to occur, can be a source of radiation. Surface currents at 20 kHz are additional sources of radiation.

Determination of the leakage of ac (20 kHz) currents and charges to the solar cell array interconnects after dc to ac conversion is worthwhile because the numerous tiny interconnects can radiate an appreciable amount of power in plasma waves

4. Wake as a Source of Plasma Waves

Wake can be a rich source of plasma waves because there are a number of non–equilibrium features present inside the wake. Some of these features are (Figure 3):

(1)   Sharp density gradients, specially in the near wake region.
(2)   Production of non–Maxwellian (non–thermal) distributions of the electrons and ions by means of plasma expansion into the wake.
(3)   Collision of the counterstreaming plasma streams in the far wake region.

We briefly address these issues one by one.

35

ELECTROSTATIC SHOCKS
$(T_e > 3T_i)$
$E \simeq 40$ V/m

V_s

B

NEAR WAKE
ELECTRON BEAMS
DRIFT WAVES
(DUE TO DENSITY AND
TEMPERATURE GRADIENTS)

MID WAKE

FAR WAKE

RAREFACTION
ENVELOPE
(NON-THERMAL PLASMA)

ENHANCED LEVELS OF
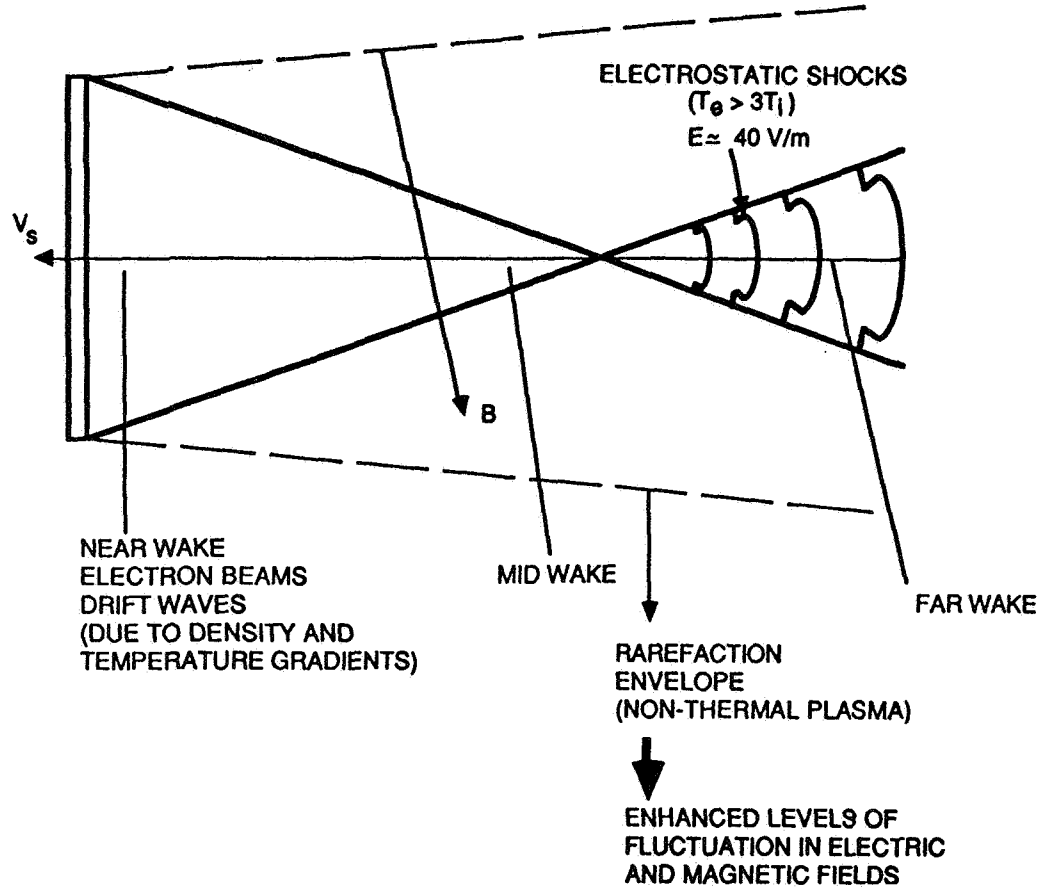FLUCTUATION IN ELECTRIC
AND MAGNETIC FIELDS

Fig. 3.   Schematic diagram showing wake of a large body in a plasma. Different types of plasma processes contributing to the enhancements of E fields are indicated.

4.1 Sharp Density Gradients

Density gradients in the wake region are likely to drive a number of drift wave modes. Since the plasma in the vicinity of the Space Station is likely to have approximately equal electron and ion temperatures, possible drift modes are the ion–cyclotron ion density drift (ICID) mode and the lower hybrid drift (LHD) mode; these modes are driven by ion drifts given by

$$V_i \simeq \frac{a_i^2}{\Omega_i} \; \frac{1}{n} \; \frac{\partial n}{\partial x} \simeq a_i^2/(L_\perp \Omega_i) \approx a_i \, \rho_i/L_\perp$$

where a_i is the ion thermal velocity, L is the scalelength of the density gradients perpendicular to B, and ρ_i is the ion Larmor radius. When $L < 2\rho_i$ or $(V_i > 0.5 \; a_i)$, lower hybrid drift waves with following parameters are likely to occur:

Frequency: $\omega \simeq kV_e \simeq \frac{a_e}{L_\perp} = \frac{a_e}{\Omega_e} \frac{\Omega_e}{L_\perp} = \frac{\rho_e}{L_\perp} \Omega_e > 2\Omega_i$

36

Wavelength: $\lambda_\perp \simeq \rho_e$

Saturation level (Gary, 1980):

$$\frac{\varepsilon}{nT} \simeq 0.1 \, (\Omega_i/\omega_{\rho i})^2 \, (\rho_i/L_\perp)^2 \ , \quad \varepsilon \simeq \frac{1}{2} \, \epsilon_0 |E|^2$$

When the density gradients have scalelengths in the range $2 \, \rho_i < L < 10 \, \rho_i$, ion cyclotron drift modes are driven with parameters as follows:

Frequency: $\omega \simeq \Omega_i$

Wavelength: $\lambda_\perp \simeq \rho_e$

The saturation level for these ICID waves are found to be similar to that for the LHD waves.

The rms electric fields for these waves are estimated to be

$$E_{rms} \simeq 4(n/10^5)^{1/2} \, (T/0.3)^{1/2} \, (\rho_i/L_\perp)^2 \ \ \text{mV m}^{-1}$$

where n is in units of cm^{-3} and T in eV.

For LHD waves $L < 2\rho_i$, $E_{rms} > 1$ mV m^{-1} is likely to occur depending on the sharpness of the density gradient. On the other hand, for the ICID waves $E_{rms} < 1$ mV m^{-1}.

The above estimates show that it is likely that density gradients in the near wake create electrostatic waves with amplitudes of the order of 1 mV m^{-1} or greater in the range of ion–cyclotron frequencies. This estimate appears to be compatible with the broadband electric field specification in JSC 30420.

4.2. Non–Thermal Plasma in the Wake

The plasmas in the wake region are expected to have non–Maxwellian velocity distribution functions. This is particularly true for the velocity components along the B field threading the plasma void in the wake. This arises because of plasma expansion; the electrons in the near wake may have counterstreaming electron beams (Singh et al., 1987) and the ions appear as ion beams in the near and mid wake regions while in the far wake they also appear as counterstreaming ion beams (Singh et al., 1986).

In the near wake regions the beam electrons are likely to excite beam–plasma modes. Some preliminary calculations for the wake of small satellites show this to be a distinct possibility. However, for large structures such as the Space Station, it remains to be investigated.

When $T_e \simeq T_i$, the ion beams in the wake region are not likely to excite instabilities. However their non–thermal distributions are likely to enhance the fluctuation level of the electric field. A systematic investigation on the enhanced electric fluctuation level is required to complete the determination of EMI effects in the wake region.

Recommendation: Contributions to the fluctuation level of electric field by non–thermal features of the electron and ion velocity distributions need attention. It is recommended that the spectrum of the fluctuation be estimated using the theoretical formulations available (Akhiezer et al., 1975).

4.3. Electrostatic Shock Formation in the Far Wake (Figure 3)

If $T_e > 3$ T_i, the ion beams are likely to excite ion–acoustic waves propagating primarily long the B field. In the far wake region the colliding ion beams are capable of creating an electrostatic shock pair; the shocks form by ion–ion instability and they move away from the wake axis (Singh et al., 1986). The electric fields in the shock fronts are typically

$$E \simeq \frac{2 \; T_e/e}{10 \; \lambda_d}$$

Assuming $T_e/e \simeq$ 1V, $\lambda_d \approx$ 0.5 cm, dc electric fields of the order of 40 V m⁻¹ are likely to be found in the far wake region. This is a large electric field from the space plasma point of view.

5. Interaction of the Contaminant Cloud with the Ambient Plasma in the Ram Direction (Figure 4)

It has been suggested that the large space structures moving across the magnetic fields with their contaminant clouds simulate the same condition as a comet. Furthermore, the motion of the contaminant cloud simulates the same situation as in Alfvén critical ionization velocity (CIV) experiments (Newell, 1985). Laboratory and space experiments along with theories show that the interaction of a neutral cloud moving across a magnetic field in a background plasma creates a rich variety of electromagnetic effects, some of which are as follows.

5.1 Generation of dc Electric Fields Perpendicular to the Ambient Magnetic Field Near the Cloud Front (Figure 4)

The electric field arises because the electron and ion pairs, formed by some ionization processes, respond differently to the ambient magnetic field; the electrons, being highly magnetized, are guided along the B field while ions continue their journey across B, at time scales of Ω_i^{-1}. This charge separation supports an electric field approximately given by

$$E_\perp \simeq \frac{1}{2} \; m_c V_s^2 / e \rho_i \approx 5 \; V/10 \; m.$$
$$\approx 0.5 \; V \; m^{-1}$$

where m_c is the mass of the contaminant neutrals. Such electric fields may be the cause of creating oblique ion beams in the ram direction of the Space Shuttle (Stone et al., 1983).

The electric potential drop, $\Delta\phi$, across magnetic field is expected to be about the kinetic energy of the contaminant neutrals. If the neutrals are predominantly H_2O, $\Delta \phi \simeq$ 6 V.

5.2 Wave Generation

The ions produced by the ionization are likely to drive lower hybrid waves, which can heat the electron population. It is likely that conditions for the critical ionization may not occur, but the processes associated with it are likely to be present in the ram direction of the Space Station (Newell, 1985).

Recommendation: It is recommended that the electrostatic and electromagnetic noise level in the ram direction because of neutral cloud–plasma interaction be investigated, and quantitative estimates of E and B fields be obtained.
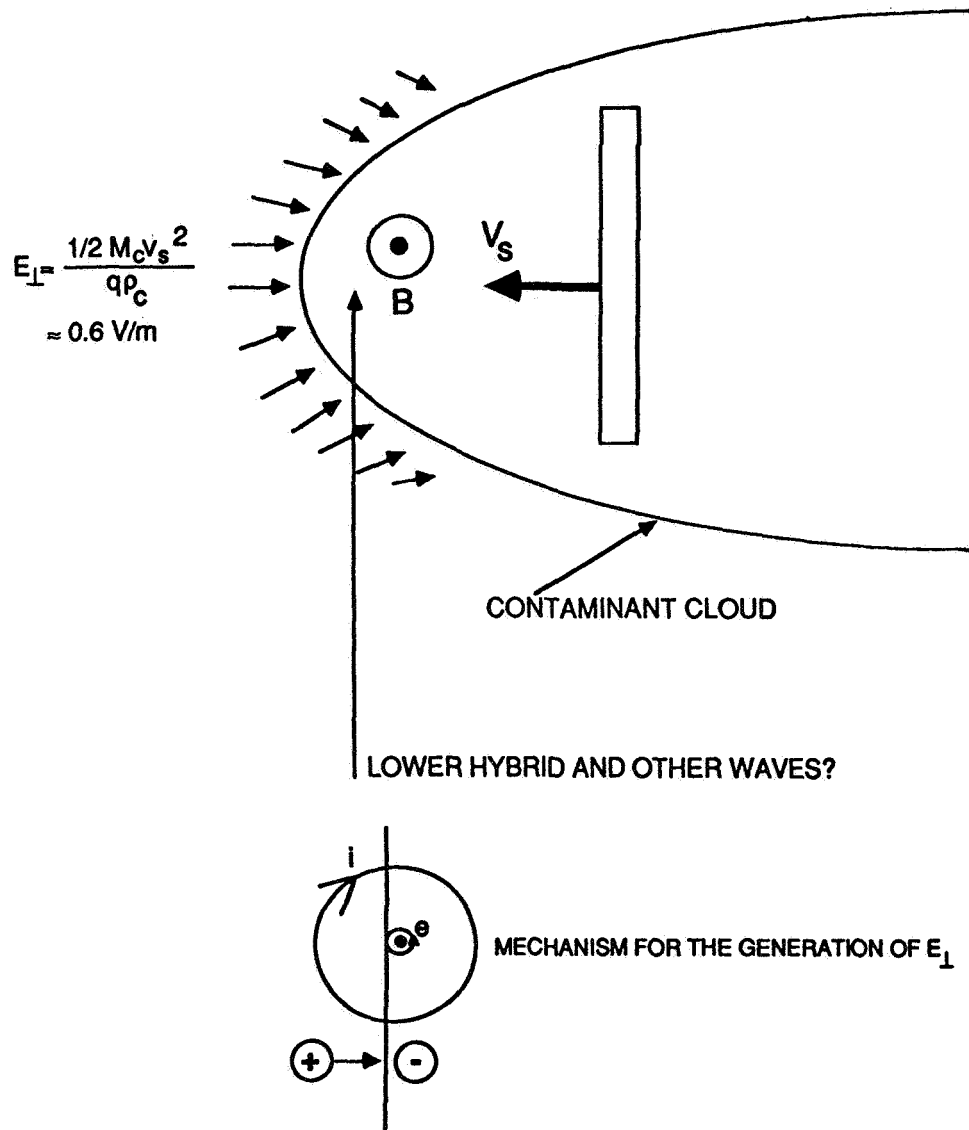
$$E_{\perp} = \frac{1/2\ M_c V_s^2}{q \rho_c}$$

$$\approx 0.6\ V/m$$

CONTAMINANT CLOUD

LOWER HYBRID AND OTHER WAVES?

MECHANISM FOR THE GENERATION OF $E_{\perp}$

Fig. 4.   Interaction of a contaminant cloud around a large vehicle in space; the processes occurring in the ram direction are highlighted.

6. EM Effects Associated with the Ionization of the Contaminants

A newly created ion of mass m_c moving with the vehicle sees an electric field $E = V_s \times B$ and as it gains a velocity in the direction of E, it is deflected by the $\underline{V} \times \underline{B}$ force. If the vehicle velocity is in x direction and B is along z, the equations of motion for a charge particle is given by

$$x = (V_s/\Omega_\alpha)\ (\Omega_\alpha t - \sin \Omega_\alpha t)$$
$$y = (V_s/\Omega_\alpha)\ (1 - \cos \Omega_\alpha t)$$

39

$$\dot{x} = V_s \left(1 - \cos \Omega_\alpha t\right)$$

$$\dot{y} = V_s \sin \Omega_\alpha t$$

where
$$\Omega_\alpha = q_\alpha B / m_\alpha$$

Thus, the position and velocity of a charge particle averaged over one cyclotron period are given by

$$<x> = V_s t \quad , \quad <y> = \frac{m_\alpha V_s}{qB}$$

$$<v_x> = <\dot{x}> = V_s \quad , \quad <v_y> = <\dot{y}> = 0$$

Thus, as the charge particles are produced they are moved along $\pm y$ direction depending on the sign of the charge. This constitutes a (pick—up ion) current in the plasma. If the ionization rate is n, number of ions produced per second, the current is given by

$$J_y = \frac{V_s}{B} \dot{n} \left(m_c + m_e\right) \approx \frac{V_s}{B} m_c$$

This current perturbs the ambient B field;

$$\frac{\partial B}{\partial X} \simeq -\mu_0 \frac{V_s}{B} m_c \dot{n}$$

The magnitude of this perturbation depends on $\dot{n}$, which depends on the contaminants densities and the various types of ionization processes. An estimate of $\dot{n}$ is needed to quantify the effects of the pick—up ion current.

Recommendation: In order to establish the effect of pick—up ion current, the ionization rate of the contaminant ions needs to be determined.

7. Solar Cell Array as a Source of Electric and Magnetic Field Noises (Figure 5)

Depending on the location of the ground, the electric potentials on the solar cell interconnects may range from large positive potentials ($>> T/e$) to large negative ones. The interconnects (pin holes) with positive potentials collect electrons while those at negative potentials collect ions. The electron current collection in the presence of the geomagnetic field becomes a very difficult problem. However, it is certain that electrons and ions in the vicinity of the interconnects or pin holes will develop non—thermal features, which will be spatially structured.

There is no experimental or theoretical work to carry out educated estimates of the electric and magnetic fields in the vicinity of the solar—cell array.

Recommendation: The practical design consideration of a solar cell array and the determination of the electromagnetic noise level in its vicinity warrant serious investigations on interactions of the high—voltage solar cell array with the plasma. At negative voltages, arcing occurs in the close vicinity of arrays. The arcs are a rich source of electromagnetic radiation. Work is needed to estimate the level of such radiation and its frequency spectrum.
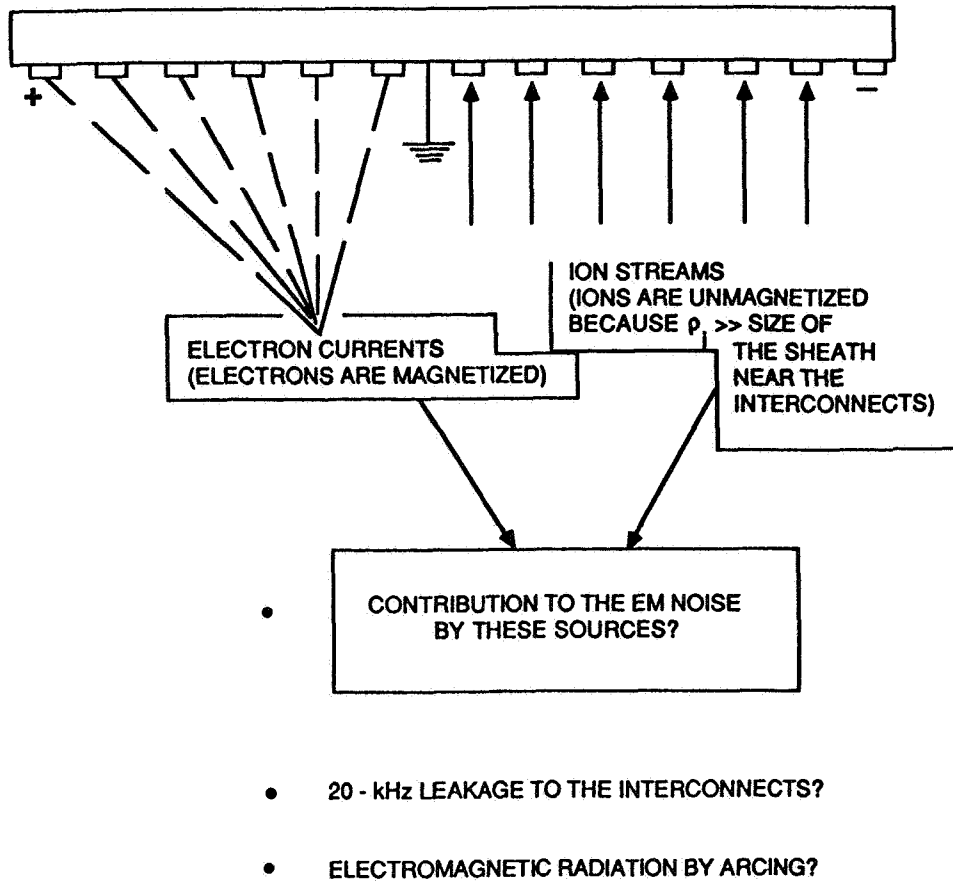
Fig. 5.   The ion and electron streams due to the voltages on the interconnects in a solar cell array are shown. Processes leading to the generation of electromagnetic fluctuations are indicated.

References

Akhiezer, A. I., I. A. Akhiezer, R. V. Polovin, A. G. Setenko and K. N. Stepanov, Plasma Electrodynamics, Vol. 2, Nonlinear Theory and Fluctuations, Pergamon, New York, 1975.

Chlouber, D., Space Station Induced Electrical Noise and Drag Interaction, McDonnell Douglas Astronautics Corp., Houston Div., TM No. 528–005–1, 1987.

Hastings, D. E., A. Barnett, and S. Albert, Radiation from large space structures in low–Earth orbit with induced ac currents, J. Geophy. Res., submitted, 1987.

Gary, P., Wave–particle transport from electrostatic instabilities, Phys. Fluids, 23, 1193, 1980.

Newell, P. T., Review of the critical ionization velocity effect in space, Rev. Geophys, 93, 1985.

Singh, N., and R. W. Gould, Radiation from a short electric dipole in a hot uniaxial plasma, Radio Sci., 6, 1151, 1971.

Singh, N., H. Thiemann, and R. W. Schunk, Studies on counterstreaming plasma expansion, Phys. Scripta, 33, 355, 1986.

Singh, N., U. Samir, K. H. Wright, and N. H. Stone, A Possible explanation of the electron temperature enhancement in the wake of a satellite, J. Geophys. Res., 92, 6100, 1987.

Stone, N. H., U. Samir, K. H. Wright, D. L. Reasoner, and S. D. Shawhan, Multiple ion streams in the near vicinity of the Space Shuttle, Geophys. Res. Lett., 10, 1215, 1983.

SPACE STATION CONTAMINATION STUDY: ASSESSMENT OF
CONTAMINANT SPECTRAL BRIGHTNESS

D. G. Torr

Center for Space Plasma and Aeronomic Research
Huntsville, Alabama 35899

1. Introduction

Recent models of the gas concentrations induced around
orbiting vehicles have predicted concentration enhancements up to
50 times ambient near ram surfaces at ˜200 km. The number
densities have yielded relatively large scale lengths, which
means that the column abundances are significantly larger that
anticipated ($˜10^{14}$ cm^{-2} at 200 km). The molecules and atoms
which make up the total abundance can either absorb, scatter, or
emit radiation at the operating or sensing wavelengths of
spectrometric, radiometric, and photometric instruments.
Conservative preliminary estimates of the collisional excitation
that could arise as a result of interactions between the
instreaming ambient atmosphere and the gases generated in the
environment of a low-Earth orbit (LEO) vehicle indicated that
these would be significantly higher than the natural zodical
background level + 10%, the criterion used in Space Station
Contamination Requirements Document JSC-30426.

Previous requirements of atomic and molecular column
densities specified in JSC-30426 appear to have been based
largely on calculations of absorption effects. In retrospect, it
is easily shown that emissive contamination is far more
significant than absorptive contamination for the same column
content.

Whereas the total column densities of 5×10^{13} cm^{-2}
specified in JSC-30426 provide adequate controls on absorption,
the same is not true for emissions. The results of this study
will demonstrate that emissive contamination is significantly
more severe than anticipated.

2. Background

The determination of the change to the natural brightness
created by contaminants around a spacecraft is not a simple task.
A host of excitation mechanisms exists and vary primarily with
the flux and composition of incident ambients, which, in turn,
depend on various geophysical parameters such as epoch of the
solar cycle, season, time of day, altitude, and geographic
location; that is, its position along the orbit. Superimposed on
the well-defined behavior patterns are more sporadic fluctuations
due to solar disturbances and magnetic activity, as well as
effects of orographic origin such as gravity waves.

The gases in the contamination environment are generated by

five main mechanisms:

(1)   Concentration enhancement of ambient gases which peaks in the ram direction

(2)   Outgassing

(3)   Leakage

(4)   Venting

(5)   Thruster firings

The effects of all five sources on contamination gases are calculated in the Science and Engineering Associates' (SEA) configuration contamination model. Table 1 lists a summary of the composition data obtained from SEA for this study.

In addition, the assessment of spectral brightness resulting from the ambient-contaminant interaction requires a knowledge of the details of cross sections and excitation mechanisms. The approach we adopted was to utilize the spectral brightness measurements made on Spacelab 1 and on the S3-4 spacecraft to identify source mechanisms, key cross sections and, hence, the abundance of contaminant species. These inferred abundances were then used to update the composition comprising the total column concentrations predicted by the SEA configuration contamination model for the Space Station and to scale the irradiances to four altitudes: 300, 350, 400, and 463 km. The contamination irradiances are compared with zodiacal natural background levels.

3. Modeling

The capability to model the spectral signatures due to the Space Station contaminant atomic and molecular species has been set in place. The model potentially provides the means for relatively accurate scaling of spectral features with altitude. However, in the current report, detailed scaling of specific features was not undertaken, because of the large demand on computer resources needed for such an effort. Instead, the full spectrum was computed at a single height (250 km for the vacuum ultraviolet, the near ultraviolet, and the visible; and 463 km for the infrared red) and scaled according to three factors given by $[N_2]^3$, $[N_2]^2[O]$, and $[N_2][O]^2$, which roughly cover the range of likely scaling factors. The curves labeled $[N_2][O]^2$ which are presented in Section 8 probably represent peak values for the computed brightnesses. The brightnesses derived are consistent with the column abundances calculated by the SEA model.

It was found that absorption effects were not significant for the species analyzed and thus results for absorption are not presented, and the JSC-30426 data provide adequate controls on

44

Table 1. Composition Data

km	Total Density Ambient	Total RAM Density	Total NCD Without Freestream	Total Flux
200	1.03E + 10	3.83E + 11	3.01E + 14	6.33E + 15
250	3.33E + 9	1.15E + 11	1.07E + 14	5.31E + 14
300	1.38E + 9	4.57E + 10	3.38E + 13	8.34E + 13
350	6.50E + 8	2.18E + 10	1.67E + 13	2.04E + 13
400	3.35E + 8	1.16E + 10	9.58E + 12	6.60E + 12
450	1.83E + 8	6.62E + 9	4.83E + 12	2.05E + 12
500	1.04E + 8	4.23E + 9	3.07E + 12	8.79E + 11

km	H_2O	Organic NCD
200	5.98E + 11	5.98E + 11
200	5.86E + 11	6.67E + 11
300	5.40E + 11	3.07E + 11
350	5.60E + 11	4.40E + 11
400	5.80E + 11	7.73E + 11
450	5.40E + 11	3.00E + 11
500	5.40E + 11	3.00E + 11

km	Ambient O	NCD O	Ambient N_2	NCD N_2
200	2.59E + 9	6.09E + 13	7.26E + 9	2.21E + 14
250	1.08E + 9	2.38E + 13	2.12E + 9	6.22E + 13
300	5.68E + 8	1.14E + 13	7.71E + 8	2.03E + 13
350	3.26E + 8	6.77E + 12	3.09E + 8	8.50E + 12
400	1.98E + 8	4.25E + 12	1.31E + 8	3.78E + 12
450	1.23E + 8	2.44E + 12	5.73E + 7	1.48E + 12
500	7.75E + 7	1.53E + 12	2.57E + 7	6.64E + 11

Units - Number Density: cm^{-3}
Number Column Density (NCD): cm^{-2}

absorption. Note, however, that these exceed the constraints estimated for emission.

Since it was found that the SEA results at 463 km did not show a significant dependence on the ram direction, only representative results are presented at this stage. The dependence on ram increases significantly with decreasing altitude. The calculations we present here are representative of worst case conditions, namely, the ram direction, maximum solar activity, and maximum likely magnetic disturbance. Future work could provide reasonably good estimates for a variety of conditions. The spectral results shown in Section 8 show the altitude at which the spectral irradiances equal the zodiacal background.

4. Database

Because of the limited available data prior to Shuttle missions of detailed spectral measurements of the natural emissions at Shuttle altitudes, it proved very difficult initially to identify what components of the spectral intensities observed on S3-4 and Spacelab 1 could be attributed to contaminant sources. The Spacelab 1 array of spectrometers – the Imaging Spectrometric Observatory (ISO) – covered the spectral range from the EUV (~50 nm) to the far visible/near infrared, namely ~800 nm. The first real progress in identifying a far-field vehicle signature was made by NRL personnel (Conway, et al., 1987) who demonstrated that nadir observations of the Lyman-Birge-Hopfield (LBH) bands of N_2 varied with altitude approximately as the cube of the concentration of N_2 – a non-natural signature. The same LBH spectral signature was observed on Spacelab 1 at 250 km at night in the nadir direction by the ISO (Torr, et al., 1985). The knowledge that this signature could be attributed to "vehicle glow" provided the information needed to identify a mechanism that could account for the LBH glow (Torr, et al., 1988). This undertaking led to predictions of similar effects for other molecular species provided by the SEA model. A series of successful identifications of spectral signatures of several molecules essentially led to a chain of predictions and confirmations of necessary accompanying emission features extending from the vacuum ultraviolet (VUV) to the near infrared (NIR), and predictions for the infrared (IR). With a working hypothesis in hand, which yielded results consistent with available measurements, irradiances could be calculated for Space Station using the mechanisms identified for Shuttle.

5. Vacuum Ultraviolet (VUV) Emissions

5.1 S3-4 LBH Glow

The fact that the LBH emissions were observed $90°$ to the ram direction suggests a gas-phase reaction, since the surfaces would

not be directly impacted. The Spacelab 1 spectral ratios
preclude electron impact excitation. In the gas-phase, the
incident ambients do not have sufficient energy to excite the LBH
emission from normal, ground-state N_2 molecules. This indicates
that the contaminant gases must have a significant population of
long-lived electronically excited species. In the case of N_2, an
obvious (if not the only) candidate is N_2 in the electronic A
state.

The ISO data were examined for emissions from this state
(the Vegard Kaplan - VK bands) and it was found that the column
abundances inferred for $N_2(A)$ comprised up to ~0.01% of the total
N_2 column concentration predicted by the SEA model. The
collision cross section needed to excite $N_2(A)$ to the $N_2(a)$ state
through collisions with ambient O and N_2 (which gives rise to the
LBH emission) was estimated to be ~3.8 x 10^{-16} cm^2 to fit the S3-
4 and Spacelab 1 data.

Consideration as to what surface chemistry could produce
$N_2(A)$ led to the conclusion that similar excited states should at
least be produced for O_2, NO, and CO, namely O_2 (a and b), NO(a),
and CO(a and a'). The presence of other diatomic and polyatomic
species is not precluded. The details of the surface chemistry
are complex, and the products of surface reactions depend on the
surfaces involved. Logically, there is no reason why collisional
excitation of $N_2(A)$ would only excite the LBH bands, since there
are several nearby upper states that should be excited. The same
rationale also applies to the other molecules in question.

The ISO vacuum ultraviolet data exhibit a large continuum
feature between ~140 and 180 nm. It was found that this
continuum could be explained by synthesis of a number of VUV
bands of N_2, NO, and CO, namely:

N_2:   LBH, VK, and Ogawa-Tanaka-Wilkinson-Mulliken bands

NO: δ and ϵ bands

CO: Fourth Positive and Hopfield-Birge bands

The vibrational distributions of the molecules could be
determined by spectral synthetic fitting of the data, and it
became evident that the desorbed long-lived electronically
excited precursors such as $N_2(A)$ were being produced in highly
vibrationally excited levels, which, in turn, determined the
vibrational distribution of the subsequent gas-phase
collisionally excited bands. Figure 1 shows the composite
synthesized spectrum for N_2, NO, and CO in the VUV at 250 km at
1.9 A wavelength resolution.

5.2   Scaling with Altitude

As mentioned in Section 3, detailed scaling of discrete
spectral features was not done for the present work.

SPACE STATION CONTAMINATION STUDY
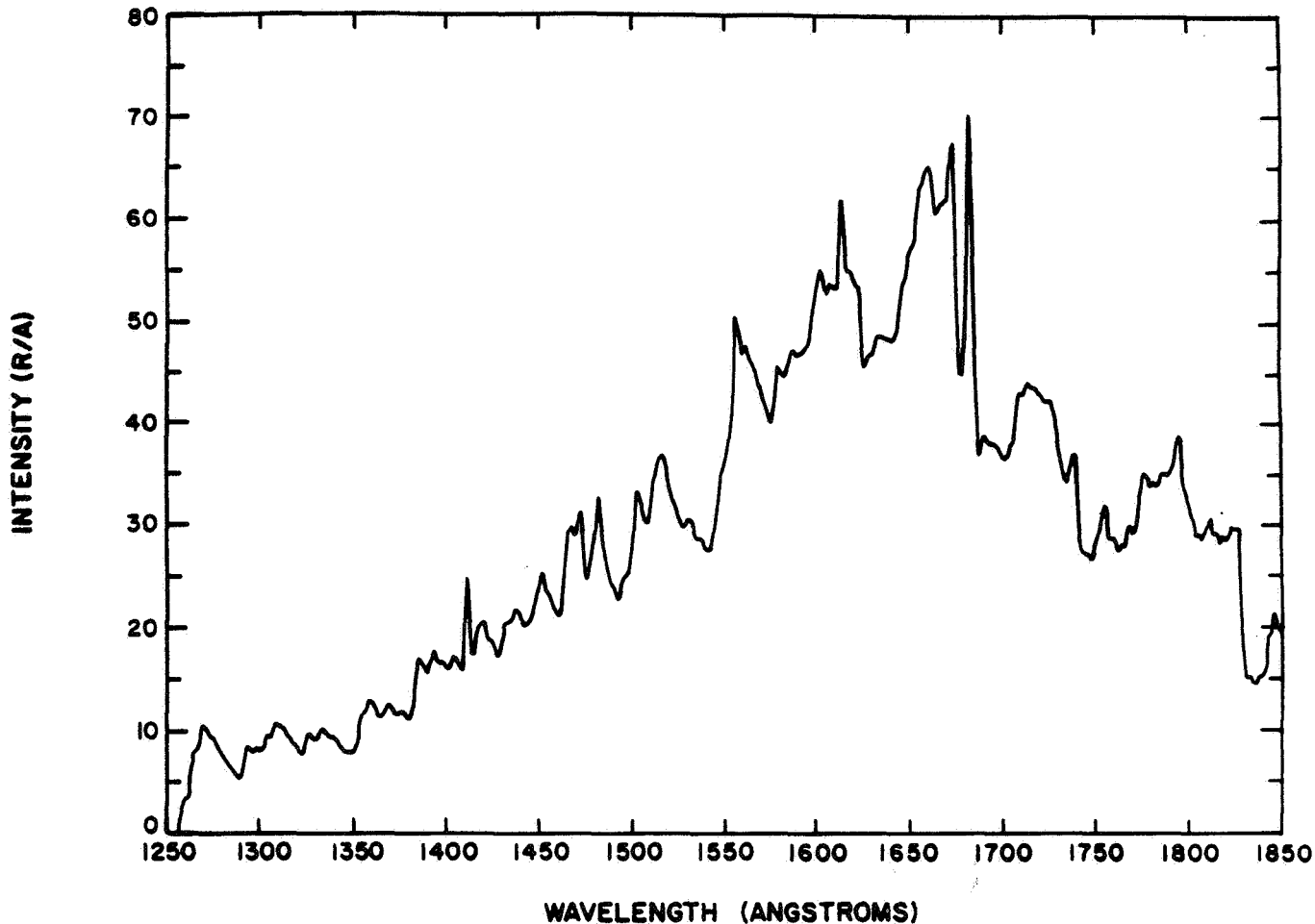
VACUUM ULTRAVIOLET AT 250 km

Fig. 1.   Synthesized vacuum ultraviolet spectrum for the
conditions of Spacelab 1:   Viewing direction - nadir (no ram data
available); Altitude - 250 km; Date - Nov./Dec. 1983 - nighttime;
Spectral resolution - 1.9A; Bands synthesized: N_2 - LBH, VK,
Ogawa-Tanaka-Wilkinson-Mulliken; NO - δ and ϵ; CO - Fourth
Positive, Hopfield-Birge.   Note: 1 R/A = 10^6 photons cm^{-2} s^{-1} A^{-1}.
The assumed steradiancy for the gas phase reactions is 4π.

Representative scaling has been done for the three factors $[N_2]^3$, $[N_2]^2[O]$, and $[N_2][O]^2$ for the overall spectrum to indicate possible or likely peak intensity levels. When the column abundance is dominated by Space Station sources, the scaling will be linear with respect to the ambient density.

6. Ultraviolet (UV) and Near Ultraviolet (NUV) Emissions

Given the information learned from the VUV on the column abundances of the various contaminant constituents, the bands expected for these molecules in the UV and NUV (~200-400 nm) were identified by synthetic spectral fitting of the ISO data, and then scaled to Space Station altitudes.

The ISO data exhibit very strong first negative bands of ionized molecular nitrogen with principal features at 391.4, 427.8, and 358.4 nm.

Although the study to date has not identified all the features observed in the ISO UV and NUV spectrum, several of the major systems were identified. These include:

CO^+: First Negative, Comet Tail

CO: Fourth Positive

N_2: Vegard Kaplan, Second Positive

O_2: Herzberg I, II, Chamberlain

NO appeared to be dominated by atmospheric emissions although a significant glow component could not be ruled out. In addition, a number of atomic lines could be matched by permitted O, N, O^+, and N^+ transitions. The forbidden transitions of O and N, namely, $O(^3P - {}^1D)$, $O(^3P - {}^1S)$, and $N(^4S - {}^2D)$, were also observed at levels which appear to significantly exceed their expected natural levels. In synthesizing the "far-field glow" spectrum, the assumption was therefore made that all the permitted and forbidden and atomic transitions are induced emissions. There is no difficulty in identifying potential source mechanisms. Preliminary estimates indicated that observed intensity levels could be accounted for, both through direct collisional excitation and chemiluminescence. While these sources would scale differently with altitude and composition, the difference is not large enough to significantly degrade the uncertainty of the present calculations. In the future, there is enormous scope for improving and quantifying the calculations. Representative synthetic UV and NUV spectra at 250 km for Spacelab 1 are shown in Figure 2.

7. Visible and Near-IR

In the case of the visible range, the assumption was made
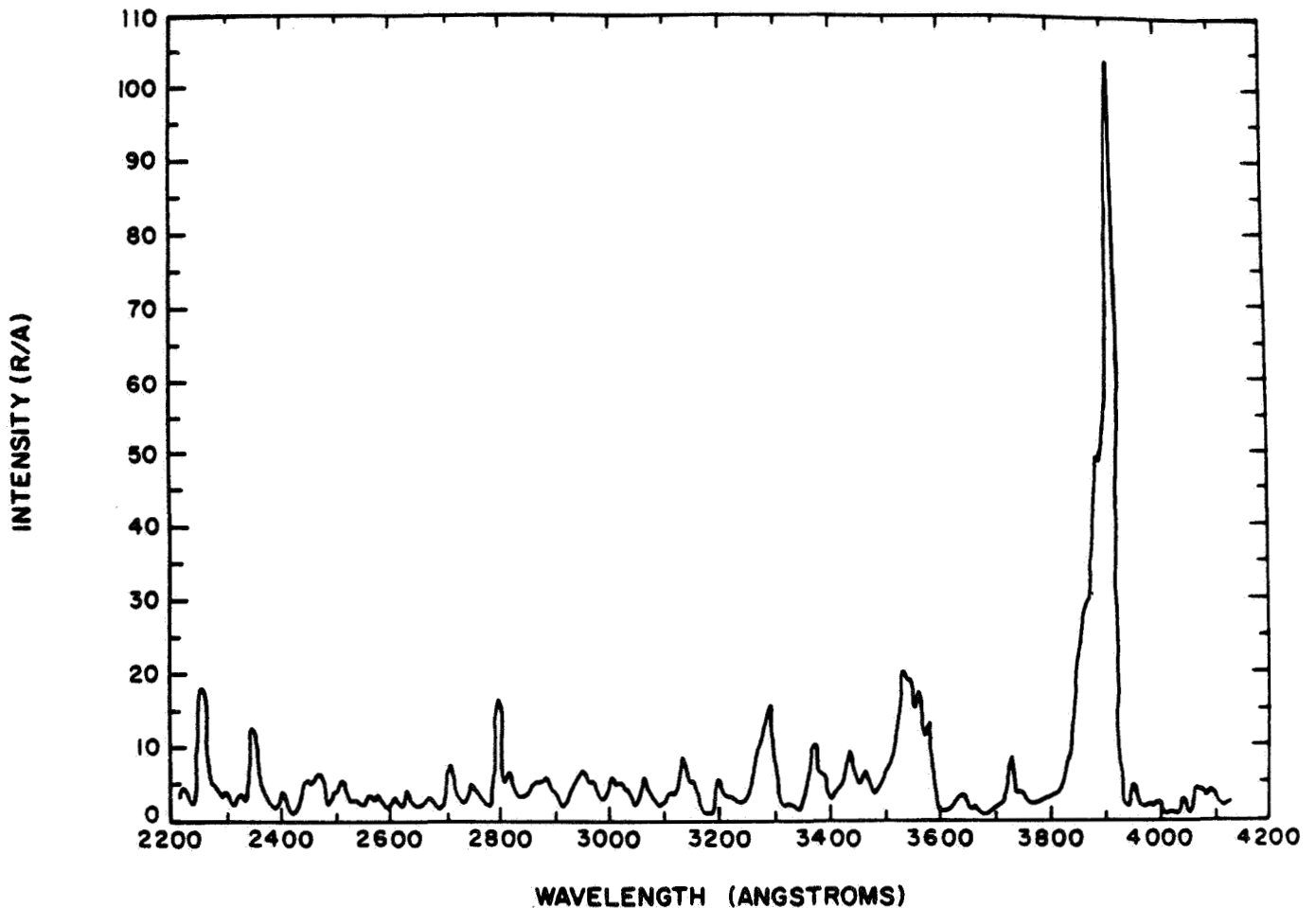
Fig. 2. Synthesized near ultraviolet spectrum for Spacelab 1
conditions: Viewing direction - ram, dayside; Altitude - 250 km;
Date - Nov./Dec. 1983; Spectral resolution - 2.5 A; Bands
synthesized: N_2 - First Negative, Vegard Kaplan, Second
Positive; O_2 - Herzberg I, II, Chamberlain; NO - γ; CO - Fourth
Positive (no Cameron bands observed); CO^+ - Comet Tail; Atomic
Lines - O, N, O^+, N^+.

that the main source of emission would arise from the molecules identified through the VUV and UV. However time has precluded inclusion of several important CO and OH emissions.

Since the intensity of several "terrestrial species" significantly exceeded their expected natural levels, it was assumed that all the observed emissions could be attributed to contaminant sources. Likely candidate bands were synthesized, with the intensities being constrained only by the overall observed intensity envelope, since the actual observed spectra appear to be more complex, with possibly unidentified features contributing significantly. The following band systems were synthesized by fitting the ISO data

N_2:   First Positive

O_2:   Atmospheric

N_2^+:   Meinel

The OH Meinel and CO Triplets, Herman, Angstrom, and Herzberg bands have not yet been synthesized, and their inclusion constitutes an important task for the future. Significant OH^+ has also not yet been ruled out. Expected atomic signatures for O, N, O^+ and N^+ were included.

Representative visible and NIR synthetic spectra for 250 km for Spacelab 1 are shown in Figure 3.

8.   Altitude Variation

Figure 4 shows the altitude scaling adopted for the calculation of irradiances at the altitudes: 300, 350, 400, and 450 km.

Figures 5 to 7 show the VUV, NUV, and VIS results scaled to an altitude of 350 km for the NUV, 400 km for the VIS, and 450 km for the VUV (approximately the proposed nominal Station altitude). As mentioned earlier, significant directional differences in column abundances did not emerge for the Space Station from the SEA calculations for 463 km, where local sources of contamination greatly exceeded ram buildup.

We re-emphasize that the calculations reported here are highly preliminary and only reflect a best attempt (based on limited knowledge) to estimate worst case conditions. Many assumptions have been made; the scaling procedures used are crude. However, during the course of this work, the method has been established and given appropriate resources, the calculations could be significantly improved.

No attempt was made to model the spectral region between 800 and 1000 nm because insufficient experimental or theoretical information is currently available to generate useful results.

51

SPACE STATION CONTAMINATION STUDY
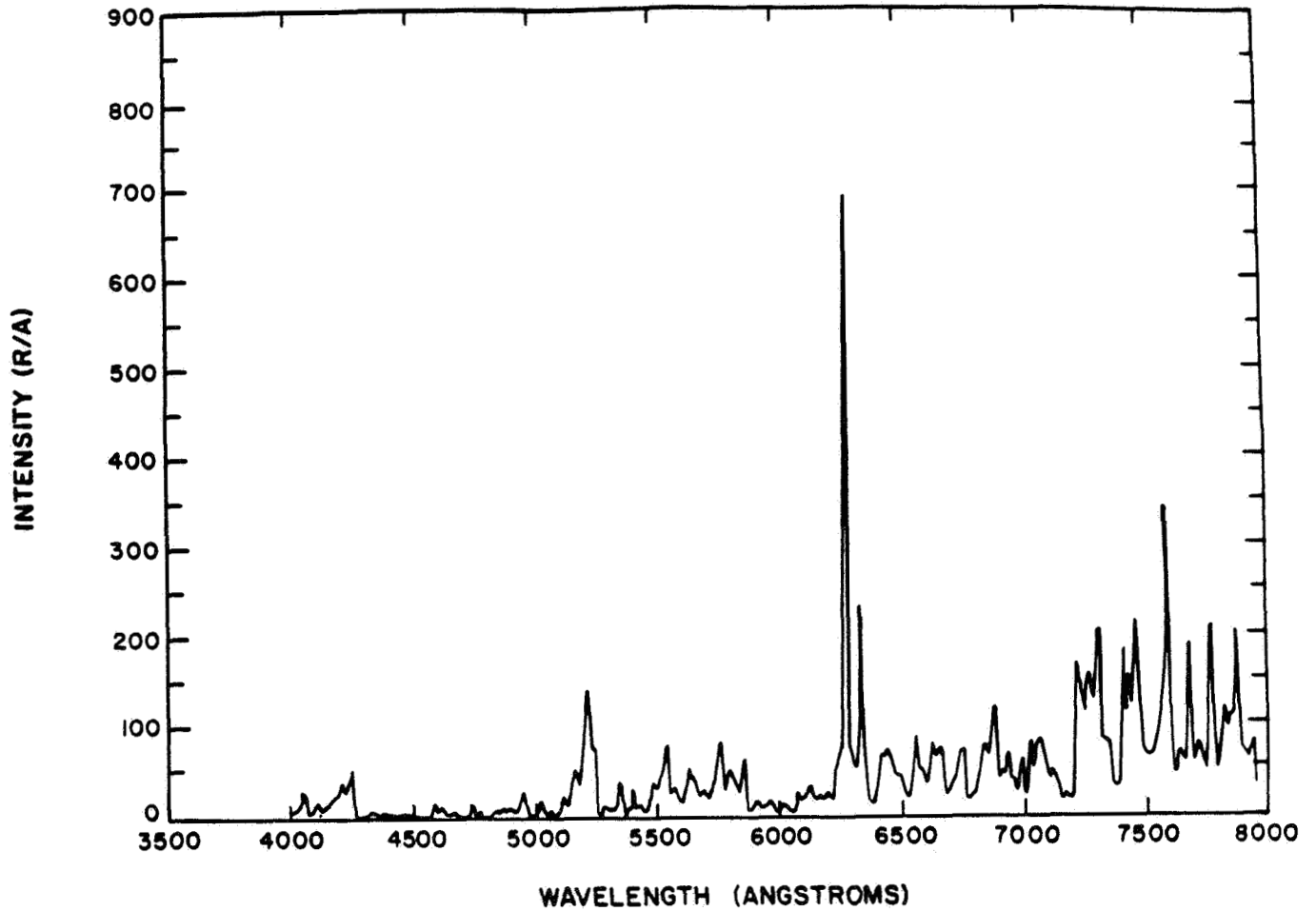VISIBLE AT 250 km

Fig. 3. Synthesized visible spectrum and near infrared for
Spacelab 1 conditions: Viewing conditions - ram dayside; Altitude
- 250 km; Date - Nov./Dec. 1983; Spectral Resolution - 5.1 A;
Bands synthesized: N_2 - First Positive; O_2 - Atmospheric; N_2^+-
Meinel; Bands not yet synthesized: OH - Meinel; CO - Triplets,
Herman, Angstrom, Herzberg; Atomic Lines - O, N, O^+, N^+.

SPACE STATION CONTAMINATION BRIGHTNESS
SOLAR MAXIMUM, DISTURBED (PEAK INTENSITIES)
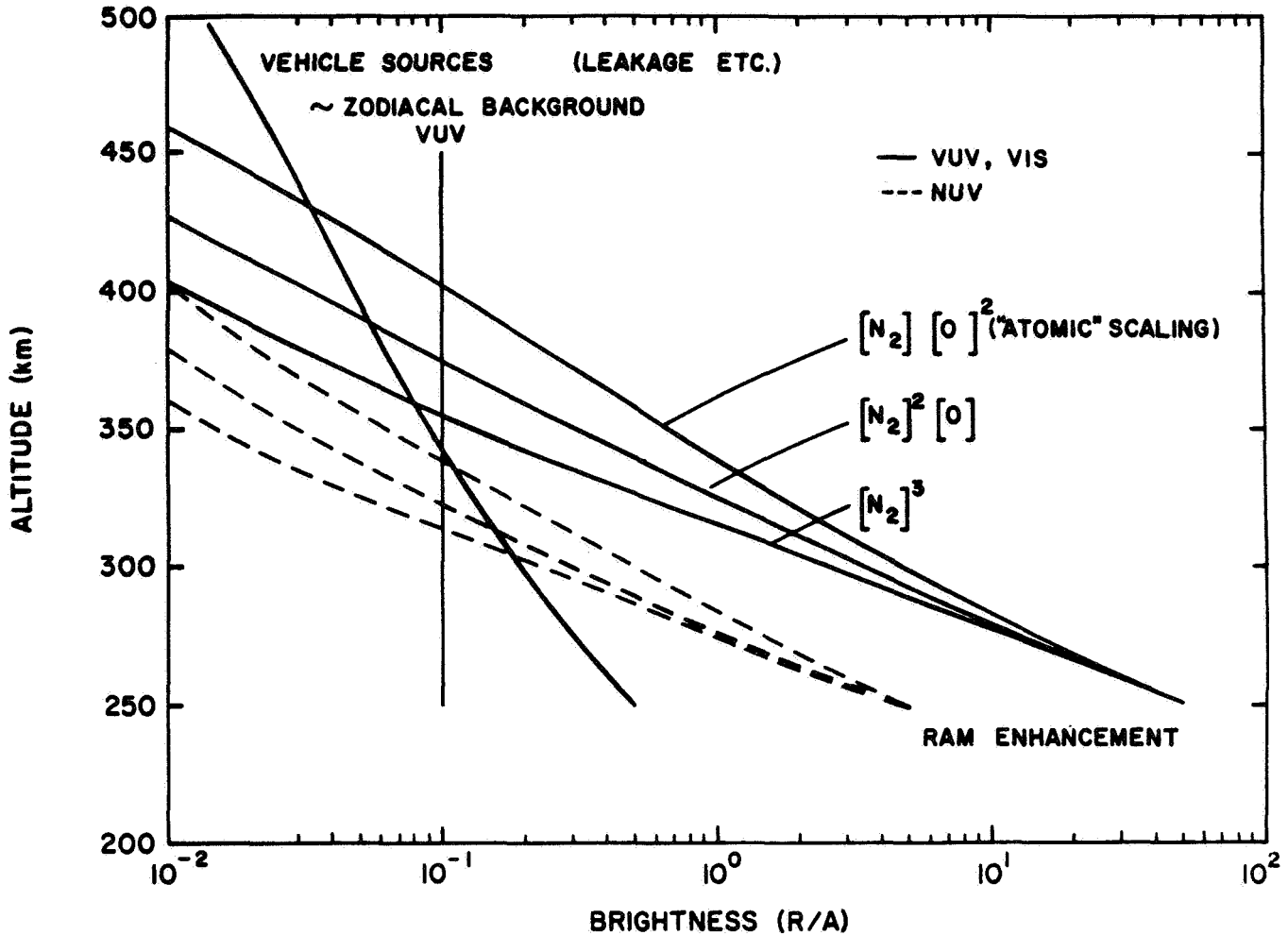
Fig. 4. Variation of the scaling factors with altitude used to extend the spectra synthesized at 250 km to high altitudes. The meanings of the scaling factors $[N_2]^3$, $[N_2]^2[O]$, and $[N_2][O]^2$ are discussed in Sections 5.2 and 8.

53

SPACE STATION CONTAMINATION STUDY
VACUUM ULTRAVIOLET AT 450 km ($[N_2][O]^2$ SCALING)
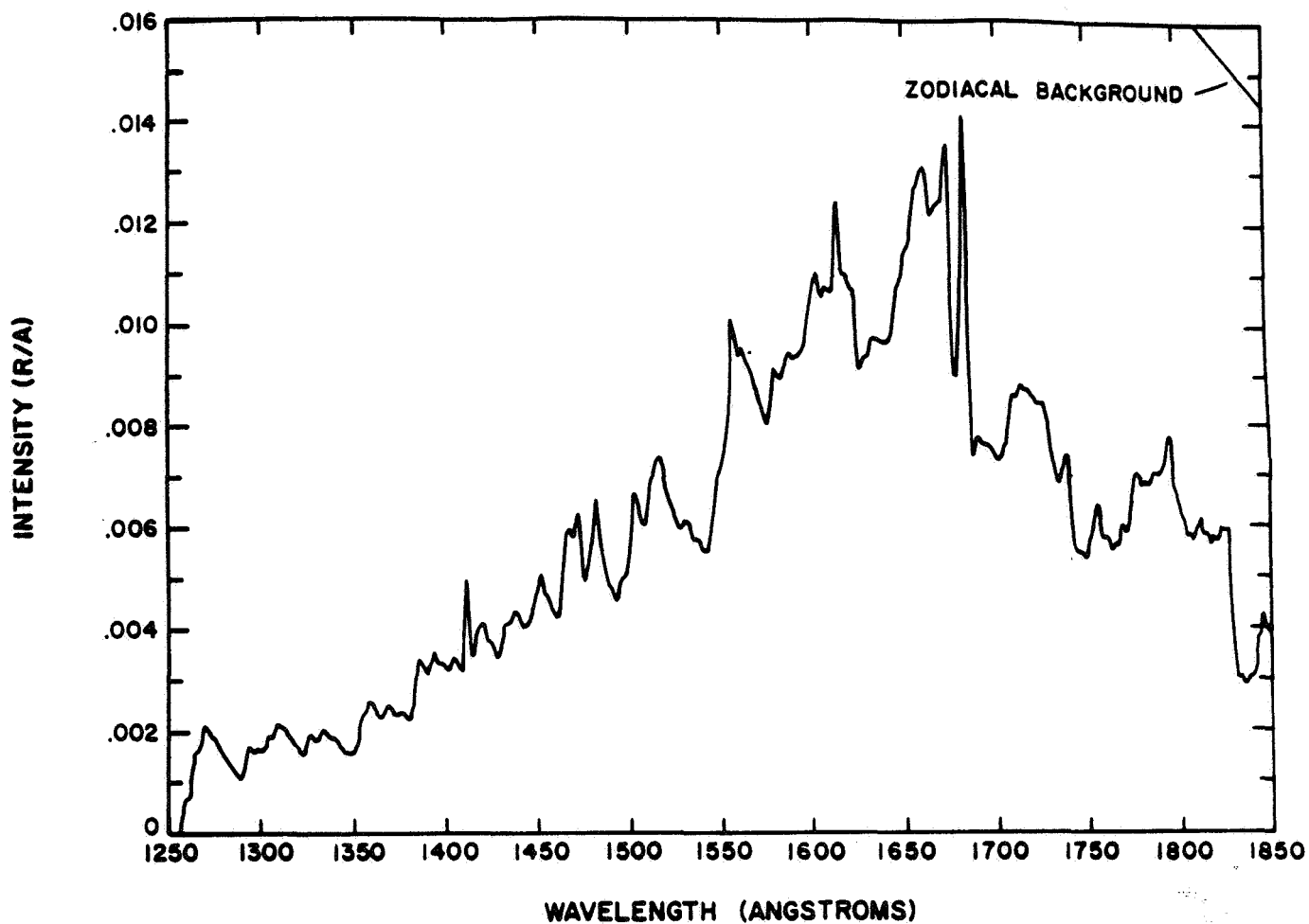
Fig. 5. Synthesized VUV spectrum at 450 km using $[N_2][O]^2$ scaling (that is, worst case). An estimated zodiacal background level is also shown.

SPACE STATION CONTAMINATION STUDY
NEAR ULTRAVIOLET AT 350 km ($[N_2] [O]^2$ SCALING)
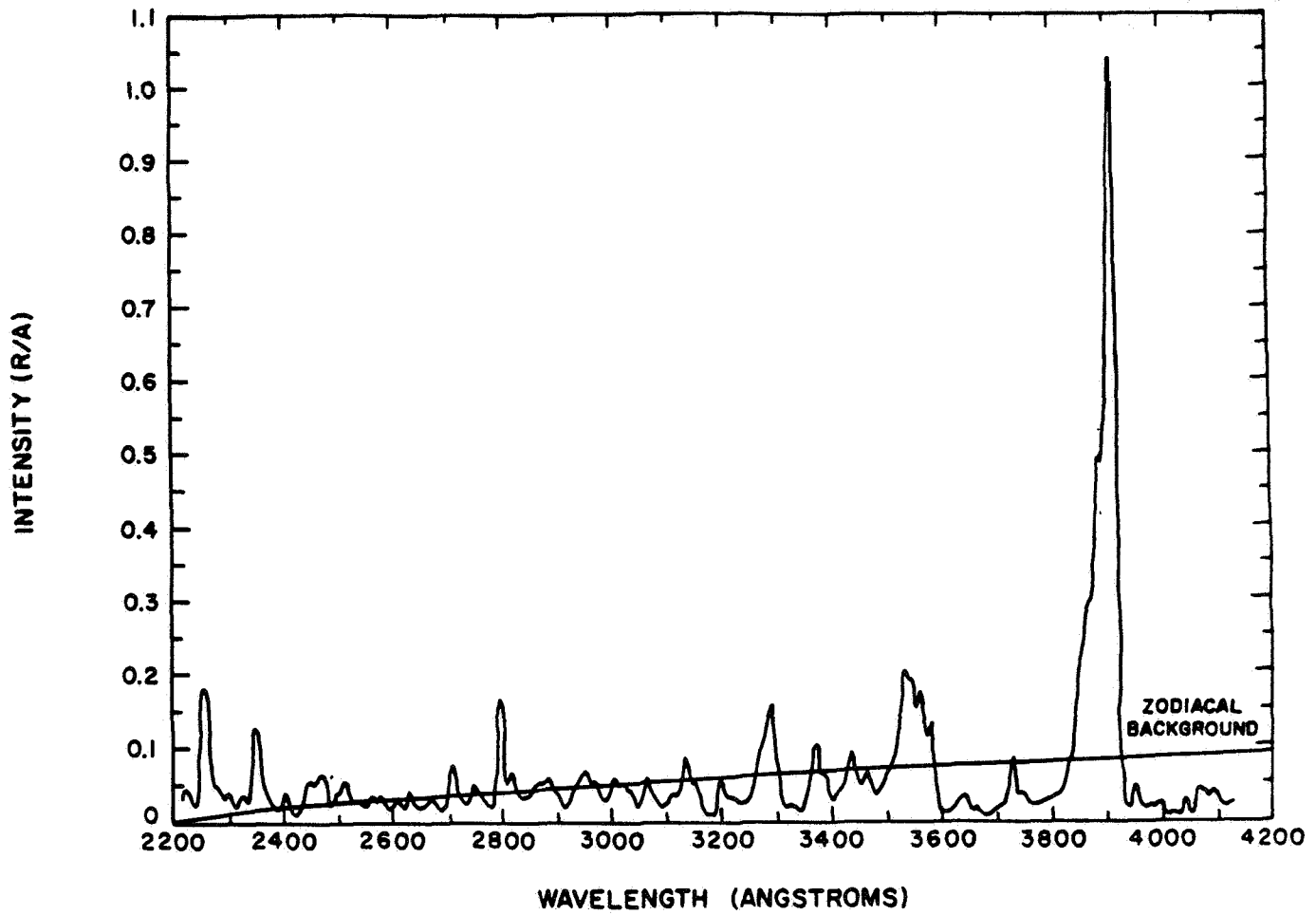
Fig. 6. Synthesized UV, NUV spectrum at 350 km using $[N_2][O]^2$ scaling (that is, worst case). The mean intensity is approximately equal to the zodiacal background at this level.

Fig. 7. Synthesized visible and near IR spectrum at 400 km using $[N_2][O]^2$ scaling (that is, worst case). At this altitude, with the exception of the $O(^3P-O^1D)$ feature, the contamination brightnesses lie well below the zodiacal background.

9.   Natural Emissions

Figure 8 shows a representative calculation of natural irradiances due to thermospheric sources at 250 km tangential viewing for Spacelab 1 conditions for comparison with the contamination brightnesses reported in the preceding sections. The wavelength resolution is 5.1 A.

10.   Conclusions and Recommendations

The results presented in this study show that spectral emissions which arise as a result of vehicle-ambient atmospheric interactions are significant and can become competitive with the natural zodiacal background up to altitudes as high as 400 km for the VUV and VIS for the worst case conditions used in this study. As mentioned in the text, the empirical database on the induced environment of space vehicles is very sparce, and these results are based on a number of assumptions and cannot be regarded as definitive at the present time. Since the technique for doing calculations of this kind was developed in its preliminary form for the purpose of this study, we are now in a position to provide greatly improved estimates of the contamination irradiances. The following tasks are considered most important in order to achieve a higher confidence level for the preliminary conclusions drawn here:

(1)   The sensitivity of the SEA model to angular dependences in the collision cross section should be included since this could result in lower emissions in the non-ram direction and the calculations should be self-consistently done for various geophysical conditions. In the calculations presented here, data were utilized where available, namely, a mixture of night, day, ram, wake, etc.

(2)   The calculations should be repeated for several viewing directions.

(3)   We used very crude altitude scaling based on an 8 m disk and not on the Space Station geometry. The SEA calculations followed by this emission model should be repeated using the appropriate Station model. This is most essential.

(4)   Several significant bands were not synthesized for the NUV visible and NIR. These should be included.

(5)   The self-consistency of emissions across the full spectral range covered (EUV to IR) cannot be guaranteed at this time. Once a self-consistent calculation is done, the column number densities of each upper state could be tabulated. The sparseness of the database was a limitation in that snapshots of data had to be used where these were not taken under the same
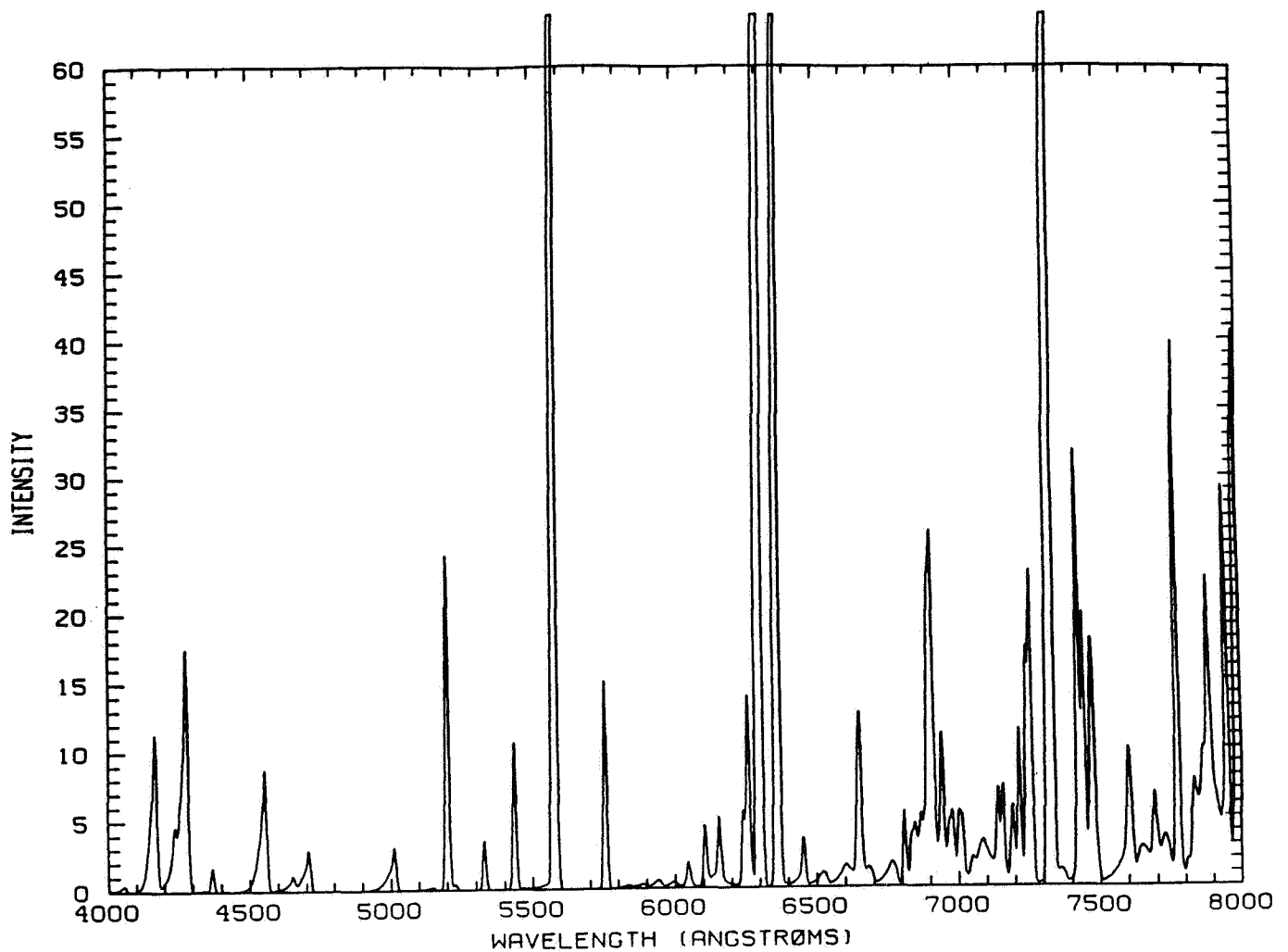
57

Fig. 8. Synthetic spectrum of the natural irradiances expected
for Spacelab 1 daytime conditions (Nov./Dec. 1983) at 250 km for
tangent viewing conditions. The sources were generated by a
comprehensive model of the photochemistry and dynamics of the
thermosphere. The units on the abscissa are (R/A).

conditions, e.g., sunlit, dark, wake, ram.

(6) Measurements of relevant neutral-neutral collision cross sections are needed for the 5 to 10 eV range.

(7) In situ optimized measurements of far-field glow are needed.

References

Conway, R. R., R. R. Meier, D. F. Strobel, and R. E. Huffman, The far ultra-violet vehicle glow of the S3-4 satellite, Geophys. Res. Lett., 14(6), 628, 1987.

Torr, M. R., D. G. Torr, and J. W. Eun, A spectral search for Lyman-Birge-Hopfield band nightglow from Spacelab 1, J. Geophys. Res., 90, 4427, 1985.

Torr, D. G., M. R. Torr, and J. W. Eun, Interpretation of the N_2 LBH glow observed on the S3-4 spacecraft and Spacelab 1, Geophys. Res. Lett., submitted, 1988.

CALCULATION OF SPACE STATION INFRARED IRRADIANCE
FROM ATMOSPHERE-INDUCED EMISSIONS

M.E. Fraser, A. Gelb, B.D. Green

Physical Sciences Inc.
Dascomb Research Park, P.O. Box 3100
Andover, MA   01810

and

D.G. Torr

Center for Space Plasma and Aeronomic Research
University of Alabama at Huntsville
Huntsville, AL   35899

Introduction

The visible emission observed from the energetic interaction of atmospheric constituents, principally O and N_2, with the material surfaces of objects in low-Earth orbit has been termed Spacecraft or Shuttle glow. Although resolved visible spectra have been taken, the emitters and the responsible excitation mechanisms have not yet been completely understood. Less is known of an infrared component of Shuttle glow. Both the orbital observations of Fazio (1985) using many bandpass radiometers as part of the infrared telescope experiment (IRT), and the ground-based observations of Witteborn raise more questions than they answer. Fazio observed no clear glow and placed an upper bound of 2×10^{11} photons cm^{-2} s^{-1} in the 2 to 3 μm bandpass.

An infrared component to the observed visible ram surface glow seems likely. Many of the species presented as possible sources of Shuttle glow also have electronic or vibrational transitions in the infrared. Even if we neglect products from thruster firings and assume unreactive surfaces, the list of potential radiometers is extensive. These include $CO_2(v)$, $H_2O(v)$, $CO(v)$, $OH(v)$, $NO_2(^2B-^2A)$, and $N_2(B^3\Pi-A^3\Sigma)$. The excitation mechanisms and radiance estimates over the 1 to 10 μm region for each of these species will be discussed.

Model

We have estimated the infrared irradiance of Space Station at an altitude of 460 km. The surface material has been presumed to be non-carbonaceous and inert. The determined number densities of various gases relevant to Space Station from both ambient and outgassing sources are shown in Table 1.

Table 1. Station Number Densities

Species	Column Density (cm^{-2})	Concentration (cm^{-3})	Fluxes[**] (molec cm^{-2} s^{-1})
Ambient O	3.45×10^{11}	1.25×10^{8}	1.0×10^{14}
Ambient N_2	2.84×10^{10}	1.03×10^{7}	8.2×10^{12}
Organics	5.7×10^{10}	2.1×10^{7}[*]	--
H_2O	1.59×10^{10}	5.9×10^{6}[*]	--
CO_2	1.24×10^{10}	4.6×10^{6}[*]	--

[*]Calculated assuming uniform density over a 27m column height.

[**]Calculated for ambient O, N_2 only using a velocity of 8 km s^{-1}

A model for the production of and emission from infrared active molecules in the Space Station environment has been constructed. The model considers two classes of radiatively active molecular production processes:

(1) Gas phase excitation of molecules in the near Station environment by collision with ambient flux, and;

(2) Surface processes that lead to molecular excitation. We have also considered secondary processes such as energy transfer from surface generated species but we have generally found these processes to contribute negligibly to the total irradiance.

The gas phase processes involve collisions between molecules in the near Space Station environment, principally CO_2, H_2O from cabin leakage and organics from outgassing, with incoming high velocity molecules. At altitudes of 460 km the ambient flux is predominantly O atoms and N_2 molecules. These species impact the station and its outgassed cloud at a relative velocity of about 8 km s^{-1} and therefore have sufficient energy to excite molecular states by direct T-E,V processes, undergo reactive collisions with gas or surface-adsorbed species, or to dissociate (in the case of N_2). Available experimental and theoretical excitation efficiencies and cross sections were used to compute production rates. Where no data were available, estimates for specific rates were made.

The primary results of our analysis are as follows. Incoming O and N_2 molecules impact gaseous CO_2 and H_2O producing vibrational excitation. Fast O atoms also react with water and organic species to form vibrationally excited OH. Considering the cross sections for these processes and the outgassing number densities, most of the incoming ambient flux impacts Space Station surfaces. N_2 impacts with sufficient energy to cause a fraction to dissociate or to populate excited states. Surface formed nitrogen atoms are presumed to remain surface adsorbed where they eventually recombine with another N atom or an O atom. Allowing the N atoms to desorb would principally effect the NO production rate. Organic species in the ambient Station environment will adsorb on Station surfaces where they react with incoming fast O atoms to produce vibrationally excited OH and CO.

The limitations and uncertainties in our treatment are due primarily to the lack of experimental data. The principal uncertainties are in the excitation efficiencies, many of which have yet to be measured. The calculated irradiance levels are therefore believed to be accurate to within only 1 or 2 orders of magnitude. Throughout the course of this study we have sought to identify key reactions/processes requiring experimental investigation.

Our model does not treat the fate of unreactive O and N_2 surface collisions. If the accommodation coefficient is small, a large fraction will rebound elastically and will pass through the Station ambient cloud once more. In this event the gas phase emissions may have been underestimated by a factor of two.

The densities of gas phase species have been presumed to be uniform. In fact, a density gradient of specific scale height is a more accurate representation. We have sought to minimize the errors in our approach by using column densities in our calculations rather than volume densities wherever possible.

We have assumed unreactive Station surfaces as well as no external carbonaceous surfaces. We have neglected species and infrared emissions from thruster firings and the effects of solar irradiance. Surface-enhanced radiative recombination reactions of triatomics such as NO_2 and CO_2 have been ignored. We have neglected all ionic processes. Incorporation of these effects would increase our irradiance predictions.

To determine the observed radiance levels, a simple model has been employed. The extent of Station is assumed to be large relative to the characteristic distances over which radiative emission occurs. Thus, a steradiancy of 2π has been assumed. In order to calculate the irradiance more accurately, a complete description of Space Station dimensions will be needed. To a first approximation, our results may be scaled by the product of the relevant Station surface area and a $1/r^2$ term,

$$\text{Scaling factor} = A/(v\tau)^2$$

where A is the surface area, v is the exit velocity, and τ is the radiative lifetime.

Results

$CO_2(v)$ and $H_2O(v)$ Emission

Since Space Station is moving at roughly 8 km s^{-1} relative to the ambient atmosphere, the interaction of energetic O atoms and N_2 molecules with CO_2 and H_2O from cabin leakage must be considered. There are several published studies of CO_2 and H_2O vibrational excitation by T-V process from fast O atoms and N_2 molecules (Dunn et al., 1973; Schatz and Redman, 1981; Rahbee, 1984; Ryali et al., 1982; Johnson, 1986). The majority of the work is theoretical trajectory analysis and one paper is shock tube data. The accuracy of the collisional cross sections is probably a factor of two. A compilation of the cross sections is shown in Table 2. The flux of vibrationally excited H_2O or CO_2 species is given by the product of the cross section, σ, the flux of reactive species, Φ, and the column density of the target species, α. Since we have assumed a steradiancy of 2π and we are at an altitude in which quenching processes are slow, the radiant intensity is given by,

$$I = 0.5 \ \sigma\Phi\alpha \quad .$$

Using the column densities tabulated in Table 1, the photon yields for $CO_2(\nu_2)$ and $H_2O(\nu_1, \nu_2, \text{and } \nu_3)$ have been calculated and are shown in Table 2. Items 1 through 4 show the results for interaction with fast O atoms and 5 to 8 for fast N_2 molecules.

OH Production

The reaction

$$O(8 \text{ km } s^{-1}, 2.6 \text{ eV center of mass}) + H_2O \rightarrow 2 \text{ OH}$$
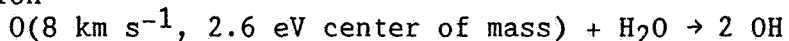
is sufficiently exothermic, 1.9 eV, to produce vibrational and electronic excitation in the OH products. This reaction has been suggested as a possible source of Shuttle glow (Slanger, 1983). The presence of organic compounds in the local Station environment indicates that the more general reaction O + R-H to be most appropriate for consideration here. A reaction (and excitation) cross section of 1 x 10^{-17} cm^2 has been employed in the radiance calculations for these reactions. The result is shown in Item 9, Table 2.

There is no experimental data for these reactions. Considering the relative abundance of H_2O and organic compounds in Station and Shuttle environment, the rates and products of these reactions represent key uncertainties.

Surface Production of NO(X,v)

The dissociation efficiency of 8 km s^{-1} N_2 molecules impacting a surface is unknown. Reasonable estimates place the dissociation efficiency between 0.1 and 10^{-5}. The upper bound has been set by energetic constraints (assuming small chemisorption energies). Clearly, the nature of the surface should greatly influence the dissociation efficiency and the fate of the atoms (i.e., chemisorbed or reflected). The dynamics of high velocity nitrogen dissociation is an area requiring detailed examination.

We have assumed a dissociation probability of 0.01. On surfaces the recombination of N atoms and O atoms is fast. Since the O atom flux exceeds

Table 2. Calculated Radiance Results

Emitter	Cross Section or Excitation Efficiency	Transition Energy (cm^{-1})	τ (s)	$I(R)$**
1. $CO_2(\nu_3)$	2.8×10^{-19}	2349	2.3×10^{-3}	0.17
2. $H_2O(\nu_2)$	8×10^{-17}	1595	4.5×10^{-2}	64
3. $H_2O(\nu_1)$	6×10^{-18}	3652	2.8×10^{-1}	4.8
4. $H_2O(\nu_3)$	5×10^{-18}	3755	2.5×10^{-2}	4.0
5. $CO_2(\nu_3)$	1.5×10^{-20}	2349	2.3×10^{-3}	7.6×10^{-4}
6. $H_2O(\nu_2)$	2×10^{-17}	1595	4.5×10^{-2}	1.3
7. $H_2O(\nu_1)$	9×10^{-19}	3652	2.8×10^{-1}	5.9×10^{-2}
8. $H_2O(\nu_3)$	9×10^{-19}*	3755	2.5×10^{-2}	5.9×10^{-2}
9. $OH(v)$	1×10^{-17}*	--	$\sim 1 \times 10^{-2}$	36
10. $NO(v)$	1×10^{-3}*	--	$\sim 2 \times 10^{-2}$	8000
11. $N_2(B-A)$	1×10^{-4}*	9552	$\sim 1 \times 10^{-5}$	400
12. $CO(v)$	1×10^{-1}*	--	$\sim 1 \times 10^{-2}$	1×10^4
13. $OH(v)$	1×10^{-1}*	--	$\sim 1 \times 10^{-2}$	1×10^4

*Estimated

**Units of Rayleighs, also 0.5 x the total flux of the excited state species. Since the entire vibrational progressions are considered for OH, CO, and NO, frequencies are not shown for these species. In addition, the radiative lifetimes shown for these species are estimates only. Vibrationally dependent values are available in the literature.

the N_2 flux, the NO flux off the surface may be as high as 2 percent of the incoming N_2 flux,

NO flux off $= 1.6 \times 10^{11}$ molecules cm^{-2} s^{-1} .

If we assume a 300 K thermal exit velocity of 4×10^4 cm s^{-1} then,

$[NO] = 4 \times 10^6$ molecules cm^{-3} .

The three states of NO which lie below the dissociation energy are $B^2\pi$, $A^2\Sigma$, and $X^2\pi$ ground state giving rise to beta, gamma, and vibration-rotation bands, respectively. Although neither the $B^2\pi$ nor the $A^2\Sigma$ states directly correlate to the ground state atoms, emission from both states is observed in the surface-enhanced recombination of these species (Dunn et al., 1973). The published account of this work, however, could not rule out energy transfer from N_2^* as the source of NO(A,B). Vibrational excitation of ground state NO should account for a major fraction of the reaction path and the infrared vibration-rotation bands should be prominent in the surface-enhanced recombination of N and O atoms. The fraction of NO which recombines on surfaces with vibrational excitation is unknown and would be a key experimental measurement. For these calculations, we have used 0.10. This fraction was chosen because it is that estimated for CO formed with vibrational excitation from the recombination of C and O atoms on metal surfaces (Tully, 1980; Kori and Halpern, 1983). The radiance estimate for NO(X,v) is shown in Item 10, Table 2.

The CO studies discussed above indicate roughly equal population of all available vibrational levels. Without experimental data for the NO system, equal populations were assumed for this system (in vibrational levels v=1-19, the full extent of our spectroscopic data base).

N_2^* Surface Production

The formation of nitrogen electronic and vibrational excited states from the collision of fast N_2 molecules may occur by direct T-E,V conversion or by dissociation followed by recombination. Neither process has yet been investigated. The only states that directly correlate with the ground state atoms are the $A^3\Sigma$ and $X^1\Sigma$ ground state. Therefore, these are the most likely products. Although the excitation efficiency for $N_2(A^3\Sigma)$ formation has not been directly determined, an estimate may be calculated from the observed Vegard-Kaplan emission intensity as seen on Shuttle by the ISO instrument during the Spacelab 1 mission. The $N_2(A-X)$ emission intensity has been measured as 5 Rayleighs/Angstrom. Assuming a resolution of 10 Angstroms, a field of view depth of 100 cm, and using the Einstein coefficient for the 0 to 6 band, the $N_2(A^3\Sigma,v=0)$ number number density is calculated to be 3×10^6 molecules cm^{-3}. This corresponds to a 2.5×10^{-4} excitation efficiency for $N_2(A,v=0)$ of the incident N_2 flux at 240 km. We have used an efficiency of 1×10^{-3} for the entire state. The $N_2(A)$ flux is therefore,

$$N_2(A^3\Sigma) \text{ flux} = 8 \times 10^9 \text{ molecules } cm^{-2} \ s^{-1}$$

and

$$[N_2(A^3\Sigma)] = 2 \times 10^5 \text{ molecules } cm^{-3} \quad .$$

The $N_2(A)$ state is long-lived, $\tau = 2s$, and may be quenched by the other species also in Station environment. The quenching of $N_2(A)$ by NO to form NO(A) is rapid, 6×10^{-11} cm^3 molecule^{-1} s^{-1}. Since we are in a region where quenching is slow, the photon emission rate will be identical to the NO(A) formation rate,

$$NO(A) \text{ formation rate} = (6 \times 10^{-11})(2 \times 10^5)(4 \times 10^6)$$
$$= 48 \text{ molecules } cm^{-3} \ s^{-1} \quad .$$

For a column height of 27m, an irradiance of 6.5×10^{-2} Rayleighs is calculated. Compared to the other processes shown in Table 2, however, these values are small. Since the NO(A) formation rate is low, NO(X,v) production from NO(A,v) radiative cascade will be negligible.

Considering the low number densities at this altitude, secondary energy transfer processes such as described above are calculated to be insignificant in comparison to direct excitation processes. Since the yields from these mechanisms scale as the square of the number densities, such mechanisms may become important at lower altitudes or during transient events that significantly increase local densities such as attitude adjustment or trimming maneuvers.

First positive emission has been observed in the recombination of nitrogen atoms on metallic surfaces (Brennan and McIntyre, 1982) and has been suggested as one of the emitters in Shuttle glow (Green, 1984). Since the $B^3\pi$ state of N_2 does not correlate to the ground state atoms, the mechanism for populating this state by surface-catalyzed atom recombination is unclear. Owing to the uncertainty in this process, we have assumed an excitation efficiency of 10^{-4} for this process. The results for this system are shown in Item 11, Table 2.

CO, OH Surface Production

Even with non-reactive surfaces, we expect near unity sticking coefficients for organic molecules. Once on the surface the organic species may react with incoming O atoms to produce CO and OH in their ground and vibrationally excited states (the electronic excited states are also possible but are not considered since this study is limited with IR radiators). The flux of organic material assuming molecular effusion onto the surface is given by,
$$\Phi = 0.25 \; \rho v$$
where ρ is the ambient density of organic species and v is the thermal velocity of the ambient organics (taken as 4×10^4 cm s^{-1}). Since the O atom flux is three orders of magnitude in excess of the organics, the product CO and OH fluxes have been taken as equal to the incoming organic flux. The resulting CO and OH fluxes are therefore,
$$CO \; flux = 2 \times 10^{11} \; molecules \; cm^{-2} \; s^{-1}$$
$$OH \; flux = 2 \times 10^{11} \; molecules \; cm^{-2} \; s^{-1} \; .$$
Assuming an exit velocity of 4×10^4 cm s^{-1}, the resulting concentrations area,
$$[CO] = [OH] = 5 \times 10^6 \; molecules \; cm^{-3} \; .$$
The radiance calculations have been performed assuming an excitation probability of 0.10. The results are shown in Item 12 and 13, Table 2. The surface produced OH(X,v) is predicted to exceed the gas phase production by a factor of 200. The surface production rates have not been measured and thus represent a key uncertainty since these processes are likely to produce significant IR emissions at Station altitude.

Total Irradiance Results

A composite spectrum of all the major emitting species is shown in Figures 1 and 2. Figure 2 shows the data from Figure 1 on log scale. The spectra for the diatomics were calculated using a spectral generation code.

The CO_2 and H_2O spectra were generated by converting all rotational lines on the HITRAN tape for these species from absorption strength to emission intensity. The band averaged Einstein coefficients agreed with published values to generally within 10 percent, verifying our methodology.

Each spectrum was produced separately then added together point by point to generate the composite spectrum shown in Figures 1 and 2. The intensity units are Rayleighs/µm. The resolution element has been chosen to be constant at 100 Angstroms.
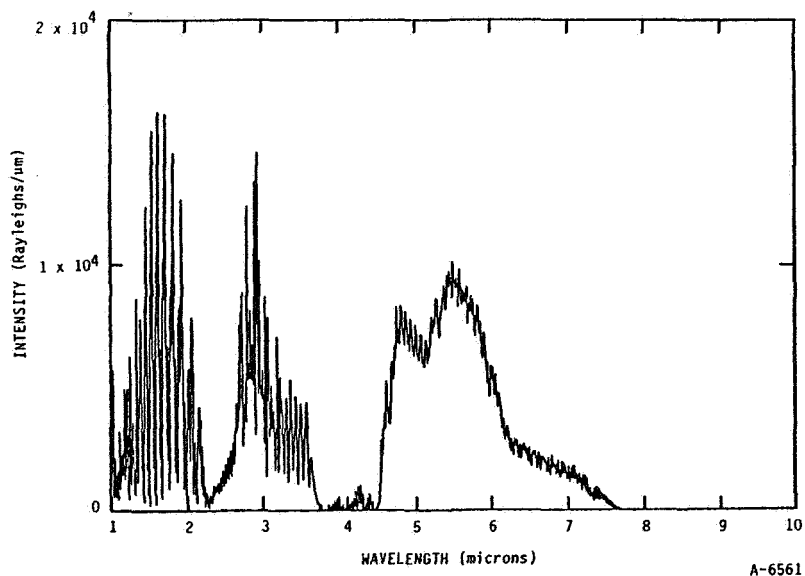
Fig. 1. Predicted Station IR irradiance.
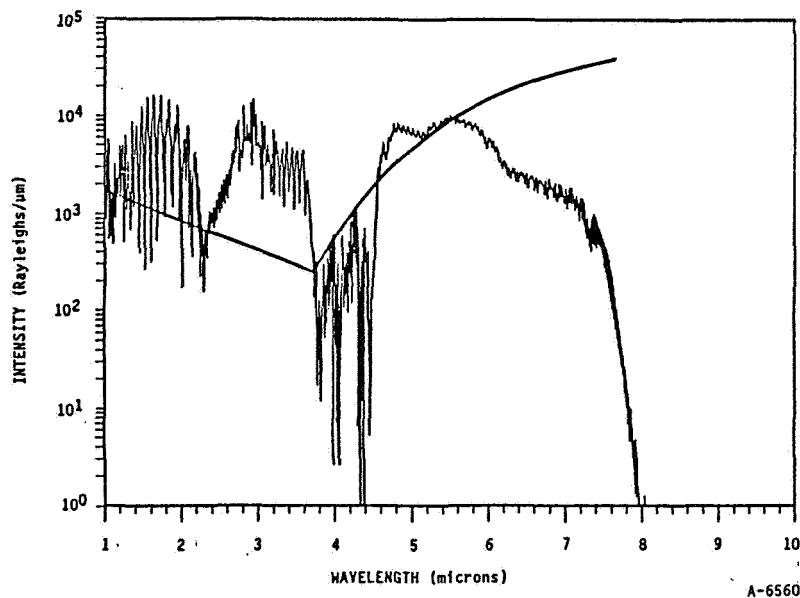
Fig. 2. Prediction Station IR irradiance, log scale.

68

Conclusions

Figures 1 and 2 show that the observed irradiance is predicted to be non-uniform over the 1 to 8 μm region. No irradiance has been predicted for wavelengths longer than this. In order to properly interpret these results they should be compared to anticipated background levels. Zodiacal light on the ecliptic in the 1 to 2, 2 to 3, and 3 to 4 μm bands have been calculated to be 1000, 500, and 300 Rayleighs, respectively (these values have been adjusted for the 2π steradiancy of our model). Figure 2 shows the predicted irradiance in comparison to the zodiacal background. The results in Figures 1 and 2 equal or exceed these predicted background levels, indicating that the Space Station IR background from atmosphere-induced emissions may be a problem of consequence.

The total irradiance shown in Figures 1 and 2 is dominated by surface processses. These are, unfortunately, the processses that are subject to the greatest uncertainty owing to the lack of experimental data. We have previously outlined our basic assumptions. Our irradiance results are estimated to be accurate to within 1 or 2 orders of magnitude. Improved estimates will require results from a detailed experimental and theoretical program.

Acknowledgment

References

Brennan, W. and P. McIntyre, Vibrational relaxation and electronic mutation of metastable nitrogen molecules generated by nitrogen atom recombination of Cobalt and Nickel, Chem. Phys. Lett., 90, 457, 1982.

Caubet, Ph., S.J. Dearden, and G. Dorthe, The specific production of $NO(B^2\pi)$ from the recombination of NO on a Nickel surface, Chem. Phys. Lett., 108, 217, 1984.

Dunn, M.G., G.T. Skinner, and C.E. Treanor, C.E., Infrared radiation from H_2O, CO_2, or NH_3 collisionally excited by N_2, O, or Ar, AIAA J., 136, 803, 1973.

Fazio, G., IR Telescope Experiment, July 1985, private communication.

Green, B.D., Atomic recombination into excited molecular states – a possible mechanism for Shuttle glow, Geophys. Res. Lett., 11, 576, 1984.

Johnson, B.R., A quantum mechanical investigation of vibrational energy transfer on $O(^3P)$ + H_2O collisions, J. Chem. Phys., 84, 176, 1986.

Kori, M. and B.L. Halpern, Vibrational energy distribution of CO in the oxidation of C on Pt, Chem. Phys. Lett., 98, 32, 1983.

Rahbee, A., Vibrationally inelastic collision of CO_2 with N_2 and Ar, J. Phys. Chem., 88, 4488, 1984.

Ryali, S.B., J.B. Fenn, C.E. Kolb, and J.A. Silver, Collisional excitation of CO_2 by N_2, O_2, and Ar, J. Chem. Phys., 76, 5878, 1982.

Schatz, G.C. and M.J. Redmon, A quasi-classical trajectory study of collisional excitation on $O(^3P)$ + CO_2, Chem. Phys., 58, 195, 1981.

Slanger, T.G., Conjectures on the origin of the surface glow of space vehicles, Geophys. Res. Lett., 10, 130, 1983.

Tully, J.C., Dynamics of gas-surface interactions: reaction of atomic oxygen with adsorbed carbon on platinum, J. Chem. Phys., 73, 6333, 1980.

E. R. Miller and K. S. Clifton   N88-25397

Space Science Laboratory, NASA Marshall Space Flight Center
Huntsville, AL 35812

Abstract. The origin of particulate contamination on the Space Station
will mostly be from pre-launch operations. The adherence and subsequent
release of these particles during space flight are discussed. Particle size,
release velocity, and direction are important in determining particle behavior
in the vicinity of the vehicle. The particulate environment at the principal
science instrument locations is compared to the Space Shuttle bay environment.
Recommendations for possibly decreasing the particulate contamination are
presented.

Introduction

Spacecraft on-orbit particulate contamination is defined as solid particles
or liquid droplets deposited on a surface or contained in a volume of
interest. Most of this material originates during ground processing, that is,
hardware manufacturing, assembly, testing, transportation, and launch site
operations.

The hardware surface cleanliness requirement presently imposed on the Space
Station hardware is level 750 as defined by MIL-STD 1246A prior to final
assembly for delivery to space; see Figure 1.
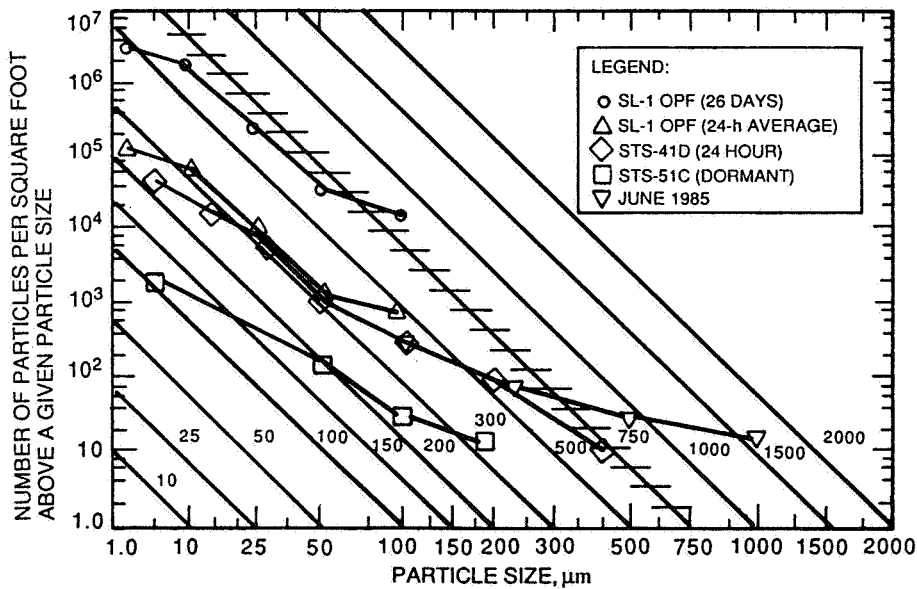
OPF AVERAGE PARTICLE FALLOUT MEASUREMENTS

Fig. 1. Depiction of MIL-STD 1246A surface cleanliness levels.
Level 750 is cross hatched for clarity. Also shown is typical
actual fallout data in Orbiter Processing Facility (OPF).

To predict the Space Station particulate contamination environment we consider how these copious particles are adhered to the surfaces, what causes removal in the low-Earth orbit environment, and, once removed, what their likely behavior may be in the vicinity of the spacecraft. Also, since the main data base on large manned spacecraft has been gained from the Space Shuttle, we consider its relevant similarities and differences to the Space Station that may apply to the particulate environment.

Sources and Mechanisms

Barengoltz and Edgars (1975) determined that the dominant particle-to-surface binding mechanism in a vacuum environment is the van der Waals force. Further, they determined a mean adhesion of $F = 0.13 \ d_p$ Newtons, where d_p is the particle diameter in meters, and found good experimental agreement using 22- to 110-μm-diameter glass beads on metal surfaces. Forces on the order of 10^3 to 10^4 g (where g is the Earth's gravitational acceleration) were required to remove half of the largest and smallest beads, respectively. Such large accelerations may be provided by meteoroid impacts.

In a further study, Barengoltz (1980) estimated the number of contaminant particulates released by such impacts on the Shuttle orbiter, using a total surface area of 1200 m^2 arbitrarily contaminated with 10^6 (10 to 100-μm-diameter) particles m^{-2}. He concluded that impact-released sources would provide an estimated 5.7×10^3 particles day^{-1} with typical release velocities of 3 cm s^{-1}. These impact-released particles are fairly uniform in size range due to the competing factors of fewer large particles which can be removed by the numerous small meteoroids and the more populous small particles which require impacts of larger but less numerous meteoroids.

Barengoltz also analyzed the "backsplash" particles (ejecta) by meteoroid impact cratering. These particles are estimated to be mostly small (2-10 μm) and numerous ($\sim 10^5$-10^7 day^{-1}) with relatively high velocities ($\sim$500 m s^{-1}).

Scialdone (1987), Clifton and Owens (1987), and Green et al. (1987) have discussed particle release by thermally-induced forces such as differential thermal expansion ("oil-canning") and friction between surfaces ("creaking"). Such forces could also be mechanically induced. Using a time decay of possible thermally-induced release of particles observed by the IECM on Spacelab 1, Scialdone derived an extremely slow average particle velocity of 1.5×10^{-3} cm s^{-1}.

Another release mechanism mentioned by Scialdone is the so-called radiometric force, or that force created when a particle is differentially heated (e.g., by sunlight) causing directional outgassing resulting in an accelerating force. Other sources include: (1) spacecraft and payload mechanical operations such as door/aperture cover opening and closing, instrument slewing/pointing, release/attach mechanisms, remote manipulating systems; (2) engine firings; (3) fluid vents and leaks; (4) astronaut EVA; and (5) spacecraft proximity and rendezvous operations. Simpson and Witteborn (1977) discuss several of the above sources and mechanisms in more detail.

For Space Station, operational controls may be applied for so-called quiescent periods. The sources that pertain during these periods are: (1) instrument mechanical operations, (2) fluid vents and leaks from the spacecraft and instruments, (3) thermal shock by terminator crossings (sunrise and sunsets), (4) instrument heating and cooling operations, and (5) meteoroid impacts.

The operations that occur during non-quiescent periods may be important due to relocation of particulate material that may subsequently be removed during quiescent operations.

Shuttle, Space Station Similarities
and Differences

The obvious similarities that the Space Station will share with the Shuttle orbiter that relate to the particulate contamination environment are: (1) both are manned vehicles having pressurized volumes, (2) both fly in low-Earth orbit, and (3) both serve as a platform for a diverse mixture of science experiments.

The differences are extensive and significant. (1) The Space Station will have repeated long period (weeks) cycles of quiescent operations, whereas the Shuttle typically has hours of similar operations. (2) The Space Station maintains attitude without engine firings, whereas the Shuttle requires almost constant attitude correction using vernier engines and requires orientation of the payload bay for various pointing requirements. (3) The Space Station will undergo only slow thermal environment (solar angle) changes, while the Shuttle payload bay experiences large thermal excursions depending on attitude to Sun, Earth, or deep space. (4) Experiments on Space Station are at large distances from expansive areas (such as photovoltaic arrays, thermal radiator, and manned modules) compared to Shuttle bay experiments. (5) The Space Station has a long on-orbit stay time (20-30 years) with months for its experiments, compared to days for Shuttle.

Shuttle Data

The Induced Environment Contamination Monitor (IECM) Camera/Photometer Experiment operated continuously throughout the STS-2, -3, -4, and -9 missions, stereoscopically recording particles and background within a 32° field-of-view. During a total of 378 hours of observations, over 18,000 frames of data were recorded by the two cameras (Clifton and Benson, 1988). However, not all of the recorded frames were conducive for particle detection, most often due to adverse lighting considerations, and the number of frames for which contamination measurements could be made was sharply reduced. Contaminant particles with radii in excess of 10 μm were recorded on over 1800 frames or approximately 42 percent of the data suitable for contamination measurements. Much of the higher activity came during the very early portions of the missions when high contamination levels are anticipated.

The results indicated high particle concentrations early in the mission decaying to a quiescent rate equivalent to approximately 500 observable particles per orbit (Clifton and Owens, 1987). With exposures normalized to 1 s, the probability of the cameras recording one or more particles at any given time was 36 percent. The average stay time for a particle was 5 s. It is evident that particle production was related to both Shuttle and experiment activities. The contamination that was observed varied greatly from frame to frame in both nature and extent, with bursts of particle activity observed frequently throughout the missions. During the cold test of STS-9, however, contamination activity was minimal as compared to the warmer and more active phases of the mission. During this cold test, only 3 frames out of 330 showed in excess of 5 particles, while 282 frames showed no evidence of contamination at all. Thermal effects were evident in producing particles during the cold test, with the preponderance of particles observed within 15 min of orbital sunrise.

One of the primary determinants in the number of particles detected appears to be the direction of the velocity vector. The residual atmosphere at orbiter altitudes acted very much as an 8 km s^{-1} wind both inhibiting and

enhancing the observation of particles. For the most part, very little contamination was observed during periods of the STS-4 and STS-9 missions in which the orbiter velocity vector had a co-elevation of less than 70°. On the contrary, large number of particles were often recorded with the velocity vector at high co-elevations.

In addition to variations of particle activity, frames often differed greatly in the populations of particle sizes that they exhibited. For example, the mean particle radii of water-dump particles as compared to non-dump-associated particles were 102 and 53 microns, respectively. The mean total velocity for particles observed in 18 selected frames was ascertained at 1.2 m s^{-1} with a mode at 0.8 m s^{-1} and a median of 1.0 m s^{-1}. (It should be noted that the selection of frames was intended to provide a sampling of different conditions that produced contamination.) Particles traveling with the mean velocities observed are often already under the influence of atmospheric drag. A number of curved particle tracks can also be observed as the particles tend to align themselves with the velocity vector. In one frame in which particles were shielded from the velocity vector, particles indicated an initial velocity on the order of 0.2 m s^{-1} or less with velocities gradually increasing as the particle-to-spacecraft distance increased. This effect, i.e., the low initial velocity increasing with distance, appears to be a general one, particularly for radial velocities.

Not unexpectedly, strong enhancements of particles were observed during water dumps. The appearance of "snowstorm" events was independent of velocity vector direction and occurred during each water dump event. However, the duration of the settling periods following water dumps did show a variability evidently dependent upon the velocity vector. For the best measured cases, nominal contamination rates were reached approximately 30 min following cessation of the dump, with an e-folding time of 5 min.

Space Station Particulate Contamination

The predominant areas of the Space Station are the solar photovoltaic arrays and dynamic collectors ($\sim$4000 m^2), the pressurized modules ($\sim$1000 m^2), and the thermal radiators ($\sim$500 m^2). If it is assumed that the number of released particles is proportional to surface area, as predicted from meteoroid impacts and perhaps to some degree from thermally-induced forces, it is important to determine where the particles are transported, especially in relation to sensitive viewing instruments located, say, on the upper and lower booms of the dual keel Space Station.

Assuming elastic collisions, a released particle will undergo an acceleration, a, due to atmospheric drag

$$a = 3 \, \frac{\rho_a}{\rho_d} \, \frac{v^2}{d} \, ,$$

where ρ_a = atmospheric density ($\sim$1 x 10^{-14} g cm^{-3} at 350 km), ρ_d = particle density, V = Space Station velocity ($\sim$8 x 10^5 cm s^{-1}), and d = particle diameter. The distance a particle will travel released into RAM is proportional to the release velocity squared, v_o^2. For example, a 100-μm-diameter particle, ρ_d = 1, v_o = 10 cm s^{-1}, will travel 0.26 m before coming to rest and begin turning around. For the same particle with v_o = 100 cm s^{-1}, the distance will be 26 m (a 50-μm particle with ρ_d = 2 g cm^{-3} will behave similarly), and for a 200-μm particle, ρ_d = 1, the respective distances will double. The optimum RAM release direction, in order for a particle to travel

74

to the upper or lower boom locations (estimated to be 30 to 50 m or more from the major surface areas) is ±45°, requiring release velocities to be increased by $\sqrt{2}$ from a RAM normal surface, or to be released from a surface ±45° from RAM. Release at other angles into RAM will require higher velocities to reach the boom regions. Particles released in the wake cannot reach the experiment areas but could possibly be detected by instruments viewing in the wake direction. In this area-dependent scenario, particle release velocity is a very important parameter for contamination in the vicinity of the experiment locations, as is the release direction.

As stated previously, Barengoltz (1980) predicts average particle velocities of ~3 cm s^{-1} while Scialdone arrives at a much lower figure. Data from the IECM indicate an upper limit to the average release velocity of about 20 cm s^{-1}. Corroborative evidence of low release velocities is the data from IECM showing very little contamination when the Shuttle bay was oriented within 70° of RAM.

The Barengoltz meteoroid impact model produces omni-directional particles, while particles released by thermal-related effects may favor the solar direction, e.g., in the general RAM direction for sunrise on Space Station and in the wake direction from sunset.

The IECM and Particle Analysis Cameras for Shuttle (PACS) (Green et al., 1987) data show a definite correlation of particulate events with instrument and system hardware operations. The Space Station instruments on the upper and lower booms will have similar mechanical operations (opening/closing of covers, slewing and pointing, extending/retracting). In addition, instrument gas venting and fluid leaks will probably occur. Also, meteoroid impact and thermal effects and particulate release mechanisms will apply to these areas. However, the linear arrangement of these instruments along a fairly open boom allows particles to be released in mostly unobstructed directions. In the case of Shuttle, Scialdone's decay model allows released particles to reflect from surfaces until they more or less directly escape from the bay. Also, on Space Station, there is less opportunity for shielding from RAM than for Shuttle bay released particles.

Both IECM and PACS data indicate particulate decay with time. The IECM data show an initial on-orbit decay to average levels in about 15 hours. Less obvious was Scialdone's 50- to 75-hour decay time constant from IECM data on Spacelab 1 after heatup from a long cold soak. The meteoroid model with an almost unlimited supply of particles of 100 µm diameter or less would not predict a significant decay except for the larger particles. It seems reasonable, however, that thermally- and radiometrically-released particles from surfaces undergoing repeated similar cycles would have some time constant. Most of the large areas of Space Station will be constructed on-orbit probably months before scientific instruments will be attached (even on the Phase I single boom). If we postulate a time constant of 1 week, particulate contaminants from these sources would be reduced by a factor of >50 per month.

Recommendations

Surface cleanliness specifications should be tighter for large areas, especially for the photovoltaic arrays (the dynamic solar power system will probably have a much better surface cleanliness requirement than level 750).

Use of low absolute values of solar absorptance and thermal emittance coatings will reduce diurnal temperature changes, thereby reducing particle release by thermal effects.

Extra cleaning should be required for instruments and equipment located on the upper and lower booms. Also, manifesting and placement of experiments must be considered (i.e., do not fly a particulate generator with an IR telescope, but if it must be done place them as far apart as possible in physical location and timelining of operations).

Do not locate satellite servicing facility near the upper boom as shown in some sketches of the full-up Space Station.

Verification and monitoring instrumentation for the Space Station particulate environment is highly recommended, especially to correlate particle production with various activities, ranging from science instrument operations to Shuttle tending. Monitoring demands a good centralized data base of all possible contamination-producing events in order that correlation studies can be performed and possible corrective action be taken. Such a data base does not exist for the Space Shuttle.

Conclusions

Particulate matter is tightly bound to surfaces in vacuo primarily by van der Waals molecular force. For space vehicles, most of this particulate matter originates during ground operations.

For Space Station quiescent operations, particles are probably released in proportion to surface areas that are mostly 30-50 m from the upper and lower boom areas.

The release mechanisms during quiescent periods are probably related to thermal effects (including radiometric), meteoroid impacts, and instrument mechanical operations.

The average release velocities are predicted and measured on the order of 20 cm s^{-1} or less, allowing transport distances of ~2 m for 200-μm-diameter particles with unit densities, or 4 m for 200-μm-diameter, density = 2 g cm^{-3}, etc. For release of particles larger than about 100 μm diameter, some decay time constant, much shorter than the many months between construction of the major area elements and the addition of sensitive instrumentation, seems to be warranted for all mechanisms other than meteoroid impacts.

Particulate release by instrument and nearby equipment operations will probably be less severe than from similar operations in the Shuttle bay, but remains a large concern.

Overall, the particulate contamination environment for the Space Station should be significantly less than for Space Shuttle.

References

Barengoltz, J., and D. Edgars, The relocation of particulate contamination during spaceflight, Jet Propulsion Laboratory, Pasadena, California, TM33-737, 1975.

Barengoltz, J., Particulate release rates from Shuttle orbiter surfaces due to meteoroid impact, J. Spacecraft & Roc., 17(1), 58-62, 1980.

Clifton, K. S., and J. K. Owens, Optical contamination measurements on early Shuttle missions, Appl. Opt., in press, 1987.

Clifton, K. S., and J. K. Owens, Analysis of contamination data recorded by the IECM Camera/Photometer, to be submitted, 1988.

Green, B. D., G. K. Yates, M. Ahmadjian, and H. Miranda, The particulate environment around the Shuttle as determined by the PACS experiment, to appear in SPIE Proceedings No. 777, 1987.

Scialdone, J. J., Particulate contamination during Shuttle ascent, to appear in SPIE Proceedings No. 777, 1987.

Simpson, J. P., and F. C. Witteborn, Effect of the Shuttle contaminant environment on a sensitive infrared telescope, Appl. Opt., 16(8), 2051–2073, 1977.

THE PARTICULATE ENVIRONMENT SURROUNDING THE SPACE STATION: ESTIMATES FROM THE PACS DATA

Byron David Green

Physical Sciences Inc.
Dascomb Research Park, P.O. Box 3100
Andover, MA 01810

Abstract. Estimates of the sources of particulates surrounding Space Station are made based on the existing orbital observations data base. Particulates surrounding the Shuttle are mostly event related or from the residual release of mass (dust) brought to orbit from the ground. The particulates surrounding the Space Station are likely to arise from additional sources such as operations, docking, erosion, and abrasion. Thus, scaling of the existing data base to long-duration missions in low-Earth orbit requires analysis, modeling, and simulation testing.

Introduction and Background

The presence of particulates in the Space Station environment could cause a variety of deleterious effects. Their settling on sensitive optical surfaces will cause decreased performance by physically obscuring or scattering emission from bright off-axis sources. Particulates above surfaces in the field-of-view of sensitive instruments will efficiently scatter and emit thermally. These near field sources could dominate remote emission levels. Sunlit particulates appear brighter than stars, entire cities, and even lightning strokes.

Additional deleterious effects will result from particle impact causing surface roughening during the lifetime of the Space Station. Drag will increase as the surface becomes rougher. Thermal balance may change as absorptivity or reflectivity of surfaces is altered. Changes in the surfaces of the solar collectors may decrease power production as aging occurs.

Ever since the first manned missions in Earth orbit, there have been visual reports of activity-induced particles surrounding the spacecraft. During the Mercury through Apollo missions many unusual particle observations were reported. The sensitivity to particle detection however strongly depends upon illumination geometry, and quantification of the observations required more controlled observations. Both video and coronagraphic investigations were undertaken on Skylab in 1973 (Schuerman and Weinberg, 1976; Schuerman et al., 1977; Giovane et al., 1977). Particles with radii as small as 5 μm were detected. Our analysis of their data has revealed that the numerous particles observed had a size distribution which followed a rough $r^{-1.5}$ dependence, i.e., on average there would be 30 times as many 5 μm radius particles as 50 μm radius particles. Moreover the particle velocities observed were in the 0.1 to 20 m s^{-1} range with the larger particles generally moving more slowly. These particles were observed after Skylab had been on-orbit for a month. Because the Shuttle orbiter was to act as an orbital observation platform carrying astronomical and aeronomical

experiments into orbit for week-long observation missions, NASA realized that the local particulate environment could seriously compromise the ability to make remote observations.

From the inception of the Shuttle program, environmental optical quality goals were set by a NASA panel. The Contamination Requirement Design Group (CRDG) guidelines specified an acceptable particulate contamination level on-orbit for the normal Shuttle operational environment as an average of less than one particle per orbit entering a 1.5×10^{-5} sr field-of-view along any line within 60° of the -Z axis (out of bay), and this field-of-view should contain no discernible particles for 90% of the operational period. A discernible particle is a particle with diameter of 5 μm within a range of 10 km.

Contamination below this level was generally deemed as undetectable or as an acceptable nuisance level. Recent advances in detector technology (especially in the infrared) may require more stringent future guidelines for Space Station or may drive the most sensitive experiments off large space structures onto free-flying platforms. The particles surrounding Shuttle observed on-orbit are believed to arise primarily from ground-based processing. The orbiter processing facilities have been improved significantly with particulate counts being carefully monitored by passive techniques, such as witness arrays, at every stage of processing. The improvements have resulted in substantially less particulate loading (area coverage) on the arrays. In spite of these improvements it is still recommended that most sensitive payloads adopt protective measures against particles until safely on-orbit. Another major contamination period is during ascent when the payload bay venting could move particles around and down onto sensitive surfaces. Simultaneously, vibrations from the solid rocket boosters and when the Shuttle goes transonic will act to redistribute particles. It has long been known that activities such as water dumps generate copious ice particles, but in this paper we report that a whole range of events such as crew activities and engine firings can shake loose or produce particles detectible to sensitive astronomical instruments. While on-orbit, micrometeorites may spall off material as modeled by Barengoltz (1980). He predicted that formation of smaller particles down to 2 μm is favored. Data from the passive collection techniques and ground processing facilities are carefully reviewed in the Particulate Environment Section of ENVIRONET which has been compiled by Barengoltz (1985). A general review of this environment has also recently appeared (Green et al., 1985).

In order to verify that CRDG guidelines were met a pair of cameras in a stereo viewing geometry were included as part of the Induced Environment Contamination Monitor (IECM) diagnostic pallet which was manifested on the earliest missions (STS-2,-3,-4) and on the Spacelab 1 mission (STS-9). This pallet was assembled under the guidance of Edgar Miller of NASA/Marshall Space Flight Center. The pallet and its results have been described by the previous speaker (see also Miller, 1983, 1984). There have been other observations of particles in the Shuttle environment. The low light level television cameras observed large particles during STS-3 as previously reported by Maag et al. (1983). They analyzed videotape data from the camera located in the forward part of the bay looking aft with a 4° field-of-view. With the tail blocking the Sun, any particles in the bay or near the tail were observed from their forward scattering lobe. This configuration provides the most sensitive

detection of particles. Particle distances from the camera were not known, but atmospheric drag was used to size/range particles. Because of the relative insensitivity of the camera only large particles could be detected even in the forward scattering configuration. Nevertheless, a large number of particles were detected. They were estimated to be in the mm-cm radius size range. Over 60 particles larger than 5 mm were observed.

Another interesting set of observations were acquired by the Temperature Controlled Quartz Crystal Microbalances (TQCM) flown on the Spacelab 1 mission by McKeown et al. (1985). Sensors were pointed along five directions ($\pm$X, $\pm$Y, -Z). The sensor facing out of the bay (-Z) acquired the least mass indicating that collisional backscattering of particulates does not appear to be a significant process. The sensor facing Spacelab 1 gained the most mass. Post-flight analysis of particulates found that most particles were in the 1 to 20 μm range, a size which is below the camera data threshold. This indicates that the cameras see only a small portion of the particles in the environment. The sources of the TQCM particulates were estimated via elemental analysis to be from ascent redistribution and solid rocket motor firings on-orbit. However, crew activity-generated particles must be substantial to explain the large accretion on the sensor facing Spacelab 1.

The Air Force realized that particulates could interfere with remote atmospheric observations of the chemical processes occurring in the thermosphere and mesosphere which are planned from the Shuttle. In order to assess the magnitude and time scales for this interference the Particle Analysis Cameras for Shuttle (PACS) experiment was developed. Analysis of the film images from the cameras would have permitted position and velocity determination. An error analysis of the digitization and correlation procedure performed by EKTRON indicated accurate determinations of position and velocity components at the few percent level were attainable from film data (Gold and Jumper, 1986). More importantly the particle's scattered intensity and persistence after orbital events could be accurately monitored from the film data.

The PACS cameras differed from the IECM cameras in several aspects, however. Film exposures were taken in sets of four. This exposure sequence was repeated every 120 s. In order to detect small particles, ASA2000 negative film was used and the cameras were focused at 25 m rather than infinity. This distance represents a compromise between enhanced near field sensitivity to particles and loss of the far field stars which allowed for orientiation and in-flight calibration. (For the 25 m focal distance, stars were observed as small, well-defined circles. Because the stellar irradiance was spread over several film resolution elements, only stars brighter than seventh magnitude have been observed in the PACS data.)

The objectives of the PACS experiment were to: (1) quantify the particulate sizes and trajectories so as to identify source locations; (2) determine the severity of events such as dumps, purges, maneuvers, and various operations and measure their decay (clearing) times. The experiment design and performance have been presented elsewhere (Green et al., 1987) and will be only briefly summarized here.

The PACS Experiment

The principal investigator for the PACS Experiment was M. Ahmadjian at the Air Force Geophysics Laboratory. PACS was part of the first Goddard Hitchhiker mission aboard STS-61C (Columbia). The Columbia had just undergone a substantial refurbishment taking 2 years. Unfortunately the launch was delayed for several weeks due to inclement weather including heavy rains while on the launch pad. Thus, this mission was likely to have a larger than representative contamination environment. Lift-off occurred at 6:55 a.m. (EST) on January 12, 1986. A nearly circular orbit of 290 km altitude was achieved at 28° inclination. After orbit stabilization and opening the payload bay doors, PACS was turned on at 3 hr 30 min mission elapsed time (day 0/3:30 MET).

Several significant events occurred during the 6-day mission. A 12,000 lb RCA TV satellite was launched at 0/9:32 MET (the first day of the mission at 9 hr 32 min). There were five water dumps, and a variety of attitudes were used including passive thermal control and several different inertial attitudes for comet Halley and astronomical missions. The measurement period of greatest interest to PACS occurred on the third day of the mission. Columbia traveled an entire orbit with the bay facing deep space with all activities suppressed (including thruster firings) then traveled another orbit in the gravity gradient attitude (nose to Earth) with the bay facing the wake direction again with all activities suppressed. These periods should be representative of the best observational conditions achievable in the bay of the orbiter.

While we were at Hitchhiker Control Center during the mission we gathered a great amount of available data on Shuttle attitude, Sun angles, velocity vector, Earth coordinates, and the mission timeline. The staff at the Control Center (NASA and its associated contractors) were extremely helpful, providing a wealth of information and assistance. We made extensive use of the Shuttle ground system attitude display which provided Shuttle position and orientation updates several times a minute. This data permitted us to begin understanding the PACS data as soon as the film reached PSI. The detailed orbiter ancilliary data tape became available approximately 6 months later and proved useful in verifying the preliminary analysis.

Access to the film canisters was provided 10 days after landing. Inspection revealed that the film in camera 1 had jammed from the start. Camera 2 recorded data during the entire mission exposuring over 400 ft of film. The film was developed by the Aerospace Corporation. Several copies were made and analysis began 16 days after touchdown. In total 14,788 frames of film data were acquired, covering parts of 83 orbits during every day of the mission.

Terminator crossings (sunrises, sunsets) provide optimal detection conditions for particulates. The fraction of film frames at terminator crossings in which particles were detected is plotted in Figure 1. Although particles were observed very often during the first day on-orbit, there appears to be a marked decrease in their occurrence with time on-orbit. By the end of the 6 day mission less than 25% of the terminator crossings have any detectable particles in any frame. The anomalously large value on day three may be due in part to the orbit attitude. The Shuttle spent most of day three in passive thermal control (rotisserie) attitude which sequentially exposes most surfaces to the Sun. We believe this generates particles due to local thermal expansions and flexing. This phenomenon will be discussed more fully below.
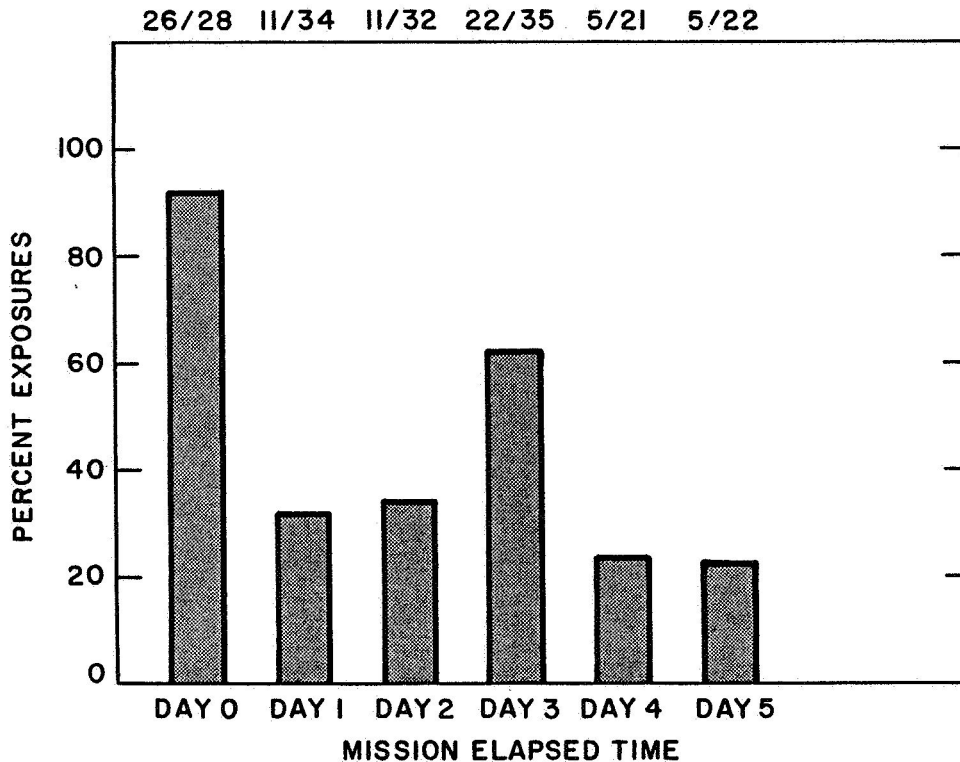
26/28 11/34 11/32 22/35 5/21 5/22

Fig. 1. Fraction of film exposures having particles
at sunrise/sunset.

The scattered intensity of each particle is an extremely sensitive func-
tion of scattering angle and also depends on particle shape, particle compo-
sition, and particle size (Rawlins and Green, 1987). Quantitative understand-
ing of particulate concentrations is hampered by the constantly varying
illumination angles and attitudes. During the first orbital sleep period the
orbiter was placed in a Sun inertial attitude with the starboard (+Y axis)
wing pointed at the Sun. In this attitude when the space above the cameras is
illuminated, particles are observed at constant solar-scattering angles of
$90° \pm 10°$. Each orbit the Shuttle crosses the terminator and is illuminated
for a few minutes before the Earth below is lit overexposing the film. The
sunlit Earth is observed for 1/4 orbit. Then the sunlit Shuttle observes deep
space for ~20 min before crossing the night terminator. The average number of
particles observed during the two periods ("sunrise" and "afternoon") are dis-
played for each orbit during the Sun inertial period. Again there appears to
be a decrease in particles with time on-orbit. In addition there are clearly
more particles per frame at sunrise than later in the orbital day. Again we
feel this is a result of thermal stresses generated at sunrise.

One of the goals of PACS was to determine the time required to return to
a clean optical environment after a water dump. Although several dumps
occurred during the mission and particles associated with those dumps were
observed, only one happened under proper illumination conditions so that a
temporal decay could be observed. Particles were observed promptly in the
first frame taken about 1 min after the start of the dump. The optical envi-
ronment is severely degraded during the dump. Several hundred particles are
observed in the 0.13 sr field-of-view. Because this dump occurred at the end
of the first sleep period the Shuttle was still in Sun inertial attitude. For
fixed solar angle the observed temporal decay of the particles reflects a real

drop in concentration, since detection sensitivity is a constant. The number of visual particles in each 2.7 s exposure is plotted in Figure 2 from the end of the dump until orbital sunset 19 min later. There is a rapid (nearly 2 orders of magnitude) decrease in the first 6 min followed by a much slower decay. The water ejection occurs from a jet on the opposite (port) side of the Shuttle well below the opened bay doors. Ice particles
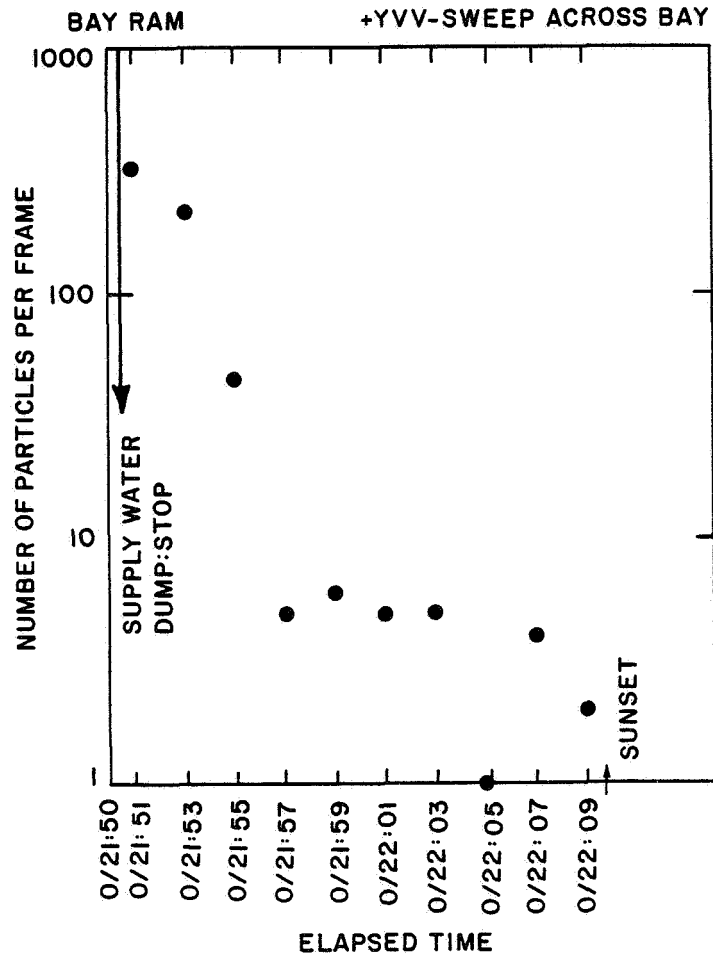

Fig. 2. Particle decay after supply water dump
(visual particle count)

formed in the expansion will undergo complex trajectories due to plume colli-sion effects and atmospheric drag. Although particles were observed with many different trajectories, the usual direction observed was across the bay - the direction from the water dump jet outlet to the PACS field-of-view. During the period after the dump, the Shuttle orientation with respect to the velocity vector changed. During the dump the bay was in the ram direction (+ZVV) so that atmospheric drag would tend to force the particles behind the Shuttle. By the end of the dump, a component of the atmospheric drag was across the bay so that some of the particles would be forced across the bay. This component changed with time so that just before sunset (22:07) the

velocity vector had rotated so that the water jet side of the Shuttle squarely faced the ram direction (-YVV). During the decay after the dump there was no obvious change in particle direction or brightness (size/distance). However, this change in attitude may have affected the temporal decay of the particles. For comparison, the decay in particles was observed after a dump by the NASA IECM cameras agrees in magnitude with the particle counts observed by PACS. The decay in that data seems to more closely follow a single exponential decay with an e-fold time of less than 5 min. The PACS data show a more rapid early time decay. However, we feel the details of the decay are dependent on the atmospheric drag velocity vector. There were eleven fuel cell purges during PACS observational periods. We detected no obvious particulates associated with these events.

The other mission event that dramatically increased the detectible particles was the TV satellite deployment at 0/9:32 MET. This satellite was located in the rear of the bay in a retractable clamshell container. Starting with the opening of the container, particles were observed moving across the camera field-of-view away from the rear of the bay. As the satellite was spun up to its 50 rpm rotation period, copious particles were continuously observed. They first moved rapidly, then more slowly as if the particles were released early in the spin-up but with a distribution of velocities. Thus, the fast moving particles reached the field-of-view first, followed by the slower moving portion of the distribution. For all particles the direction of motion was mainly away from the rear of the bay. During the 15 min prior to satellite launch, the optical environment was the worst for the entire mission.

At several times during the mission, groups of particles were observed within the field-of-view for several sets of exposures. Groups of ~75 particles were observed to be in the same relative positions in frames taken 2 min apart. One particle took 8 min to traverse the field-of-view. These nearly immobile particles were observed in several different attitudes including the velocity vector across the bay (so that the entire column in the field-of-view was subjected to atmospheric drag) and even when the bay was in ram. Because several of these particles had clear disks they were not on the camera lens but rather quite remote, >10 m. Based on drag calculations they must have been quite large (larger than cm diameters) in order to persist with negligible motion in the field-of-view. We can offer no better explanation at this time.

Particles were often observed with rapidly oscillating radiance levels as if they were presenting different geometric aspects to the camera. We believe they were non-spherical particles rotating. One particle exhibited 47 periodic oscillations during a 2.5 s exposure. We are unable to postulate a source mechanism which would give rise to such rapidly rotating particles. Drag would tend to damp these rotations.

Besides the events which obviously degrade the optical environment around the Shuttle, there were two key observational periods during which all activities were suppressed. On mission day two, after 50 hr on-orbit, the Shuttle maneuvered into a deep space viewing attitude (nose into the velocity vector, Earth below the port wing). No further thruster firings were used to maintain this attitude. Data were acquired for 105 min in this mode, then the Shuttle maneuvered into gravity gradient attitude (nose to Earth, bay facing wake). Again thrusters were disabled. The Shuttle attitude varied only slightly

(<5°) during this orbit. The numbers of particles observed within the field-of-view during the two sequences are shown in Figures 3 and 4.
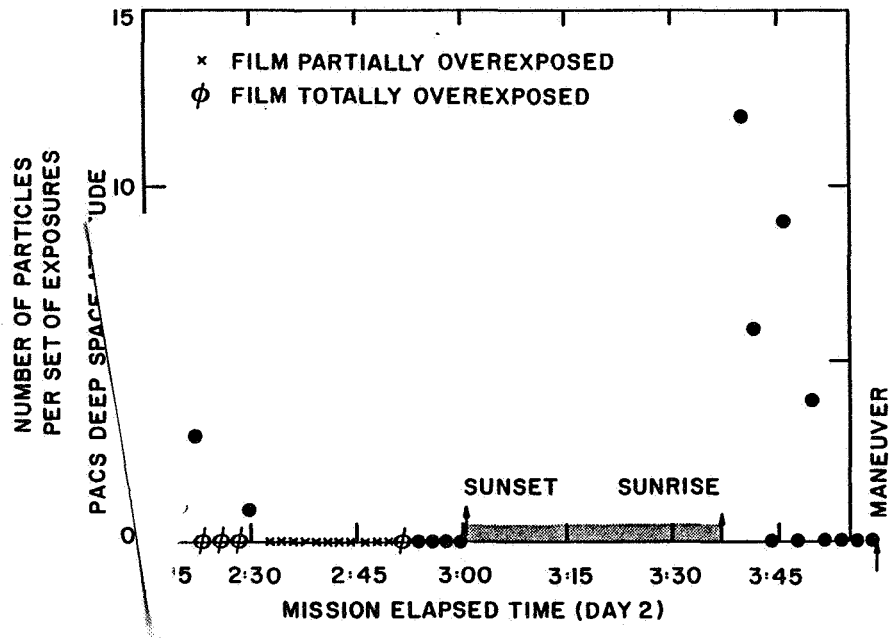

Fig. 3. Particles in field-of-view during PACS prime measurement sequence (deep space viewing - all disabled).
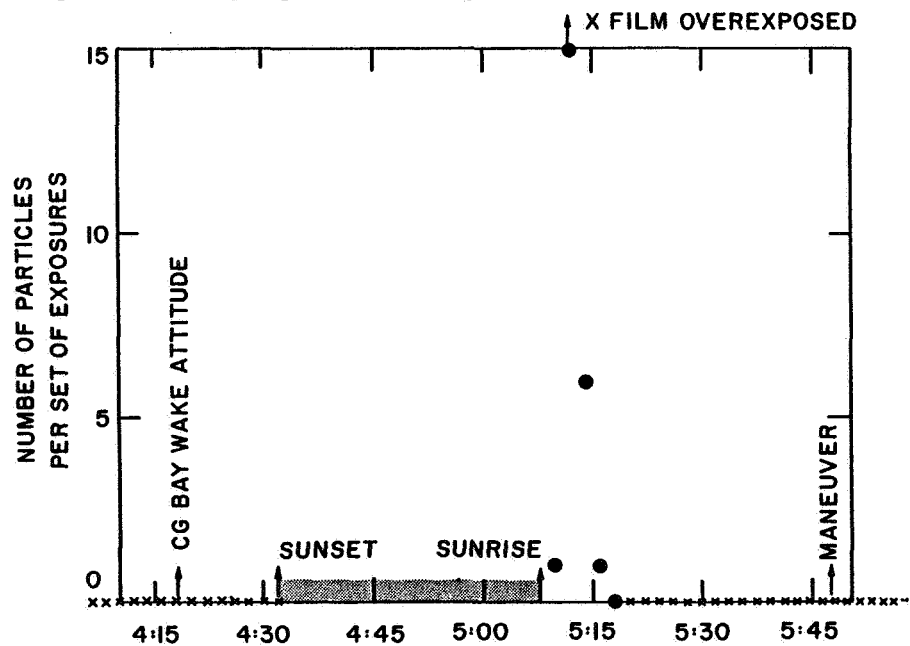

Fig. 4. Particles in field-of-view when gravity gradient attitude bay in wake (all disabled).

The frames taken in deep space viewing attitude have near optimum viewing geometry; the Sun is nearly perpendicular to the bay so that even near field particles are solar illuminated and observed at a 90° scattering angle. In Figure 3 there are two clear periods when particles were observed: just after the maneuvering was completed and just after orbital sunrise. Note there is no corresponding feature at sunset. The illumination conditions are quite constant so that the fluctuations in the particle counts after sunrise should be real. Several very different trajectories were observed. (A nose-to-tail direction of motion should have been favored due to drag.) Because the bay was not illuminated during this period (shadowed by cabin), the observed particles may have arisen from very different parts of the orbiter.

In Figure 4 the gravity gradient data are presented. The film is most often overexposed in this attitude. The Earth is in the field-of-view so that the sunlit Earth overexposes the film. The best viewing conditions are when the Shuttle bottom is illuminated and the Earth is still dark as occurred from 2/05:10 to 05:18. Here again a flurry of particles is observed just after orbital sunrise. They are observed with a solar illumination angle of ~160°. This is a very sensitive configuration (Rawlins and Green, 1987). The bay is shadowed, but the field-of-view begins to be illuminated about 3.5 m from the cameras. The particle trajectories seem to be mainly rear to forward. The bay is in wake and not solar illuminated; thus, any particles observed most probably are swept into the field-of-view by drag.

Scialdone (1986) has recently suggested that several thermal processes could drive particles off surfaces. We feel that the current data show clear evidence that sunrise-related thermal stresses induce particle generation.

Summary of PACS Data and Particle Model

The PACS camera successfully gathered data on the orbital particulate contamination environment during mission STS-61C. The film data clearly indicate that the solar illumination angle is the key parameter. We suspect particles were often present but we were able to observe them only under proper illumination conditions. At terminator crossings (when illumination conditions were reasonably good) particles were observed about one-third of the time within the 17° x 24° field-of-view of the PACS cameras. Particles were observed: when all activity was suppressed, after maneuvering, after payload bay door operations, during the preparations for a satellite launch, during and after water dumps, and after sunrise. During active events such as dumps and the satellite launch, the particle trajectories observed extrapolated back to the vicinity of the source. Atmospheric drag accelerations only slightly perturb the trajectories of detected particles during these events. Only a few particles were detected by the strobe-illumination. This indicates that the particles were nearly always beyond 2 m from the cameras. It also appears that particles are often very asymmetric offering different geometrical areas to the cameras at an angular rate of up to 20 per second. Particles with trajectories from every direction were observed.

We can attempt to compare the PACS observations with the CRDG guideline standards. Roughly particle occurrence is on average 1/3 particle per 0.3 s exposure (~1 particle per second) late in the mission within the 0.126 sr field-of-view of PACS. This corresponds to approximately 2/3 particle per

orbit within a 1.5 x 10^{-5} sr field-of-view. The PACS observations would satisfy the CRDG guidelines except that PACS is unable to sense particles down to 5 μm diameters and certainly is not sensitive enough to see one at 5 km. However, the PACS results are encouraging in that there may be quiescent times when the optical environment is quite clean. Unfortunately there are many times when it is not.

The PACS data in conjunction with other orbital data bases have been used to create the framework model of the Shuttle environment. Excluding orbiter activities (dumps, thruster firings) the clearing time for the environment appears to have characteristic clearing times (e-fold) of 5 hr in a solar inertial attitude, and of 11 days for a variable attitude mission. The solar-induced particle cloud produces 100 particles sr^{-1} during a 10-min period. The clearing time (e-fold) following a water dump is 2 to 10 min depending on attitude. On average there were 8 particles sr^{-1} s^{-1} larger than 40 μm surrounding the Shuttle during the middle of mission.

In order to compare the various observations of particulates on-orbit, a $r^{-1.5}$ scaling was applied to achieve a 5 μm detection threshold for all measurements. Additionally, fields-of-view were adjusted to 1.5 x 10^{-5} sr. The scaled observations from PACS (STS-61C), STS-4 star cameras, Infrared Telescope (Spacelab 2), and Skylab are all presented in Figure 5 as a function of time on-orbit. Considerable variation is observed. The temporal decay of particulates (which are dominantly residual particles from ground accumulation) is shown as observed (solid line) and extrapolated (dashed line). From the figure it is seen that based on this extrapolation, CRDG design goals would be met after 20 to 40 days on-orbit. Based on surface area alone, the initial particulate generation rate surrounding the Space Station would be about 1000 particles per 10^{-5} sr per orbit.

Station Particulate Environment

Somewhat at odds with these Shuttle observations is the Skylab coronagraphic data. Taken after 25 days on-orbit, substantial particulate contamination was observed. This brings into doubt the ability to extrapolate a decay of the particulate cloud density. Observational data from later during the 9-month mission would provide critical insight into this behavior. Skylab data represent the only practical existing data base beside any Soviet observations.

At some level, particulates generated by orbital processes will establish a quasi-steady state level. A careful engineering approach may permit scaling of Shuttle observations to a Space Station scenario. The effects of thrusters (used for orbit and attitude maintenance), docking activities, crew activities (internal and EVA), dumps, and residual particles from ground accumulation may all be estimated roughly based on Shuttle observations. A detailed model of size distribution, spatial transport, and temporal behavior of each source must be developed and applied to the Space Station configuration. The effects of particle redistribution may be simpler due to small geometric obstruction factors. Unfortunately, additional processes are likely to generate particles, whose magnitudes are much more difficult to assess. The variety of mechanical operations to be undertaken on Space Station are likely to generate unusual distributions of particles. Modeling these sources will be most difficult. Additionally, erosion will result in particle generation. Oxygen atoms will
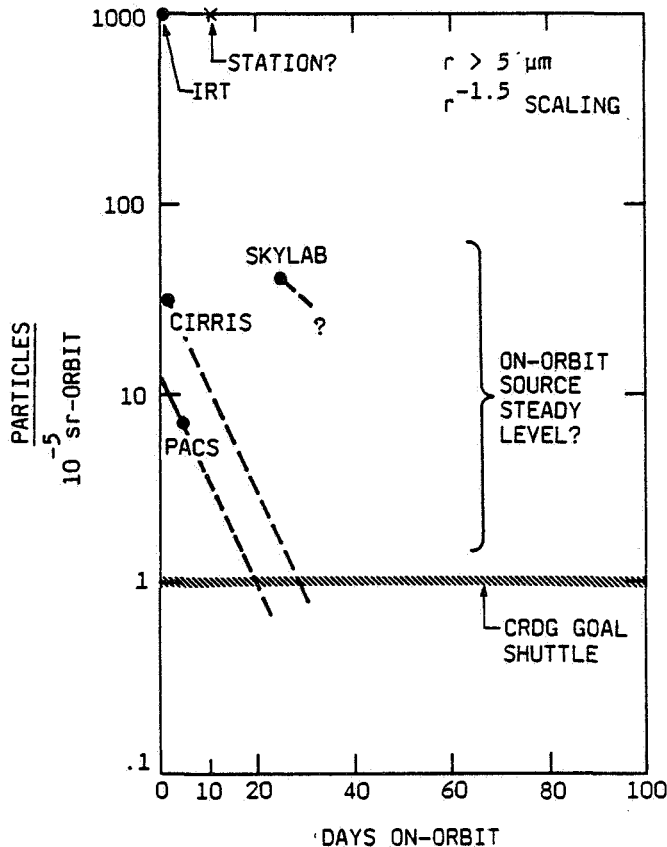
88

Fig. 5. Residual particulate environment surrounding spacecraft.

penetrate protective coatings at pinholes or fractures leading to undercutting and eventual particle/flake formation. Accelerated laboratory tests have clearly demonstrated this effect and its potentially serious impact. In order to achieve a similar goal for Space Station as was set by the CRDG for Shuttle from any source, less than 1 particle (r > 5 μm) may be generated per 10 m^2 of surface area per orbit.

The key unknowns which must be addressed to more accurately predict the particulate environment surrounding the Space Station are: the details of the particle dynamics, the generation rates for each process and size distributions; and a predictive two-dimensional model. The velocities and angular distributions of particles leaving surfaces must be determined as input to the model. Drag and effects of particle charging must be included in the model. The goal of this model should be to guide development of guidelines for Space Station users: to minimize their impact on observational capabilities yet permit a range of activities to be undertaken. Thus, the magnitude of particle generation and its spatial and temporal extent for each source or activity can guide location on Space Station and observational time period selection.

The coupled activities of: (1) further analysis of existing data from on-orbit, (2) ground-based and orbital tests of particle production upon abrasion or erosion, and (3) modeling to permit scaling relationships for the

89

Space Station configuration will provide an improved insight into the environment to be encountered by Space Station.

References

Barengoltz, J., Particulate release rates from Shuttle orbiter surfaces due to meteoroid impact, J. Spacecraft & Roc., 17, 58-62, 1980.

Barengoltz, J. (ed.), The particulate environment around Shuttle, panel report (Section 10) located on ENVIRONET computerized database operated by NASA/Goddard Space Flight Center, 1985.

Giovane, F., D.W. Schuerman, and J.M. Greenberg, Photographic coronagraph, Skylab particulate experiment T025, Appl. Opt., 16, 993-998, 1977.

Gold, B. and W. Jumper, PACS image processing, Ektron Applied Imaging Final Report, November 1986.

Green, B.D., G.E. Caledonia, and T.D. Wilkerson, The Shuttle environment: gases, particles and glow, J. Spacecraft, 22, 500-511, 1985.

Green, B.D., G.K. Yates, M. Ahmadjian, and H. Miranda, The particle environment around the Shuttle as determined by the PACS experiment, SPIE Paper 777-01, 1987.

Maag, C., J. Barengoltz, and F. Keykendall, STS-3 "snow flake" study, A291-A294 in The Shuttle Environment Workshop (J. Lehmann, organizer), February 1983.

McKeown, D., J.A. Fountain, V.H. Cox, and R.V. Peterson, R.V., Analysis of TQCM surface contamination adsorbed during the Spacelab 1 mission, AIAA paper 85-7008, in AIAA Shuttle Environment and Operations II Conference Proceedings, Houston, Texas, pp. 108-115, November 1985.

Miller, E.R. (ed.), STS-2,-3,-4 Induced Environment Contamination Monitor (IECM) Summary Report, NASA TM-82524, NASA/Marshall Space Flight Center, Alabama, February 1983.

Miller, E.R. (ed.), Induced Environment Contamination Monitor - Preliminary Results for the Spacelab 1 Flight, NASA TM-86461, NASA/MSFC, Alabama, August 1984.

Rawlins, W.T. and B.D. Green, Spectral signatures of micron-sized particles in the Shuttle optical environment, Appl. Opt., 26, 3052, 1987.

Schuerman, D.W. and J.L. Weinberg, Preliminary Study of Contaminant Particulates Around Skylab, NASA CR-2759, 1976.

Schuerman, D.W., D.E. Beeson, and F. Giovane, Coronagraphic technique to infer the nature of the Skylab particulate environment, Appl. Opt., 16, 1591-1597, 1977.

Scialdone, J.J., Particulate Contaminant Relocation During Shuttle Ascent, NASA TM-87794, NASA/GSFC, Greenbelt, Maryland, June 1986.

EFFECTS OF METEOROIDS AND SPACE DEBRIS ON THE PARTICULATE ENVIRONMENT FOR SPACE STATION

W.R. Seebaugh

Science & Engineering Associates, Inc.
Englewood, CO 80111

Abstract. A large orbiting platform such as Space Station will be subjected to numerous impacts by meteoroids and space debris fragments. These hypervelocity impacts will produce clouds of ejected structural material in the vicinity of the spacecraft. In this paper we report the development of a preliminary model for impact-generated ejecta production which combines the fluxes of meteoroids and space debris fragments with a description of the number of ejecta particles produced by hypervelocity impacts. Modeling results give mean ejecta densities from 30% to 100% of the present particulate background limitation of 1 particle 5 microns and larger per orbit per 1×10^{-5} sr field-of-view as seen by a 1-m-diameter aperture telescope in the 1990s time frame. Projected increases in the space debris flux raise this density to 300% of this limitation after 2010. The model is also applied to estimate the vulnerability of metallic claddings on composite structural members to penetration by hypervelocity projectiles, thereby exposing the substrate to atomic oxygen. The estimated annual number of penetrations is from 4 to 8 per m^2 of cross-sectional area in the mid 1990s, increasing to more than 40 penetrations per m^2 after 2010.

Introduction

The probability of penetration of the habitation volumes of prior manned spacecraft by natural meteoroids was low (Cour-Palais, 1987); it remains low for spacecraft with cross-sectional areas not exceeding tens of m^2. This probability increases somewhat for Space Station, which will have a cross-sectional area of 100-300 m^2 (depending on its orientation relative to the meteoroid flux). The current space debris environment, which is not well known, appears to pose a similar threat to spacecraft habitation volumes. The future space debris environment may increase dramatically, possibly exceeding the meteoroid environment by an order of magnitude during the lifetime of Space Station (Su and Kessler, 1985).

The potential for impacts of natural meteoroids and space debris fragments with spacecraft surfaces has generated sufficient concern over penetration of habitation volumes that structural means of distributing the impact energy have been developed. The usual mitigation measure is the construction of a thin "bumper" some distance outboard of the pressure wall. When a hyper-velocity projectile (natural meteoroid or space debris fragment) penetrates a properly designed bumper, a cloud of projectile and bumper material (solid, liquid, or vapor, or a combination) strikes but does not cause severe damage to the pressure wall (Cour-Palais, 1987).

Hypervelocity projectiles that are smaller than those for which a bumper was designed and those that impact unshielded areas of the spacecraft (presumably with wall thickness sufficient to preclude penetration) will produce clouds of ejected structural material in the vicinity of the spacecraft. A significant fraction of this ejected material will be in the form of solid particles with diameters exceeding 5 microns. Gault et al. (1963) showed that the ejecta particle flux will greatly exceed (by 3-4 orders

of magnitude) the flux of impacting particles of the same mass. This potentially major particulate source for large orbiting platforms such as Space Station has not been considered previously. Impacting meteoroids and space debris fragments may also increase the potential for atomic oxygen erosion of vulnerable materials by penetrating the protective metallic cladding being considered for such materials.

In this paper, we report the development of a preliminary model for impact-generated ejecta production. The model is similar to that reported by Seebaugh and Linnerud (1984) for explosively generated ejecta. The major parameters in the model are the fluxes of meteoroids and space debris fragments at the orbital altitudes of interest and the number of ejecta particles generated by a hypervelocity impact on a spacecraft surface. In the following sections we briefly describe the components of the model and results obtained for Space Station.

Fluxes of Meteoroids and Space Debris Fragments

The undisturbed meteoroid flux is given by Cour-Palais (1987)

$$\log N = -14.37 - 1.21 \log m \quad \text{for } 10^{-6} \text{ g} < m < 1 \text{ g} \tag{1}$$

$$\log N = -14.34 - 1.58 \log m - 0.06 (\log m)^2 \text{ for} \tag{2}$$

$$10^{-9} \text{ g} < m < 10^{-6} \text{ g}$$

where N is the flux (per m^2 per sec) and m is the projectile mass in g. The lower limit of application of equation (2) is extended to 10^{-12} g in JSC 30000. Since the undisturbed meteoroid flux is omnidirectional with respect to the Earth, a correction for Earth shielding must be applied to equations (1) and (2). The Earth's gravitational field also attracts (focuses) the meteoroids. The current estimate of the meteoroid flux at an orbital altitude of 400 km is given in Fig. 1 (using shielding and focusing factors from JSC 30000). The mass density of meteoroids is 0.5 g cm^{-3} (Cour-Palais, 1987). The meteoroids impact the Space Station at a mean velocity of 20 km s^{-1}.

The projected space debris flux from JSC 30000 is also given in Figure 1 (lower solid line, here extrapolated from a fragment diameter of 100 microns down to 5 microns). As argued in JSC 30000, this baseline is probably the minimum flux. Higher fluxes suggested in JSC 30000 are given by the dashed line (current flux) and by the dotted line (projected for 1990s). The mean mass density of space debris fragments is that of alumimum, 2.7 g cm^{-3} (Cour-Palais, 1987). The impact velocity ranges from about 2 to 16 km s^{-1}; a mean impact velocity of 10 km s^{-1} is assumed in this paper.

Ejecta Particle Generation

Seebaugh and Linnerud (1984) developed a phenomenological model for the ejecta environment created by high-explosive detonations near the Earth's surface. Oberbeck (1977) and others have shown that the crater produced by a hypervelocity impact is similar to that produced by a slightly buried high-explosive charge. It is reasonable, therefore, to expect that the ejecta environments are also similar. With this in mind, we have begun development of a model for the ejecta environment created by the hypervelocity impact of a
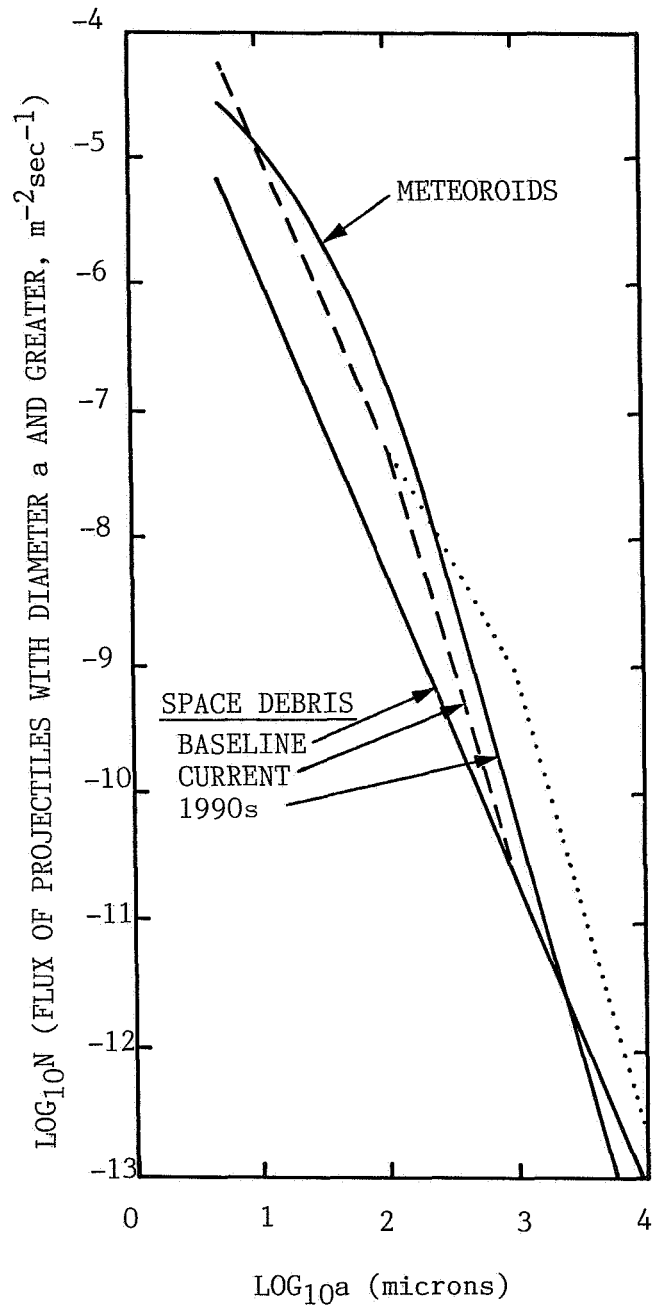
Fig. 1. Flux levels for meteoroids and space debris fragments at an altitude
        of 400 km.

small projectile (meteoroid or orbital debris fragment) on a spacecraft
surface. For the cases modeled, the impact energy is insufficient to cause
spallation of surface material; that is, the target can be considered to be
semi-infinite (Cour-Palais, 1987).

The model development parallels that of Seebaugh and Linnerud (1984), substituting empirical relationships more appropriate to hypervelocity impacts for those developed for explosively generated ejecta. The mass of ejecta created by each projectile impact on a spacecraft surface is given by (Su and Kessler, 1985)

$$M_e = V^2 m \qquad (3)$$

where M_e is the mass of ejecta, V is the impact velocity in km s^{-1}, and m is the mass of the projectile. The mass of the largest ejecta particle created by a hypervelocity impact is given by (Gault et al., 1963)

$$M_m = 0.1 \, M_e. \qquad (4)$$

The cumulative mass of ejecta particles with mass greater than M is given by (Seebaugh, 1977)

$$M_c = M_e [1 - (M/M_m)^{1/6}] \qquad (5)$$

where M is the mass of the particle under consideration. This corresponds to the cumulative number of ejecta particles N_e with mass M or greater

$$N_e = 0.2936 \, (M/M_e)^{-0.8333} - 2 \qquad (6)$$

which is in the form of equation (5) of Su and Kessler (1985). Equation (6) above has the advantage (relative to the distribution of Su and Kessler, 1985) that it gives no particles with mass greater than M_m, which is not the case with Su and Kessler's distribution.

The explosive model of Seebaugh and Linnerud combines relationships equivalent to equations (3)-(6) above with a theoretical description of the ejecta mass as a function of ejection velocity to provide initial conditions for calculation of trajectories of ejecta particles. This approach may also have merit for hypervelocity impacts on spacecraft surfaces; however, insufficient theoretical cratering calculations have been performed for the projectile energies of interest here. Some qualitative conclusions regarding ejecta velocities are advanced herein following the presentation of the results obtained for the particulate environment for Space Station.

Particulate Environment for Space Station

An orbiting platform such as Space Station presents a varying surface area to the highly directional meteoroid flux at varying positions in its orbit. The projected areas of the module cluster of Space Station are approximately 100 m^2 in the direction of the velocity vector, 200 m^2 in the direction normal to the velocity vector and the orbital plane, and 300 m^2 from above or below. For convenience, a representative area of 150 m^2 was used to represent the mean area exposed to the meteoroid flux. The space debris flux is less directional, and it is unlikely that the 300 m^2 upper and lower surfaces would be subjected to this flux. For this reason, the same area, 150 m^2, was used for space debris impact calculations.

Impacts of meteoroids and space debris fragments will occur with spacecraft surfaces at all angles from normal to essentially parallel to the surfaces. The individual impact angles will be highly dependent on the relative directions of travel of the projectiles and the target, and on the local

orientation of the target surface. The number of ejecta particles produced by a given impact will vary with impact angle; however, there is a dearth of data on this effect. Only normal impacts are considered in the present analysis.

The model outlined above was applied to determine the number of ejecta particles generated by meteoroids impacting a 150-m^2 aluminum surface representing Space Station. The impacting meteoroid flux was partitioned into six size classes: 5-10 microns, 10-50 microns, 50-100 microns, 100-500 microns, 500-1000 microns, and 1000-5000 microns. The number of projectiles per orbit for each size class was determined using Figure 1. The ejecta mass for each size class was determined from equation (3) using the mean projectile mass for the size class. The number of ejecta particles generated per orbit was calculated (using the same size classes for these particles) for each representative projectile. Ejecta particles were considered to be released into the hemisphere above the target (2π sr solid angle).

Figures 2 and 3 summarize the number of projectiles with diameter greater than "a" impacting per orbit and the mean number of ejecta particles with diameter greater than "a" created per orbit per sr for the entire array of projectiles, respectively. The solid curves represent the sum of the meteoroid and the baseline space debris fragment environments (corresponding to solid lines of Figure 1). The dashed curves sum the meteorite and current space debris contributions (corresponding to the dashed space debris line of Figure 1). Similarly, the dotted curves represent the sum of the meteoroids and the curve for space debris for the 1990s (see dotted line on Figure 1).

The particulate background limitation (quiescent period) is given in JSC 30426 as one particle 5 microns or larger per orbit per 1 x 10^{-5} sr field-of-view as seen by a 1-meter-diameter aperture telescope. This criterion is represented by the ordinates of the curves in Figure 3 at 5 microns diameter. These particulate backgrounds approach or slightly exceed the JSC 30426 limitation; however, it must be stressed that these results are averages for many orbits. Any given projectile impact will create many more particles than shown in Figure 3 for a short time. For example, an 860-micron space debris fragment (mean diameter for 500-1000 micron size class) creates 6 ejecta particles in the 5 to 10 micron size class per 1 x 10^{-5} sr. The number of small particles generated by a single impact increases as the diameter of the projectile increases. This effect many be limited by phase change phenomena as the impact energy increases. Analysis of this effect is beyond the scope of the present study.

The relatively high ejecta particle density immediately following an impact is mitigated by the relatively low number of impacts occurring during a given time period. For the example given in the preceding paragraph, there are only 0.02 impacts per orbit (on the average) for the 1990s space debris environment. For this scenario, there is an average of just over one impact per orbit of sufficient particle generating capacity to approach the one particle per 1 x 10^{-5} sr limitation.

The ejecta environment caused by meteoroid and space debris fragment impacts on Space Station surfaces may best be described as a moderate density background caused by small (5-50 microns) projectile impacts with occasional spikes caused by larger (50-500 microns) projectile impacts. The spikes will exceed the above criterion for time intervals that depend on the ejection velocities of the particles. As discussed in the Introduction, the model does not currently address this issue. The ejecta particles will leave the target surface with velocities from tens of m s^{-1} to several times the impact velocity relative to the target (Gault et al., 1963), The larger particles will tend to have the lower velocities (Seebaugh, 1977). For order-of-
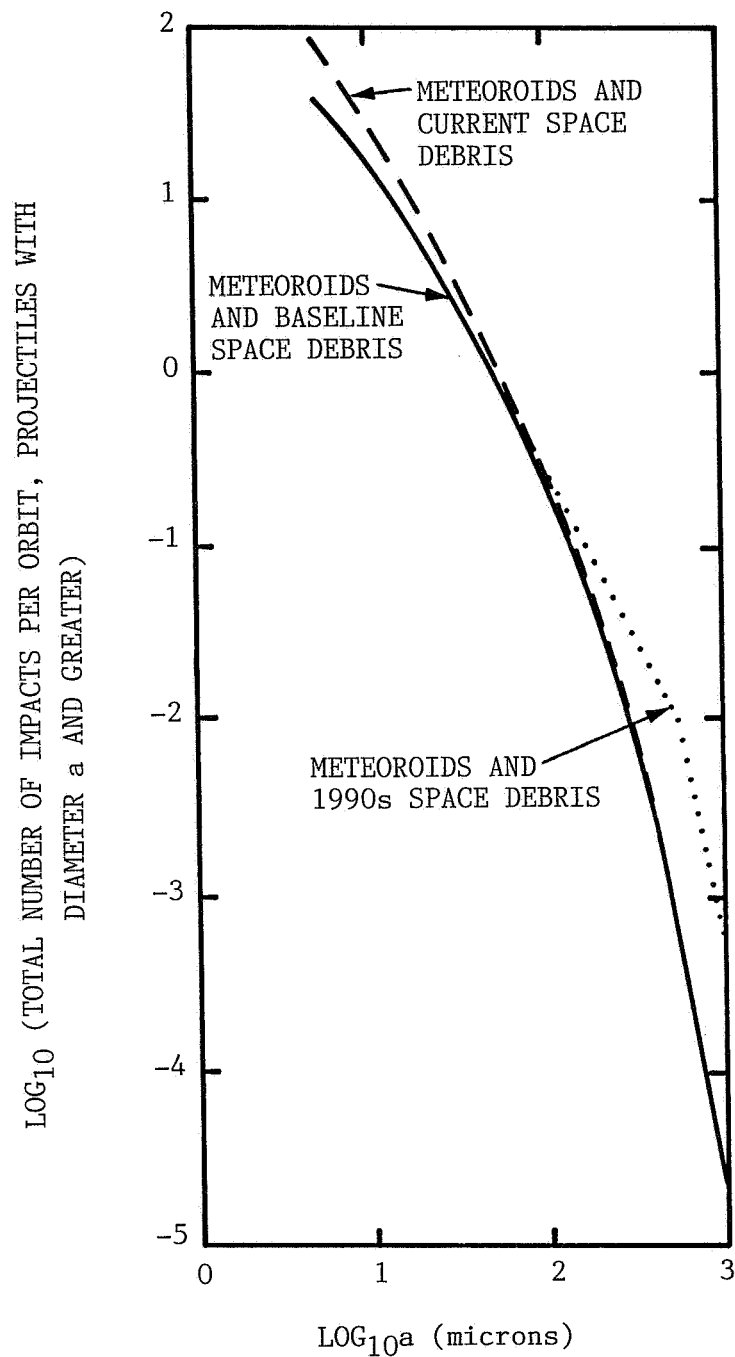
95

Fig. 2. Number of impacts of meteoroids and space debris fragments with 150-m^2 module cluster at an altitude of 400 km.

magnitude analyses, a particle velocity equal to the critical impact velocity (70 m s^{-1} for aluminum targets) may be used (Sewell and Kinney, 1968). If a particular instrument is sensitive to particles to a range of 1 km, then the above limitation would be exceeded for an interval of approximately 15 s following these occasional impact events.
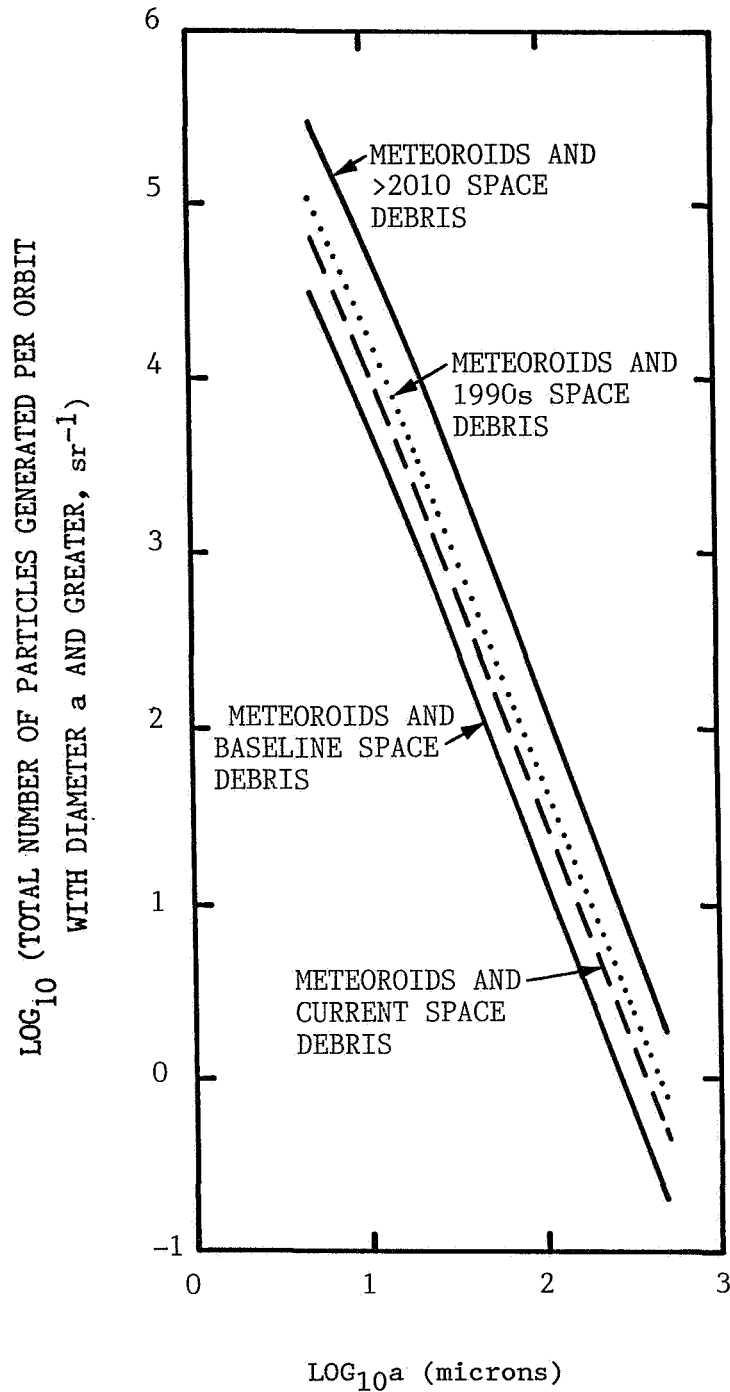
Fig. 3. Total number of ejecta particles generated per orbit per steradian for 150-m^2 module cluster at an altitude of 400 km.

Estimates of future space debris populations (Su and Kessler, 1985) indicate that this population may exceed the meteoroid flux by a substantial amount, perhaps as much as a factor of 10 for years beyond 2010. If this high flux level occurs, the number of ejecta particles generated will increase to the level of the line labeled ">2010" in Figure 3. This particulate environment exceeds the 1 x 10^{-5} sr criterion by a factor of 3.

The planned truss structure for Space Station is an assembly of aluminum-clad composite tubes. Impacts of meteoroids and space debris fragments on the truss structure will produce craters in the cladding. If the craters penetrate through the full depth of the cladding, the composite substrate will be exposed to erosion by atomic oxygen. The projectile diameter required to penetrate 0.018-cm-thick aluminum cladding (LAR-13562) was calculated as a function of projectile velocity and impact angle for meteoroids and space debris fragments (Seebaugh, unpublished). The expected number of impacts resulting in complete penetration of the specified cladding for a truss structure with 17-m^2 cross-sectional area (cross boom configuration for Space Station) are given below for an impact angle of 45° (Cour-Palais, 1987):

Scenario	No. Penetrations Per Year
Meteoroids only	65
Meteoroids with baseline space debris flux	70
Meteoroids with 1990s space debris flux	140
Meteoroids with ">2010" space debris flux	

The lowest value in the above table represents approximately one penetration in each truss member per year. The highest value exceeds 10 penetrations in each truss member per year, or about two penetrations in each meter of truss member length. These values will increase with decreasing thickness of the cladding.

Conclusions

Modeling results show that the mean ejecta density produced by impacts of meteoroids and space debris fragments with Space Station surfaces is from 30% to 100% of the particulate background limitation of 1 particle 5 microns or larger in diameter per orbit per 1×10^{-5} sr. No other particulate sources are included in this estimate, which applies to the 1990s time frame. The uncertainty, which is primarily a result of the lack of information on the space debris flux at Space Station altitude, may be larger than a factor of 3. New knowledge is more likely to increase the estimate of particulate production by impact processes. As a result of future orbital activity, these particulate densities will probably increase by an additional factor of 3 after 2010.

The particulate densities given in the preceding paragraph are mean values over many orbits. Ejecta densities will exceed these mean values following impacts of larger projectiles for a few tens of seconds.

Meteoroids and space debris fragments in the diameter range of 100 to 500 microns produce 80% of the impact generated ejecta. Further work on defining the space debris environment, which is required for many reasons, should provide firmer estimates for the projectile flux in this size range.

Experimental results for hypervelocity impacts of particles in the 5 to 1000 micron range into potential Space Station surface materials are required to increase confidence in the ejecta generation model. This includes determination of ejecta particle sizes and ejection velocities for impact angles from normal to about 75°. The model should be extended to incorporate these data and develop a predictive capability for the attenuation of the

particulate environment following an impact. Monte Carlo calculations, similar to those performed by Su and Kessler (1985), would be useful in determining how the variations in projectile flux with time, relative velocities between spacecraft and projectiles, and spacecraft surface orientation affect the particulate environment.

Composite structural members with thin metallic cladding will be vulnerable to atomic oxygen erosion at the locations of impact craters which completely penetrate the cladding. Impacts of larger projectiles will produce both metallic and non-metallic ejecta (the latter from the substrate). The estimated number of penetrations for 0.018-cm-thick aluminum cladding is from about 60 to 140 per year during the 1990s, increasing to about 740 per year after 2010.

Co-orbiting platforms with smaller cross sections than Space Station will have proportionally less severe particulate environments associated with impact ejecta. If these platforms use cladded composite structural members, they will be vulnerable to atomic oxygen erosion to the same degree as Space Station.

References

Contamination Control Requirements Document, NASA, JSC-30426, 1986.
Cour-Palais, B.G., Hypervelocity impact in metals glass and composites, Int. J. Impact Engrg., 5, 221, 1987.
Gault, D.E., E.M. Shoemaker, and H.J. Moore, Spray Ejected from the Lunar Surface by Meteoroid Impact, NASA TN-D-1767, 1963.
Oberbeck, V.R., Application of high explosive cratering data to planetary problems, in Impact and Explosion Cratering, edited by D.J. Roddy, R.O. Pepin, and R.B. Merrill, Pergamon Press, New York, p. 45, 1977.
Seebaugh, W.R., A dynamic crater ejecta model, in Impact and Explosion Cratering, edited by D.J. Roddy, R.O. Pepin, and R.B. Merrill, Pergamon Press, New York, p. 1043, 1977.
Seebaugh, W.R., and H. J. Linnerud, Crater ejecta environment from near-surface high-explosive detonations, Int. J. Impact Engrg., 2, 239, 1984.
Space Station Program Office, Space Station Program Definition and Requirements, Section 3: Space Station System Requirements, Appendix A: Natural Environment Definition for Design, NASA, JSC 30000, Sec. 3, App. A (JSC 30425), 1986.
Sewell, R.G.S., and G.F. Kinney, Response of structures to blast: A new criterion, Annals N.Y. Academy, 152, 532, 1968.
Su, S.-Y., and D.J. Kessler, Contribution of explosion and future collision fragments to the orbital debris environment, Adv. Space Res., 5, 25, 1985.
Technical Support Package, Metal-Clad Graphite/Epoxy Tubes, NASA, LAR-13562, undated.

CONTAMINATION OF OPTICAL SURFACES

Graham S. Arnold and David F. Hall

Chemistry and Physics Laboratory
The Aerospace Corporation
P.O. Box 92957
Los Angeles, CA 90009

Introduction

Self-contamination has long been recognized as potentially limiting the performance and ultimately the useful life of spacecraft. Demands for increasing system lifetimes have increased the need for understanding and control of contamination. The proposed NASA Space Station, with its requirement for 30 years performance, has potentially the most challenging contamination requirements ever to be considered.

If the Space Station is to provide a clean and durable environment for research in space science, Earth observation, and space exploration, then contamination control must be considered continuously, from the very outset in defining and refining the Space Station configuration. This workshop, and the efforts of other workshops and working groups, stand in recognition of this fact. Furthermore, the very performance life of major elements of the Space Station itself will be limited if contamination control is not effectively implemented.

This paper addresses the effect of molecular contamination on Space Station optical surfaces. One can imagine all sorts of optical surfaces which might populate the Space Station at some time in its life. The examination in this paper will be primarily directed at two sorts: solar voltaic power sources and optical solar reflectors for thermal control or solar dynamic power generation. The effect of contaminants on optical surfaces has been the subject of multiple theoretical, laboratory, and space flight investigations. An exhaustive review of these various investigations is clearly beyond the scope of this short paper. Rather, an examination of the published Space Station requirements for molecular contamination accretion and for the monitoring of such accretion will be discussed, in the context of the historical performance of space systems.

The ML12 experiment which is flying on the USAF Space Test Program's P78-2 vehicle, more commonly known by the acronym SCATHA (Spacecraft Charging at High Altitudes), provides a benchmark against which satellite contamination performance can be judged. This experiment has provided some 7 years worth of data on contamination accretion and thermal control coatings performance in the geosynchronous environment. A bibliography of papers, presentations, and reports describing this data base appears at the end of this paper.

Contamination Accretion

The requirement for molecular contamination by and on the Space Station (Aaron, 1986) is:

The flux of molecules emanating form the core Space
Station must be limited such that... The mass
deposition rate on two 300 K surfaces both located at
the PMP with one perpendicular to the +Z axis and the
other whose surface lies ... at critical power
locations with an acceptance angle of 2 π sr shall
be no more than 1 $\times$ 10^{-14} g cm^{-2}s^{-1} (daily average).

Comparison of this requirement to the performance of actual satellite
systems reveals that it is an ambitious requirement, indeed. Table 1 shows
such a comparison.

Table 1. Comparison of Spacecraft Contamination Accretion
to the Space Station Requirement.[*]

	dM/dt (g cm^{-2} s^{-1})	dx/dt[+] (Å yr^{-1})	dα/dt (Å yr^{-1})	Solar Array Loss[#] (% yr^{-1})
Space Station budget	1 $\times$ 10^{-14}	30	0.0003	0.015
SCATHA belly band TQCM	6 $\times$ 10^{-14}	190	0.002	0.1
Typical OSR radiator	6 $\times$ 10^{-13}	1900	0.02	1
Sunlit, vent-viewing OSR	1.2 $\times$10^{-12}	3800	0.04	2
Mature, large satellite	2 $\times$ 10^{-13}	600	0.007	0.35

[*]dα/dx = 0.001/100 Å assumed, measured/specified property underlined
[+]Assuming a density of 1 g cm^{-3}
[#]100(dα/dt)/2

This comparison shows contaminant mass accretion rates for the Space Station
requirement (Aaron, 1986) and the deposition rate on a quartz crystal
microbalance on the SCATHA ML12 experiment (Hall, 1982) along with fused
silica mirror degradation rates for SCATHA, typical geosynchronous satellite
silica mirror radiator performance (D. Gluck, private communication, 1982),
degradation of a warm, vent-viewing, sunlit radiator in elliptic Earth orbit
(Hall et al., 1985), and the performance of the cold radiator on a large,
mature (late edition) geosynchronous satellite (Hall et al., 1985; D. Gluck,
private communication, 1982).

For the purposes of this comparison, the solar absorptance increase has been related to the mass accreted by the simple, linear approximation of

$$d\alpha/dx = 0.001/100 \text{ Å} \qquad (1)$$

which results from the SCATHA experiment (Hall, 1982) The measured, or specified quantity shown in Table 1 is underlined. (There is some room for debate on the exact value of the proportionality constant in equation (1), but this debate does not affect the qualitative conclusions on draws from Table 1.) Spacecraft radiator degradation can be simply related to the increase in solar absorptance (Kan, 1985), as can be the decline in solar dynamic power production. The decay of solar voltaic power generation is approximately one half the increase in solar absorptance (of a solar reflector) (D. Marvin, private communication, 1987).

Note that the quartz crystal microbalance on SCATHA had a very small portion of its field-of-view filled with potential outgassing sources. Note further that the solar absorptance data shown in Table 1 are for fused silica mirror radiators, which are not subject to degradation in solar absorptance as a result of natural geosynchronous radiation damage (Kan, 1985).

The lessons to be gleaned from the information summarized in Table 1 are:

(1) The Space Station specification requires a vehicle environment which is substantially cleaner than experienced by the nearly clear field-of-view SCATHA contamination monitor.

(2) The typical performance of geosynchronous spacecraft radiators of fused silica is dramatically worse than required by Space Station.

(3) Sunlit silica surfaces which are warm in comparison to the typical radiator but which have a direct view of major spacecraft vents accrete even more deleterious contamination by photochemical deposition.

(4) Mature satellite programs can effect substantial reduction in contamination (by a combination of materials control and re-direction or sealing of spacecraft vents).

A reminder that contamination is a space system problem is provided by the experience of the Space Shuttle (McKeown et al., 1985; Miller, 1983). Table 2 shows the rate of contamination of 273 K surfaces (of various orientation) on the Induced Environment Contamination Monitor on four flights of the Shuttle. The accretion rates on the the early flights define a contamination level inherent to a relatively empty Shuttle bay. The STS-9 Spacelab flight shows that loading the bay with a variety of experimental hardware can seriously degrade the environment.

Table 2. Space Shuttle Induced Environment Contamination
Monitor Contamination Rates for a 273 K Surface.

Mission	Contamination Rate[*] (Å hr^{-1})				
	-X	+X	-Y	+Y	-Z
STS-2[+]	0.9	3.5	-.2	1.5	
STS-3[+]	3.8	6.0	1.9	2.2	2.8
STS-4[+]	0.9	1.2	0.9	0.6	0.4
STS-9[#]	0.7	16.4	6.7	3.1	0.5

[*]For various sensor orientations (vehicle fixed coordinates)
[+](Miller, 1983)
[#](McKeown et al., 1985)

Contamination Monitoring

The Space Station requirements document (Aaron, 1986) states that

...monitoring of the environment to a limited extent will be
required. Verification and monitoring measurement requirements
shall consider ... molecular and particulate deposition ... and
returned gas flux.

It is conventional to use 10 MHz quartz crystal microbalances (QCM) for
monitoring molecular contamination rates. These devices have a sensitivity of
about 4.4 ng cm^{-2} Hz^{-1}. The Space Station mass accretion rate requirement
therefore corresponds to about 70 Hz/year decrease in QCM frequency. One
usually measures the beat frequency between two quartz crystals, one exposed
to the contaminant flux and one shielded, to enhance the sensitivity of the
QCM. Even so, one must anticipate QCM frequency/temperature coefficients on
the order of ± 5 Hz/K. Although the nature of long-term fluctuations in QCM
frequency is not well understood, one can expect slow drift on the order of ± 1
Hz/week in QCM beat frequency (D. F. Hall, private communication, 1987).
Therefore, even monitoring the required contamination level on Space Station
will be difficult if straightforward conventional approaches are used.

Conclusions

The Space Station contamination requirements are so stringent that they
cannot be approached without considering contamination at every step in the
design of the Station. Numerical contamination models of proposed geometries
should be assembled early and exercised often, as the basis for estimating the
contamination risk presented by a given geometry or operation. Such models
have been described by Fong et al. (1987) and elsewhere in this volume.

Furthermore, a contamination model of the final configuration can serve as a guide for locating contamination monitoring devices near major sources of contamination, and interpreting the impact on sensitive surfaces. In this way, one can hope to provide a monitoring system which provides early warning of problems.

Because the Space Station requirements are so stringent, the generosity in margin and systematic error in contamination predictions that have been used in the past may no longer be acceptable. This means that modeling must incorporate more physically realistic information. In addition to the obvious requirements for more accurate and detailed data on outgassing and thermal/vacuum aging of materials, models must include (substrate temperature dependent) photochemical deposition and a better accounting of non-line-of sight (NLOS) contaminant transport.

The mass accretion on the SCATHA QCM is a case in point. First, is the preponderance of the detected mass accreted by photochemical deposition. Second, one is unable to account for the mass deposition rate measured, by many orders of magnitude, if one uses simple models of NLOS transport by contaminant self-scatter described by Scialdone (1983).

More elegant contamination modeling tools have been developed, the code SPACE II being one well-known example (Bareiss et al., 1987). This sort of code is a powerful tool, indeed. However, one must recognize that at the current state-of-the-art even these powerful tools have their limitation. For example, SPACE II accounts for a significant source of NLOS transport in low Earth orbit with which the Space Station must contend: atmospheric return flux. The validity of SPACE II predictions of return flux were tested on the Atmosphere Explorer (AE) satellite (Bareiss et al., 1987). The test was to measure the return of vented neon by mass spectrometry. The SPACE II prediction overestimated the return flux by 50%. Note that rare gas scattering by the atmosphere around a small vehicle like AE is probably the least stringent test of the scattering dynamics approximations conventionally used in contamination codes. Herm et al. (1987) and Harvey and Herm (1981) have demonstrated the risk in using simple hard-sphere scattering models for spacecraft design, even for helium-ambient collisions.

The comments in the previous paragraph are not intended to be specific criticisms of SPACE II, but rather to point out that the current state of contamination modeling admits to uncertainties which may loom large when one tries to meet the Space Station design requirement. Improvement in modeling, and verification of models with more realistic tests (for example with hydrocarbon rather than rare gas vents, with long-term instrumented vehicle tests, and with laboratory measurement of reactive, elastic, and inelastic scattering cross sections), would facilitate the assignment of margins in contamination budgeting.

Furthermore, an improvement in the state of understanding of contaminant effects would help in the design of the Space Station. The uncertainty in the thickness dependence of contaminant solar absorptance was mentioned above is a case in point. This uncertainty currently stands at about an order of magnitude (Hall, 1982). Therein lies an order of magnitude in contamination budget margin. This subject, too, admits to further laboratory and space flight research.

Summary

The Space Station requirements for performance life and cleanliness are among the most stringent ever considered for a space vehicle. The historical experience of space systems suggests that the contaminant mass accretion rate required for the Space Station will be extremely difficult to realize. Therefore, these requirements mandate the quantitative consideration of molecular contamination at every stage of Space Station design.

There is an active national effort of space flight and laboratory research in the various aspects of spacecraft self-contamination. It is clear that the Space Station can benifit from these efforts. However, the specific requirements of orbit, size, and lifetime of the Space Station may warrant an advance in the quantitative understanding of non-line-of-sight contaminant transport, of contamination effects, and in verification of modeling techniques.

Bibliography of the SCATHA ML12 Experiment

D.F. Hall and A.A. Fote, Long-term performance of thermal control coatings at geosynchronous altitude, AIAA Paper 86-1356, AIAA/ASME 4th Joint Thermophysics and Heat Transfer Conference, Boston, Massachusetts, June 1986.

D.F. Hall, T.B. Stewart and R.R. Hayes, Photo-enhanced spacecraft contamination deposition, in Proceedings of the Third European Symposium on Spacecraft Materials in the Space Environment, ESA SP-232, pp. 39-47, Noordwijk, The Netherlands, October 1985.

D.F. Hall, T.B. Stewart and R.R. Hayes, Photo-enhanced spacecraft contamination deposition, AIAA Paper 85-0953, AIAA 20th Thermophysics Conference, Williamsburg, Virginia, June 1985.

A.L. Vampola, P.F. Mizera, H.C. Koons, J.F. Fennell, and D.F. Hall, The Aerospace Spacecraft Charging Document, SD-TR-85-26, June 1985.

D.F. Hall and J.N. Wakimoto, Further flight evidence of spacecraft surface contamination rate enhancement by spacecraft charging, AIAA Preprint 84-1703, AIAA 19th Thermophysics Conference, Snowmass, Colorado, June 1984.

D.F. Hall and A.A. Fote, $\Delta\alpha_s/\Delta\varepsilon_H$ measurements of thermal control coatings over four years at geosynchronous altitude, Progress in Astronautics and Aeronautics, 91, 215-234, 1984.

D.F. Hall, ML12 Spacecraft Contamination and Coatings Degradation Flight Experiment, AFWAL TR-83-4140, December 1983.

D.J. Carre and D.F. Hall, Contamination measurements during operation of hydrazine thrusters on the P78-2 (SCATHA) Satellite, J. Spacecraft & Roc., 20, 444-449, 1983.

D.F. Hall, Current flight results from the P78-2 (SCATHA) Spacecraft Contamination and Coatings Degradation Experiment, in Proceedings of the ESA/CNES/CERT International Symposium, Spacecraft Materials in the Space Environment, ESA SP-178, pp. 143-148, Toulouse, France, June 1982.

A.A. Fote and D.F. Hall, Contamination measurements during the firing of the Solid Propellant Apogee Insertion Motor on the P78-2 (SCATHA) Spacecraft, Proceedings of the SPIE, Vol. 287, pp. 95-101, 1982.

D.F. Hall and A.A. Fote, $\Delta\alpha_s/\Delta\varepsilon_H$ measurements of thermal control coatings on the P78-2 (SCATHA) Spacecraft, Progress in Aeronautics and Astronautics, 78, 467-486, 1981.

H.A. Cohen, D.F. Hall, et. al., P78-2 Satellite and payload responses to electron beam operations on 30 March 1979, in Proceedings of the Third AF/NASA Spacecraft Charging Technology Conference, NASA CP-2182, pp. 509-560, November 1980.

D.M. Clark and D.F. Hall, Flight evidence of spacecraft surface contamination rate enhancement by spacecraft charging obtained with a quartz crystal microbalance, in Proceedings of the Third AF/NASA Spacecraft Charging Technology Conference, NASA CP-2182, pp. 493-508, November 1980.

H.C. Koons, P.F. Mizera, J.F. Fennell, and D.F. Hall, Spacecraft charging - Results from the SCATHA Satellite, Astronautics and Aeronautics, 18, November 1980.

D.F. Hall, Flight experiment to measure contamination enhancement by spacecraft charging, in Proceedings of the SPIE, Vol. 216, pp. 131-138, 1980.

D.F. Hall and A.A. Fote, Preliminary flight results from the P78-2 (SCATHA) Spacecraft Contamination Experiment, invited paper to ESTEC Symposium on Spacecraft Materials in Space Environment, Noordwijk, Holland, in ES SP-145, pp. 81-90, October 1979.

D.F. Hall, E.N. Borson, R. Winn, and W. Lehn, Experiment to measure enhancement of spacecraft contamination by spacecraft charging, in AIAA 8th Space Simulation Conference, NASA SP-379, pp. 86-107, Silver Spring, Maryland, November 1975.

D.F. Hall and W.C. Lyon, Low thrust propulsion system effects on communication satellites, Progress in Astronautics and Aeronautics, 33, MIT Press, 1974.

References

Aaron, J.W., Space Station Program Office Space Station External Contamination Control Requirements, NASA Johnson Space Center, JSC 30246, November 19, 1986.

Bareiss, L.E., R.M. Payton, and H.A. Papazian, Shuttle/Spacelab Contamination Environment and Effects Handbook, NASA Contractor Report 4053, Martin Marietta Aerospace Denver Division, Denver, Colorado, March 1987.

Fong, M.C., A.L. Lee, and P.T. Ma, External Contamination Environment of Space Station Customer Servicing Facility, AIAA Paper 87-1623, AIAA 22nd Thermophysics Conference, Honolulu, Hawaii, June 8-10, 1987.

Hall, D.F., Current flight results from the P78-2 (SCATHA) spacecraft Contamination and Coating Degradation Experiments, in Proc. Int. Symp. on Spacecraft Materials in the Space Environment, ESA SP-178, pp. 143-148, 1982.

Hall D.F., T.B. Stewart, and R.R. Hayes, Photo-Enhanced Spacecraft contamination deposition, AIAA Paper 85-0953, AIAA 20th Thermophysics Conference, Williamsburg, Virginia, June 19-21, 1985.

Harvey, N.M., and R.R. Herm, Helium Purge Flow Prevention of Atmospheric Contamination of the Cryogenically Cooled Optics on Orbiting Infrared Telescopes: Calculation of the He-O Differential Cross Section, SD-TR-81-53, The Aerospace Corporation, El Segundo, California, June 5, 1981.

Herm, R.R., B.R. Johnson, and S.J. Young, Prevention of Primary Mirror Contamination by Helium Purging, SD-TR-87-17, The Aerospace Corporation, El Segundo, California, February 27, 1987.

Kan, H.K.A., Space environment effects on spacecraft surface materials, in Proc. SPIE, 541, 164-179, 1985.

McKeown, D., J.A. Fountain, V.H. Cox, and R.V. Peterson, Analysis of TQCM surface contamination adsorbed during the spacelab 1 Mission, in Proceedings of the AIAA Shuttle Environment and Operations II Conference Houston, pp. 108-115, Texas, November 13-15, 1985.

Miller E.R., Update of Induced Environment Contamination Monitor Results, AIAA Paper 83-2582-CP, AIAA Shuttle Environment and Operations Conference, Washington, D.C., October 31-November 2, 1983.

Scialdone, J.J., Shuttle Measured Contaminant Environment and Modeling for Payloads, AIAA Paper 83-2583-CP, AIAA Shuttle Environment and Operations Meeting, Washington, D.C., October 31-November 2, 1983.

SURFACE INTERACTIONS RELEVANT TO SPACE STATION CONTAMINATION PROBLEMS

J. T. Dickinson

Department of Physics
Washington State University
Pullman, WA 99164-2814

Abstract. The physical and chemical processes at solid surfaces which can contribute to Space Station contamination problems are reviewed. Suggested areas for experimental studies to provide data to improve contamination modeling efforts are presented.

Introduction

A number of consequences have been recognized as serious and problematic in terms of contamination and materials degradation from placing platforms and vehicles in various earth orbits. (Roux and McKay, 1984; Leger et al., 1986; Bareiss, 1987).

Identified Sources of Contamination:

■ outgassing, leaks, dumping, and thruster engine firing

■ interaction of "source" surfaces with above

■ the ambient space environment ($h\nu$, e^-, $\pm$ions, neutrals)

■ interaction of "source" surfaces with environment

■ possible electrostatic discharges

■ mechanical failure (microcracking, fracture, spallation)

Consequences:

■ "space-phase" particles and particulates (=>absorption, glow, etc.)

■ condensation/deposition on "receiving" surfaces

■ modification/degradation of surfaces-materials (roughness, optical, electrical, mechanical properties)

■ charging

Figure 1 shows schematically the surface interactions in a general sense that contribute to the emission or uptake of matter at a substrate. Surface Science has traditionally focused on: (1) describing, quantifying, and explaining phenomena, and (2) surface analysis (quantitative and qualitative analysis). Although the latter can contribute to our understanding of the

contamination-surface effects, the former is more important.
Also, it should be emphasized that both surface and near surface
phenomena need to be considered and coupled. For relatively
simple processes, we might expect:

Emission OR Condensation/Absorption Probability =

f (Flux$_P$, Energy$_P$, Concentration$_A$, Temperature, Surface   (1)
    Roughness, Mechanical Stress, Relevant Cross ·
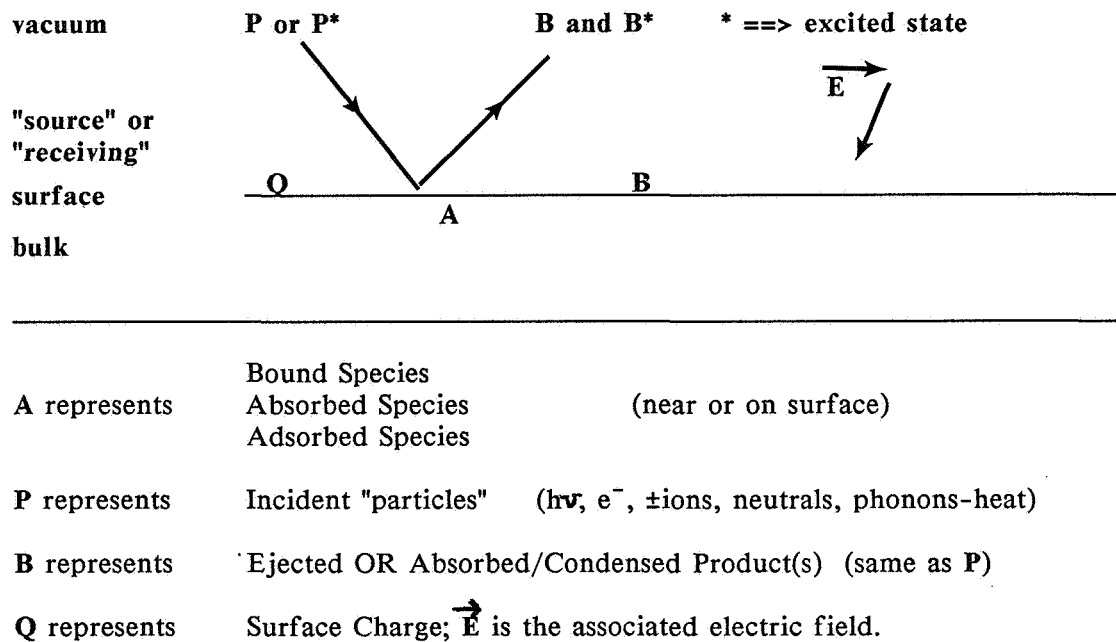   Sections, Activation Energies, Rate Constants).

vacuum   P or P*   B and B*   * ==> excited state

"source" or
"receiving"

surface   Q_____B_____

bulk

A represents   Bound Species
                Absorbed Species   (near or on surface)
                Adsorbed Species

P represents   Incident "particles"   ($h\nu$, e^-, $\pm$ions, neutrals, phonons-heat)

B represents   Ejected OR Absorbed/Condensed Product(s) (same as P)

Q represents   Surface Charge; $\vec{E}$ is the associated electric field.

Fig. 1.   Schematic of possible interactions with a surface that
          can lead to the release of particles.

Thus, quantitative predictions may require a detailed
understanding of the physics and chemistry of the process as well
as the appropriate parameters and constants.   In many cases,
synergisms (e.g., Effect of (P_1 + P_2) >> Effect of P_1 + Effect of
P_2), internal electronic/rotational/vibrational energy, angles of
incidence, and interfaces (e.g., coating/substrate interface) may
also have to be considered.   As an example, it is entirely
possible that simultaneous electron bombardment and O atom
exposure would result in significant increases in the oxidation
of a polymer.
For modeling purposes, empirical equations might suffice to
predict relatively complicated effects.   An example might be the
outgassing rate of volatile compounds from a thermally cycling

polymer matrix or the production of decomposition products from fast atom bombardment of a polymer. Of utmost importance is to be able to predict the rates of emission/uptake, the direction and velocity of the emission, the sticking probability of a emitted species at another surface, and the possible changes in properties caused by the presence of this new species.

Important Surface Phenomena are listed in Table 1.

Table 1. Important Surface Phenomena which can play a role in Contamination Processes.

Equilibrium Processes:

Permeation and diffusion (may be rate limiting in many processes) (Jost, 1952)

Adsorption (physisorption, chemisorption), absorption, desorption, sublimation   (thermally regulated) (Redhead et al., 1968)

Catalytic Reactions (Somorjai, 1981)

Non-equilibrium Processes:

"Hot" atom, ion, and radical/surface reactions including activated adsorption/desorption (Ceyer et al., 1987)

Electron and photon induced desorption (Knotek, 1984)

Electron, ion, and photon induced/enhanced chemistry (Chuang, 1981)

Photoelectron and secondary electron emission (Cardona and Ley, 1978)

Chemically and radiation induced luminescence/electron emission from surfaces (Chen and Kirsh, 1981)

Sputtering (Stuart, 1983)

Emission of excited and/or reactive species (Hagland and Tolk, 1986)

Radiation induced polymerization and cross-linking of organic molecules (Wright, 1978)

Incident particle/stressed substrate interactions (Dickinson, 1987)

Electrostatic breakdown (Kendall et al., 1986)

The phenomena listed under Equilibrium Processes are well known; diffusion and the ad(b)sorption/desorption phenomena

111

certainly are critical in the outgassing and build-up of contamination layers on exposed surfaces. The catalytic behavior of metals and metal oxide surfaces should not be ignored if large areas of such materials come under consideration, particularly in possible reactions involving oxygen, hydrogen, nitrogen, and water.

Under Non-Equilibrium Processes, we have listed a set of irreversible phenomena, usually involving incident particles with non-thermal internal/translational energies. Space limitations do not allow a detailed description of all of these effects to be given here; references have been cited for obtaining additional information.

Examples and Discussion

A simple example of a non-equilibrium process is the emission of electrons from a polymer surface exposed to UV radiation. For illustration we consider the polymer Kapton-H and radiation consisting of pulses of 248 nm Excimer laser light (20 ns pulse width). Figure 2 shows the time-of-flight of the electrons over a distance of 5 cm, digitized at 5 ns/channel. (Tonyali et al., 1988). The data were taken for unstressed and stressed material, showing that the elongated Kapton actually yields considerably more photoelectrons. The sources of these charged particles are weakly bound electrons in electron traps located above the valence band of the polymer. In this case, mechanical stress in the presence of intense 248 nm radiation
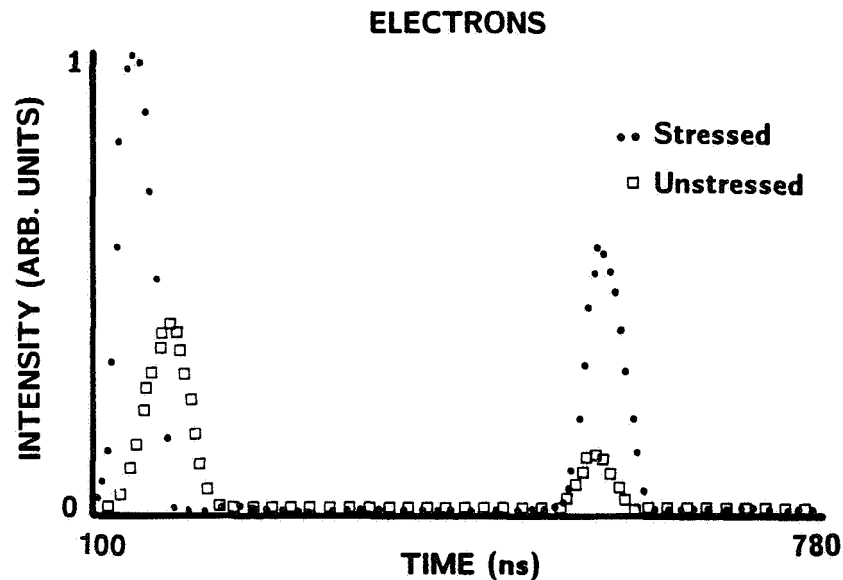

Fig. 2.   Electron emission TOF spectrum of stressed and unstressed Kapton-H samples. The specimens were elongated to 70% strain and then subjected to 0.7 J cm^{-2} pulsed laser radiation @ 248 nm.

significantly alters the population of these states. For a given density of trapped electrons in a single state, n_e, the yield of photoelectrons is first order in the photon flux. If $h\nu$ is larger than the binding energy of this state, the yield is weakly dependent on hv, particularly over the range of the solar spectrum. Thus, if we assume that n_e is constant, the photoelectron yield, Y, is simply:

$$Y = (\text{fluence}) \ (\text{"cross-section"}) \ n_e \quad\quad (2)$$

Einstein's equation predicts the energy of the photoelectrons:

$$E = h\nu - E_b. \quad\quad (3)$$

The UV photon flux incident on an orbiting structure should be fairly accurately known and cross-sections could be measured. Correct modeling of the yields of emission of such charge would require relatively accurate n_e.
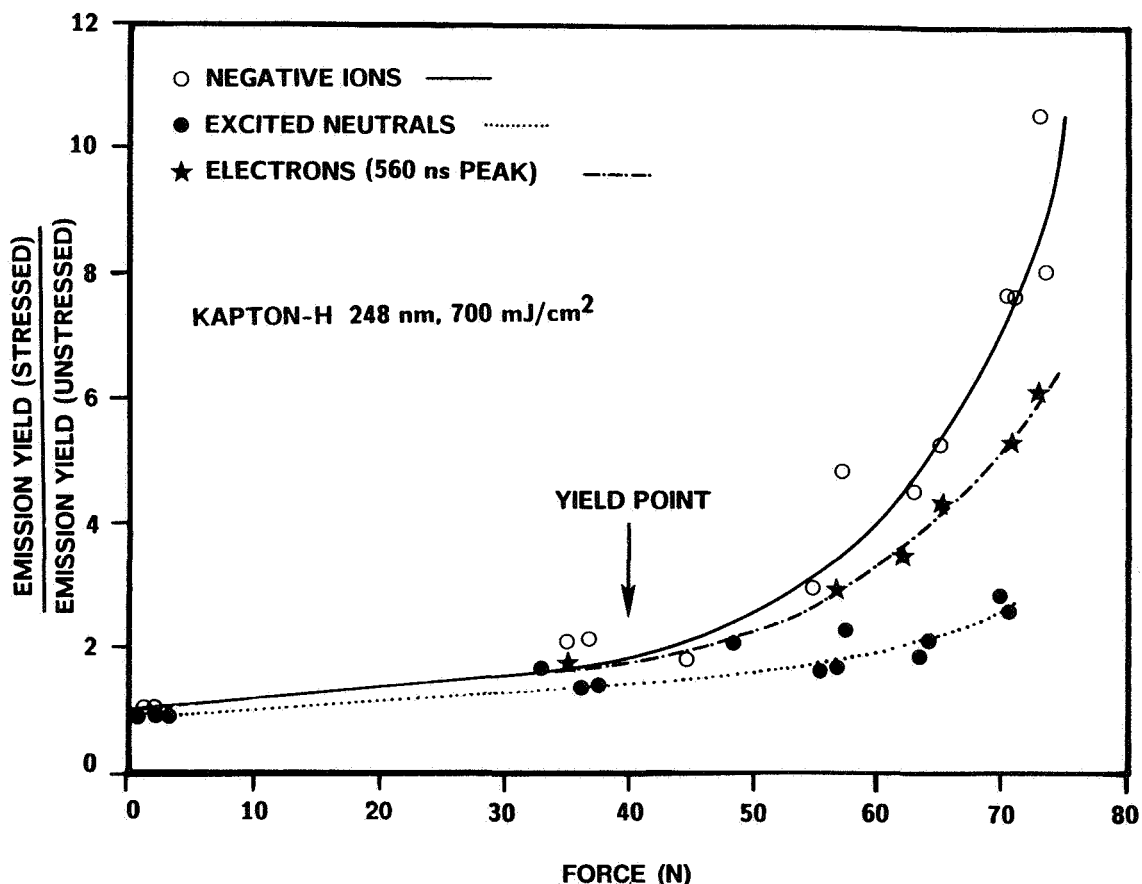
Fig. 3. The effect of an applied force on the negative ion, electron, and excited neutral emission yield. The laser fluence to the sample was 0.7% J cm^{-2} @ 248 nm.

We have also shown (Tonyali et al., 1988) that mechanical deformation influences the yield of other products of UV laser bombardment at 248 nm of Kapton-H. Figure 3 shows the dependence of the negative ions, excited neutrals, and one of the electron peaks (at 560 ns), all showing increases with applied force, particularly at forces beyond the onset of plastic deformation of the Kapton. The emitted negative ions are principally in the region of mass 28.

Another example of an electron emission process involving traps is thermally stimulated electron emission (TSEE). If a wide bandgap material (e.g., ceramic, glass, polymer) is irradiated with electrons, x-rays, ions, etc. of sufficient energy to create defects such as color centers and free radicals, trapped charge can be stimulated thermally to react with these defects. Energy that is released during this reaction can result in luminescence (radiative decay) or electron emission (via an Auger process). An example of the latter is shown in Figure 4a,

ELECTRONS FROM BR AFTER BOMBARDMENT

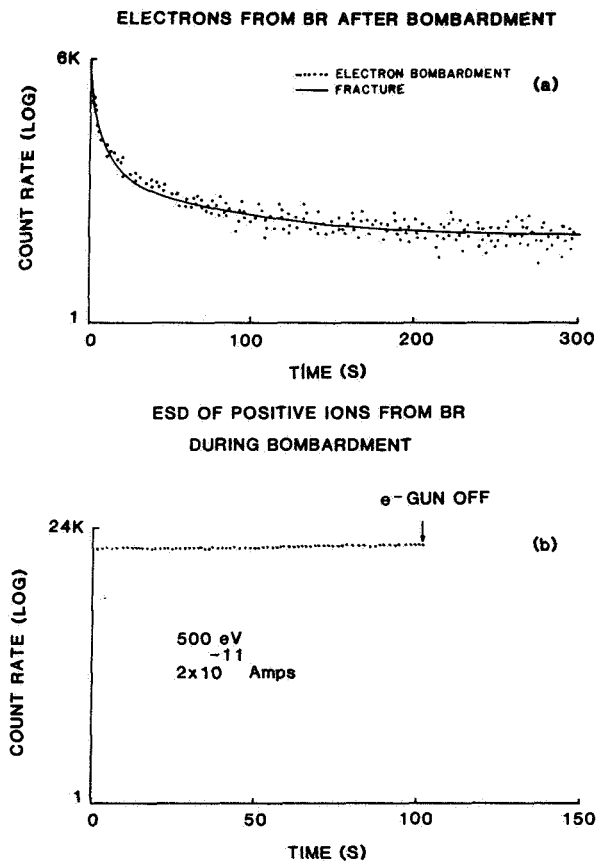**ESD OF POSITIVE IONS FROM BR**
DURING BOMBARDMENT

Fig. 4.   (a) Emission of electrons from a thin film of polybutadiene (BR) following bombardment of the film with 500 eV electrons(...). The solid line is a typical fracto-emission (electrons) curve following fracture of BR, normalized at a single point. (b) Electron stimulated desorption of positive ions during bombardment of the BR with 500 eV electrons at 2 x 10^{-11} A.

114

where an elastomer surface (polybutadiene) has been irradiated
with 500 eV electrons (2 x 10^{-11} Amps) for a few seconds only
(Dickinson and Jensen, 1985). The TSEE which follows this
bombardment is shown; it decays away according to a well
described set of equations (Halperin and Braner, 1960) involving
moving trapped electrons to recombination sites near and on the
surface of the polymer. If we now thermally stimulate the
material with a linear temperature sweep, we obtain a "glow-
curve" in the emitted electrons which give the activation energy
for mobilizing the electrons, in this case 0.6 eV. If we observe
the surface with a detector sensitive to positive ions, we see
that during bombardment, we see electron stimulated desorption of
positive ions (Figure 4b) which disappears immediately when the
electron current is turned off. Although we did not measure the
mass of these ions at the time, from other work we have done on
similar polymers, a likely candidate is H^+. The ion yields for
this particular experiment were 2 x 10^{-4} ions/electron.

Catalytic reactions involving oxygen may be important on
inorganic substrates, e.g., metal oxides. As an example of a
surface science experiment involving a clean metal surface, we
examine the oxidation of CO on the surfaces of small, supported
Rh particles. The method used involves chemisorbing a saturated
layer of oxygen on the Rh, then quickly introducing a step
function of CO partial pressure above the sample. A quadrupole
mass spectrometer monitors the resulting desorbed CO_2, shown in
Figure 5 for four different metal particle sizes. This type of
data can assist in working out the reaction mechanisms. In this
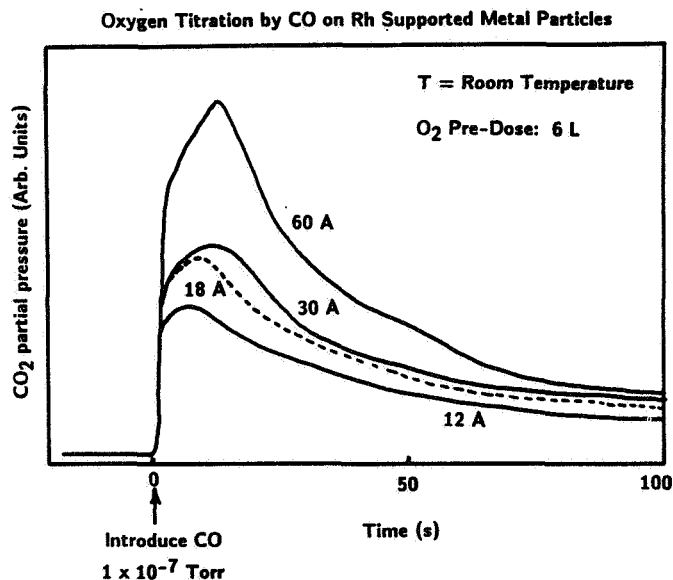case, all of the data can be computer-fit very well by a simple

Fig. 5. CO_2 partial pressure produced by the titration of
           O(ads) by CO(gas) from the surface of small Rh metal
           particles supported on an oxide substrate. The
           different curves represent different average particle
           sizes.

Langmuir-Hinshelwood mechanism (CO_{ad} reacting with O_{ad}) and yields absolute reaction rates.

A surface process that is analogous to chemiluminescence was studied in much the same way for the system involving the chemisorption of molecular fluorine on tungsten. One finds that when the clean surface is exposed to a beam of F_2, electrons are emitted during the uptake of the fluorine. In Figure 6, we show the resultant electron emission vs. time at three different substrate temperatures (Loudiana et al., 1985). The lines represent a model we developed for fitting these emission vs. time curves. The mechanism involves a dynamic electronic transition resulting in an excited surface intermediate that can again decay via the emission of a photon or an electron. The temperature dependence (increased yield with increasing temperature) is a consequence of raising the electron energies above the Fermi level in the metal, making them easier to eject into the vacuum. The number of electrons emitted/adsorbed atom
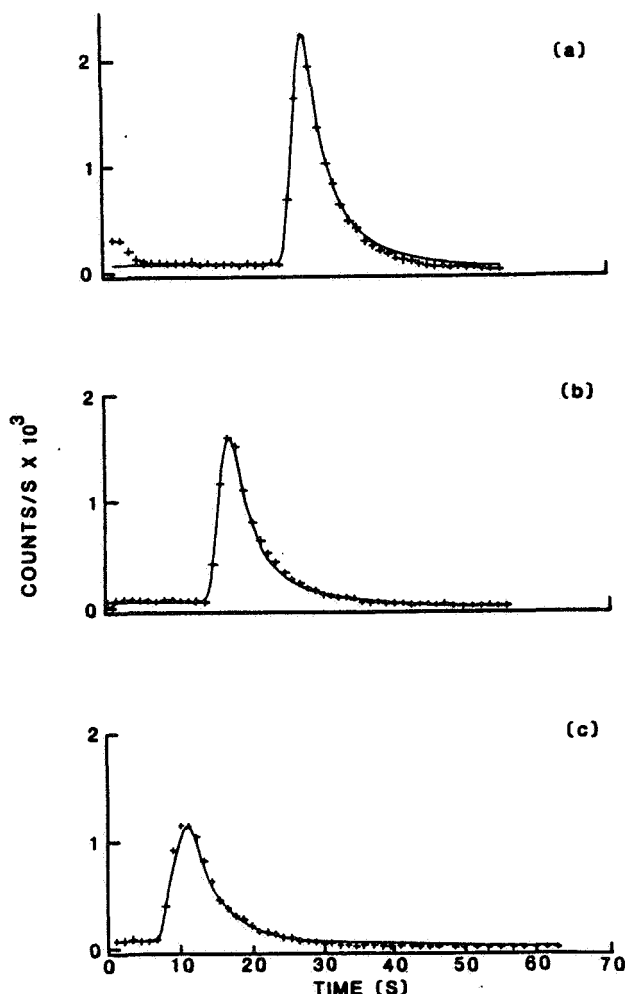

Fig. 6. Chemisorptive electron emission created by exposing a clean W metal surface to nearly a step function of F_2(gas). The three curves are for different W surface temperatures; the largest yield of electrons occurs for the highest temperature.

ranges from 10^{-6} to 10^{-10} for reactive molecules such as O_2 and F_2. Chemisorptive luminescence, a parallel process, have much higher yields because they are one electron processes vs. two for chemisorptive electron emission.

XeF$_2$ is a relatively unstable noble gas compound such that when it hits a surface, it easily dissociates, yielding atomic fluorine, a species not all that different from atomic O. Exposure of a material such as SiO$_2$ to a beam of XeF$_2$ shows chemisorption of fluorine, as detected by a mass microbalance and Auger Electron Spectroscopy. No evidence for removal of substrate atoms has been observed for gas exposure alone. However, if we bombard the surface simultaneously with electrons, ions, or energetic photons, we see quite high yields of surface etching. (This happens to be a reaction of considerable interest to the semiconductor processing industry.) In Figure 7, we show mass spectrometer measurements (Dickinson et al., 1988) of two mass peaks, mass 16 (atomic O and O$_2$) and mass 104 (SiF$_4$) which are the principal product gases released during electron induced etching of SiO$_2$. The etch rates at high reactive gas coverages can be as high as unity (e.g., SiO$_2$ units lost/incident particle). We have also shown that in a number of inorganic thin films, chemisorbed F atoms are dramatically driven into the film (absorbed) due to electron bombardment. The rate for this process was a maximum for 50 eV electrons.

Using simultaneous microbalance measurements and pulsed electron sources, one can get quite accurate yields, energy dependences, and product kinetic energy information for this type of etching reaction. Similar results for O atom plus radiation exposures of materials should be possible in conjunction with the NASA-sponsored laboratory studies. In addition to radiation, O atom exposure of mechanically stressed polymers should also be tested.

An example of an adsorption process that normally has zero sticking coefficient is the activated adsorption of CH$_4$. When thermal methane molecules at reduced pressures are incident on clean metal surfaces such as single crystal (111) Ni, no evidence of chemisorption is observed. When the translational velocity of the CH$_4$ is increased to a few tenths of an eV, Ceyer et al. (1987) have shown that the molecules begin to dissociatively chemisorb (forming adsorbed CH$_3$ and H); the sticking probability increases exponentially with the normal component of kinetic energy. The mechanism for this process is believed to involve collisionally induced distortion of the molecule which greatly enhances quantum mechanical tunneling of the hydrogen atom into a surface bonding state. It should be noted that some molecules decrease their sticking probability with increased kinetic energy due to reduced time in the interaction region. Also, recently Cardillo (private communication) has shown direct evidence that fast atom collisions with surfaces can generate electronic excitations in the substrate, indicating energy transfer channels not normally considered.

We briefly mention the work by Kendall et al. (1986) utilizing TOF mass spectroscopy. They have analyzed the neutral atoms and molecules emitted during electrical breakdown of thin
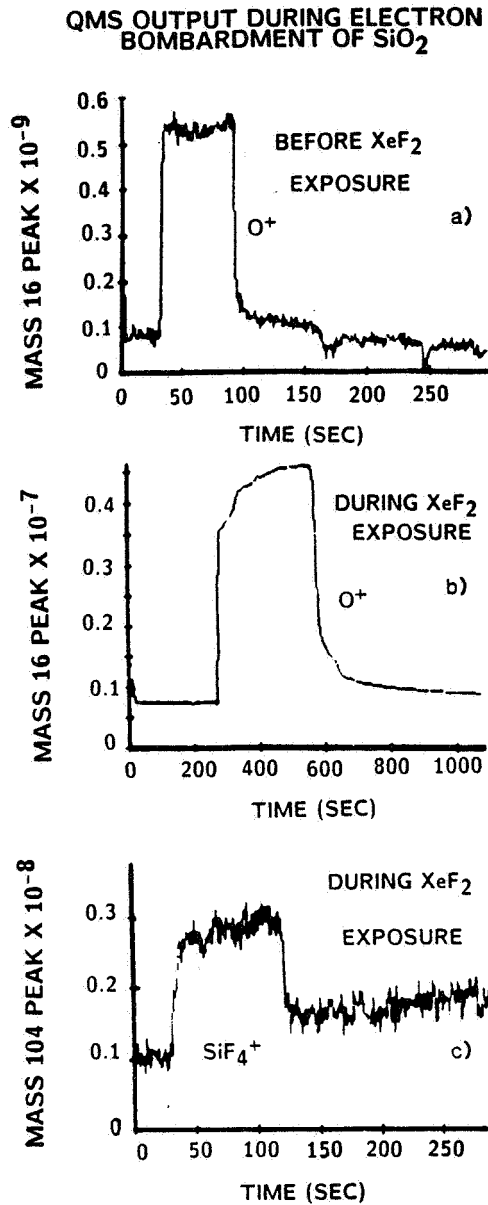
QMS OUTPUT DURING ELECTRON BOMBARDMENT OF SiO_2

Fig. 7. Output of a quadrupole mass spectrometer during the exposure of SiO_2 thin films to electron bombardment. (a) Curve shows the mass 16 response due the electron stimulated desorption from SiO_2. (b)-(c) Curves show the mass 16 and mass 104 responses, respectively, for the simultaneous exposure of the SiO_2 to the same electron bombardment and XeF_2.

sheets of Kapton and Teflon. The spectra provide the product species, quantity emitted, and the time evolution of the emission relative to the breakdown event.

We also mention a recent study by Dursch and Hendricks (1987) on the consequences of exposure to an oxygen plasma of a anodized Al foil protected graphite/epoxy tube. In particular, they examined the consequences of a pin hole in the foil, showing considerable etching beneath the hole. This should be examined

in terms of the contamination problem.

Finally, of relevance to the production of excited species that contribute to the glow phonomena, we mention a series of experiments by Lebsack (1977) which showed that the escape probability of a number of metastable species (including N_2^*) increased with normal velocity and surface condition. The more "passive" a surface (e.g., highly oxidized, hydrocarbon covered, etc.), the less quenching of long-lived excited states would occur. The implications concerning the production, survival, and resulting angular distributions of metastable species are evident.

Conclusion

We conclude by presenting a list of surface science problems that should be investigated to provide improved information to address Space Station contamination problems. It is assumed that the surfaces of interest have been identified, i.e., the range of materials, coatings, and substrates are reasonably well defined, and are available for study.

Relevant Surface Science Problems

- Measurements of necessary sticking probabilities, reaction and process rates, product species.

- Measurements of dependence on process rates on incident particle internal and kinetic energies, incident angle.

- Measurements of product internal and kinetic energies, angular distributions. (This includes, for example, metastable molecules such as N2* which may play a key role in glow phenomena.)

- Determining "State of the Surface" for the various materials of interest as a function of time (months, years). Chemical, physical characteristics of the surfaces of interest (both "source" surfaces/"receiving" surfaces).

- Determining potential Synergisms: e.g.,
    -- O atoms/Electrons
    -- O atoms/electric fields
    -- UV or O atoms/mechanical stress
    -- UV/chemisorbed organics

- Determining mechanisms of the important processes will facilitate making design changes, materials choices in the long run.

- Studies related to protective coatings (including adhesion), repair/resurfacing of "sources", and removal of contaminants from critical surfaces.

- Studies on the interaction of penetrated foil/G-E Composite structures with O atom environment. (Fluxes of released products, composition, angular distributions, etc. of gases released from pinholes).

- Experimental tests of models for solar release of particulates.

- Determination of a complete description of the environment experienced by these surfaces.

Acknowledgments

References

Bareiss, L. E., Payton, R. M., and Papazian, H. A., Shuttle/Spacelab Contamination Environment and Effects Handbook, NASA Contractor Report 4053, NASA Scientific and Technical Information Branch, 1987.

Cardona, M., and Ley, L. (Eds.), Photoemission in Solids I, Springer Verlag, Berlin, 1978.

Ceyer, S. T., Beckerle, J. D., Lee, M. B., Tang, S. L., Yang, Q. Y., and Hines, M. A., J. Vac. Sci. Technol. A 5, 501, 1987.

Chen, R., and Kirsh, Y., Analysis of Thermally Stimulated Processes, Pergamon, Oxford, 1981.

Chuang, T. J., J. Vac. Sci. Technol. 18, 638, 1981.

Dickinson, J. T., and Jensen, L. C., J. Poly. Sci.: Poly. Phys. Ed. 23, 873, 1985.

Dickinson, J. T., J. Vac. Sci. Technol. A 5, 1076, 1987.

Dickinson, J. T., Loudiana, M. A., and Schmid, A., to appear in Adhesives, Sealants, and Coatings for Space and Harsh Environments, edited by L.H. Lee, Plenum Publishing Co., New York, 1988.

Dursch, H. W. and Hendricks, C. L., SAMPE Quarterly, 19, No. 1, pp. 14-18, Oct. 1987.

Hagland, Jr., R. F., and Tolk, N. H., Short Wavelength Coherent Radiation: Generation and Applications, AIP Conference Proceedings, 147, 103, 1986.

Halperin, A., and Braner, A. A., Phys. Rev., 117, 408, 1960.

Jost, W., Diffusion in Solids, Liquids, and Gases, Academic, New York, 1952.

Kendall, B. R. F., Rohrer, V. S., and Bojan, V. J., J. Vac. Sci. Technol. A 4, 598, 1986.

Knotek, M. L., Physics Today, pp. 24-32, 1984.

Lebsack, D. E., The Scattering of Metastable Molecules from Gas Covered Si(100) and W(100) Surfaces, Ph.D. Thesis, Washington State University, 1977.

Leger, L., Visentine, J., and Santos-Mason, B., Selected
    Materials Issues Associated with Space Station, <u>SAMPE
    Technical Conference Proceedings</u>, <u>18</u>, 1015, 1986

Loudiana, M. A., Bye, J., Dickinson, J. T., and Dickinson, D. A.,
    <u>Surf. Sci.</u> <u>157</u>, 459, 1985.

Redhead, P. A., Hobson, J. P., and Kornelsen, E. V., <u>The Physical
    Basis of Ultrahigh Vacuum</u>, Chapman and Hall Ltd, London,
    1968.

Roux, J. A., and McCay, T. D. (Eds.), Spacecraft Contamination:
    Sources and Prevention, <u>Progress in Astronautics and
    Aeronautics,</u> <u>91</u>, AIAA, New York, 1984.

Somorjai, G., <u>Chemistry in Two Dimensions: Surfaces</u>, Cornell
    University Press, Ithaca, 1981.

Stuart, R. V., <u>Vacuum Technology, Thin Films, and Sputtering</u>,
    Academic Press, New York, 1983.

Tonyali, K., Jensen, L. C., and Dickinson, J. T., <u>J. Vac. Sci.
    Technol.</u> <u>A</u>, to be published, 1988.

Wright, A. N., in <u>Polymer Surfaces</u>, edited by D. T. Clark and W.
    J. Feast, pp. 155-184, John Wiley-Interscience, New York,
    1978.

LABORATORY EXPERIMENTS OF RELEVANCE TO
THE SPACE STATION ENVIRONMENT

G.E. Caledonia

Physical Sciences Inc.
Dascomb Research Park, P.O. Box 3100
Andover, MA   01810

Introduction

One might expect that contamination effects would be negligibly small in the highly rarefied atmosphere appropriate to Space Station orbit. Observations taken over the several years on the Space Shuttle have demonstrated that this will indeed not be the case unless careful design measures are taken. Specifically, it has been found that the interaction between Space Shuttle and the ambient environment produces a "contaminant cloud" around Shuttle which can provide for deleterious effects. This interaction can provide for structural disfunction by material erosion as well as operational disfunction through oxidation or coating phenomena. Furthermore, the contaminant cloud can provide a more difficult environment for external probes to operate in because of increased radiative backgrounds due to surface and "cloud" glows, enhanced plasmas and surface charging, and also direct deterioration of diagnostic equipment. Although it is clearly desirable to reduce contaminant levels so as to obviate such effects there is a cost associated with such reductions and it is critical not to significantly overestimate the required levels of cleanliness for successful Space Station operation.

At the present time, the required contamination levels can only be specified by models which can be correlated with the available empirical data base. These models themselves require a significant amount of physical information for successful application. In the next section we will provide a brief overview of the phenomenologies which produce the contaminant cloud and review the physical data required to characterize it. This discussion will be followed by a brief description of laboratory techniques which can be utilized to provide the required data.

The Contaminant Cloud

Of course the dominant source of the contaminant cloud is the Space Station itself. Contaminant species are naturally introduced around Station and on Station surfaces during operational events such as thruster firings, water dumps and other vents. Furthermore, particles will shake off of surfaces and outgassing will occur. The ambient hard UV flux will also act to enhance desorption and outgassing, and indeed may interact with some species to provide polymerization on surfaces. As will be seen, the specification of the chemical form of these outgassed species is critical to determining their ultimate impact on Space Station performance.

Ambient species, primarily O and N_2, but also lesser species such as N, O_2, and H, will impact Station surfaces at orbital velocities of 8 km s^{-1}. It has been found that in many materials this interaction produces material erosion. It is generally assumed that this erosion is the result of oxygen atom attack and for many hydrocarbon materials mass loss is estimated to occur in one out of ten impacts (Leger and Visentine, 1986; Green et al., 1985). The reaction products of these interactions have not been measured, but in many cases can be estimated from mechanistic arguments. Erosion species identification is, of course, critical for specification of subsequent reaction, evaluation of deposition tendency, and understanding of erosion induced glows. It has been suggested in the past that limited key components could be protected from oxygen atom attack by the application of sacrificial coatings. The ultimate impact of these eroded materials on the local environment must be carefully evaluated prior to such applications.

Oxygen atom attack can also provide for functional deterioration in more insidious ways. For example, Leger and Visentine (1987) have recently pointed out that moly-disulfide, a common lubricant, will oxidize under oxygen atom attack, becoming abrasive. Such a transformation would provide increased particle loading and decreased mobility for moving parts. Other materials, while not eroding, will oxidize, resulting in changing thermal and radiative properties. Furthermore, possible synergistic effects on material erosion resulting from UV loading or surface charging remain to be evaluated.

The catalytic properties of various materials in high velocity interactions must also be evaluated. For example, knowledge of the surface accommodation coefficient for momentum is critical to specifying the local cloud density. Specifically if the ambient species accommodate their momentum on the surface they will then effuse away thermally, resulting in a higher local gas density than if they had scattered elastically from the surface. The momentum accommodation coefficient is a key parameter in contaminant cloud models. As another example, catalytic reactions of ambient species on surfaces have long been suggested (see, for example, Green et al., 1986) as possible sources for excited states which could then either further interact or themselves produce a surface glow. No data are presently available on such catalytic effects at orbital velocities for the various materials of importance to Space Station.

The ambient gasses will also interact with outgassed species around the Space Station. This interaction, initially occurring at orbital velocities but also of importance at lower velocities, will produce a scattering pattern which plays a role in defining the density profile and extent of the contaminant cloud. To the author's knowledge there are no measurements of the angular differential cross sections or momentum transfer resulting from such heavy body collisions. Furthermore, inelastic collisions will also occur producing radiation from direct excitation or chemi-excitation, as well as species transformation. The data base for such interactions is very sparse in the energy range of interest.

Lastly, the importance of positive ion reactions must be evaluated. Although ambient ion concentrations are typically small compared to neutral concentrations there can be charge buildup around the Space Station. One way this can occur is through reactions between ambient ions and contaminant neutrals. Many reactions of this type will move charge between species

without significant momentum transfer. Thus, charge initially at rest in the Earth frame may be swept along with Shuttle (see discussion in Caledonia et al., 1987a). Such reactions can also produce excited species which can radiate and new ionic species which are more likely to provide surface deposition. The efficiencies for ion neutralization on various Space Station materials remain to be evaluated. We note that enhanced ionization levels have been proposed as a source of Shuttle glow (Papadopoulos, 1974).

The various data requirements discussed above have been summarized in Table 1. Potential laboratory techniques for developing this data base are examined below.

Table 1. Required Data For Space Station Contamination Level Specification

Data Required		

• Material behavior under UV loading
  − Outgassing rates
  − Products
  − Surface effects
  − Particle formation
 	
• Material "erosion" studies under energetic species impact
  − Erosion rates
  − Passivation effects −
    nonlinear behavior
  − Species produced
    ∗ state changes
    ∗ deposition
  − Surface property
    changes
  − Erosion induced glows
  − Synergistic effects
    ∗ UV loading
    ∗ charged surfaces
	• Ambient/surface inter-
	  actions
	  − Momentum transfer/
	    accommodation
	  − Surface reactions
	    e.g., fast N_2 →
	    $N + N$ → $N_2(A)$
	  − Surface collision
	    induced glows
	  − Material dependence of
	    all above
	
	• Ambient/contaminant cloud
	  interactions
	  − Differential scattering
	    cross sections
	  − Inelastic collisions
	    ∗ chemical reaction
	    ∗ radiative inducing
	      e.g., $0 + M$ → $0 + M^*$;
	      $0 + AB$ → $OA^* + B$
		• Ionic interactions
		  − Surface neutraliza-
		    tion efficiencies
		  − Ambient ion/
		    contaminant
		    reactions
		    ∗ ion velocity
		      separation
		    ∗ quasi−neutrality
		  − Non−linear effects

Laboratory Studies

Material behavior under UV loading may be investigated by standard techniques and will not be reviewed further here. A research program in this area is presently in progress at NASA Lewis Research Center (S. Rutledge, private communication, 1987).

Development of the remaining data base requires the use of state-of-the-art neutral and ionic beams exhibiting characteristic velocities of 8 km s^{-1}. A number of neutral oxygen atom beams have been under development in response to the Shuttle observations of significant material erosion. These sources may be broken into four types:

(1) Thermal sources, such as microwave discharges or plasma ashers which can produce copious oxygen atoms at thermal or near-thermal energies. These devices are of no value in providing information of the type required.

(2) Plasma torches, where a gas is highly excited by RF, dc, or microwave sources and subsequently expanded through a free jet or supersonic nozzle converting the sensible heat to velocity. These devices can produce high fluxes of oxygen atoms, but are generally limited to oxygen atom energies below 1 to 2 eV (one investigator has proposed the potential to reach oxygen atom energies of 4 eV; however, see Table 2).

(3) Ion beam techniques, where sources of positive or negative oxygen ions are electrostatically accelerated and focussed to achieve the proper velocity, at which point the charge is stripped by various techniques such as charge exchange or surface neutralization. Such beams can readily achieve the appropriate velocity, however, are typically limited to low fluxes because of Coulombic repulsion effects. For standard ion sources achievable fluxes as high as 10^{15} cm^{-2} s^{-1} have been predicted but not demonstrated (note, however, the Princeton source in Table 2).

(4) Laser sustained plasmas, where lasers are used to produce a high temperature plasma which is subsequently expanded in a free jet or supersonic nozzle to produce a high velocity neutral beam. Such sources have been demonstrated to produce beams of the desired velocity of 8 km s^{-1} at flux levels of 10^{17} to 10^{18} cm^{-2} s^{-1} and thus are of great value for aging studies.

The status of neutral oxygen atom beams presently under development or in operation has recently been reviewed by Visentine and Leger (1987) and a slightly updated version of their tabulation is provided in Table 2. As can be seen a wide variety of sources should be available to develop various aspects of the required data base. At present for 8 km s^{-1} beam applications the laser discharge techniques appear to be the most mature and in the remainder of this text the PSI pulsed molecular beam source will be used for example. In principal alternate sources will provide similar utility.

The Physical Sciences, Inc. (PSI) source has been described in some detail elsewhere (Caledonia et al., 1987b; Caledonia and Krech, 1987) and will only be briefly reviewed here. In operation a fast acting valve is used to introduce a pulse of oxygen molecules into a previously evacuated supersonic nozzle. A pulsed CO_2 laser focussed near the nozzle throat is used to break down this gas and form a high temperature plasma. The plasma subsequently expands producing a high velocity beam made up primarily of oxygen atoms. A schematic of the PSI system, as it is used for material erosion studies, is provided in Figure 1. The laser beam enters from the left and the molecular beam propagates to the right striking material targets as shown. A mass spectrometer is available for beam characterization and radiative diagnostics are available to monitor both beam properties and radiation from the beam target interaction. A second mass spectrometer head will soon be installed to allow monitoring of erosion products.

Table 2. Extant Oxygen Beam Apparati
(Updated from Visentine and Leger, 1987)

Type	Technique	Source	Species	Energy
Microwave Discharge	Electrostatic accel.	LeRC, Ferguson	$O^+(O_2)$	0-50
Microwave Discharge	Free jet	Utias, Tennyson et al.	$O,O_2(98\%He,2\%O_2)$	2 eV
Plasma Torch	Free jet	Utias, Tennyson et al.	$O(98\%He,2\%O_2)$	~4 eV
Plasma Torch	Supersonic nozzle	Aerospace, Arnold and Peplinski	$O,O_2(98\%He,2\%O_2)$	1-2 eV
Plasma Torch	Supersonic nozzle	Ari, Freeman	$O(He,O_2)$	1.3 eV
Electron Bombardment	Electrostatic accel., focusing	Martin Marietta	O^+,O_2^+,O	5 eV
Electron Bombardment	Electrostatic accel., focusing	Vanderbilt U., Tolk and Albridge	O	5-10 eV
Electron Bombardment	Electrostatic accel., focusing	G.E., Amore	$O_2/O_2^+(O)$	3-10 eV
Electron Bombardment	Electrostatic accel., focusing	LeRC, Banks and Rutledge Albridge	$O+,O,O_2$	3-15 eV
Electron Bombardment (plasma toroidal)	Electrostatic accel., focusing	Princeton U.	$O,N(N_2/O_2)$	~10 eV
Electron Bombardment	Electrostatic accel., focusing	Aerospace, Mahadaven	O,O_2,N,N_2	3-100 eV
Laser Discharge	Pulsed breakdown	PSI, Caledonia and Krech	$O(O_2)$	2-14 eV
Laser Discharge	CW breakdown cross	Los Alamos	$O(He/O_2)$	2-5 eV
Laser Discharge	Laser blowoff	JPL, Brinza	O (solid films)	2-7 eV

PROPOSED SAMPLING
QUADRUPOLE MASS
SPECTROMETER
(FROM ABOVE)

TARGETS

BEAM SAMPLING
QUADRUPOLE MASS
SPECTROMETER

PULSED
CO_2 LASER

RADIOMETERS
(FROM ABOVE)
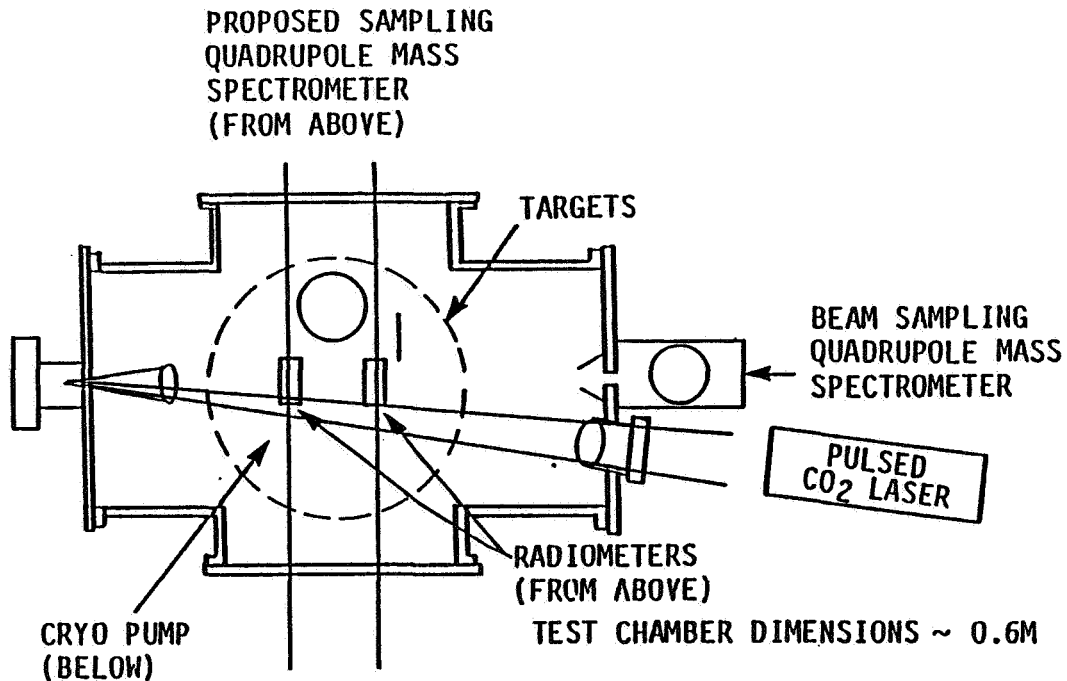
CRYO PUMP
(BELOW)

TEST CHAMBER DIMENSIONS ~ 0.6M

Fig. 1. PSI Oxygen Atom Test Facility under development.

A number of materials have already been studied with this device with
spectrometer is available for beam characterization and radiative diagnostics
are available to monitor both beam properties and radiation from the beam
total 8 km s^{-1} O-atom irradiation levels typical of those encountered during a
few weeks operation at Shuttle altitudes, $\leq 10^{21}$ O-atoms cm^{-2}. In general
mass removal rates and surface properties have been found to be similar to
those observed during Shuttle operation (Caledonia et al., 1987b; Caledonia
and Krech, 1987). As soon as the second mass spectrometer head is operational
this system will be capable of addressing many of the issues discussed in the
previous sections. These include mass loss rates, erosion species identifi-
cation, and surface property changes. Synergistic effects resulting from UV
loading, heating cycles, stress, and flexing can also be investigated with
modest system improvements.

Although the system was not developed specifically to study glows, such
observations can readily be performed above irradiated surfaces using standard
radiative diagnostic techniques. We have seen numerous material specific
radiative signatures above surfaces both visually and using an optical multi-
channel analyzer (OMA). We are presently configuring an experiment to study
erosion-induced infrared signatures above surfaces. An early study will
involve oxygen irradiation of carbon surfaces which is expected to produce
vibrationally excited CO. Possible catalytic surface glows can be studied in
a similar manner. PSI has developed an 8 km s^{-1} beam of a mix of nitrogen
atoms and molecules using similar phenomenology and anticipates no problem in
incorporating oxygen in the mix as well. The neutral species mix in such
beams will be evaluated using the mass spectrometer.

A ballistic pendulum was used within the PSI O-atom device as part of a
calibration of the system flux. The pendulum can provide a measurement of the
material momentum accommodation coefficient inasmuch as elastic collisions
provide twice the momentum transfer as fully accommodating collisions. In our

128

previous measurements we could only use a pendulum material which was transparent to CO_2 laser radiation, we found that energetic oxygen atom collisions with Saran Wrap were largely elastic. The present system is not so limited and other materials can be readily investigated. More sophisticated techniques, for example, targets connected to stings mounted on pressure or torsion transducers can be envisioned. Note that pure beams rather than rare gas-seeded beams are decidedly more advantageous for such measurements.

Gas-gas interactions provide more of a challenge. In particular scattering cross sections are best measured in a crossed molecular beam experiment. A movable time-of-flight mass spectrometer would be a critical diagnostic in such an experiment. The present trend is to use pulsed beams at right angles to optimize detectability. Standard beam techniques cannot provide center of mass energies sufficiently high for the present application; thus, one of the energetic oxygen atom sources under development would be required. The ionic exchange beams are probably the most appropriate, although a skimmed laser discharge beam could also be used.

PSI has developed a crossed beam experiment to study infrared excitation resulting from energetic oxygen atom collisions with species such as CO, CO_2, and CH_4. A schematic of the device is shown in Figure 2. Here a skimmed beam of fast oxygen atoms is crossed at right angles with a skimmed pulse (again using a fast pulsing valve) of thermal target molecules. The IR detection system is downstream of the interaction zone since momentum transfer will sweep the excited molecules in that direction. This experiment design is challenging in that the measurement must be made under single collision conditions; i.e., both the target molecules and the oxygen atoms are required
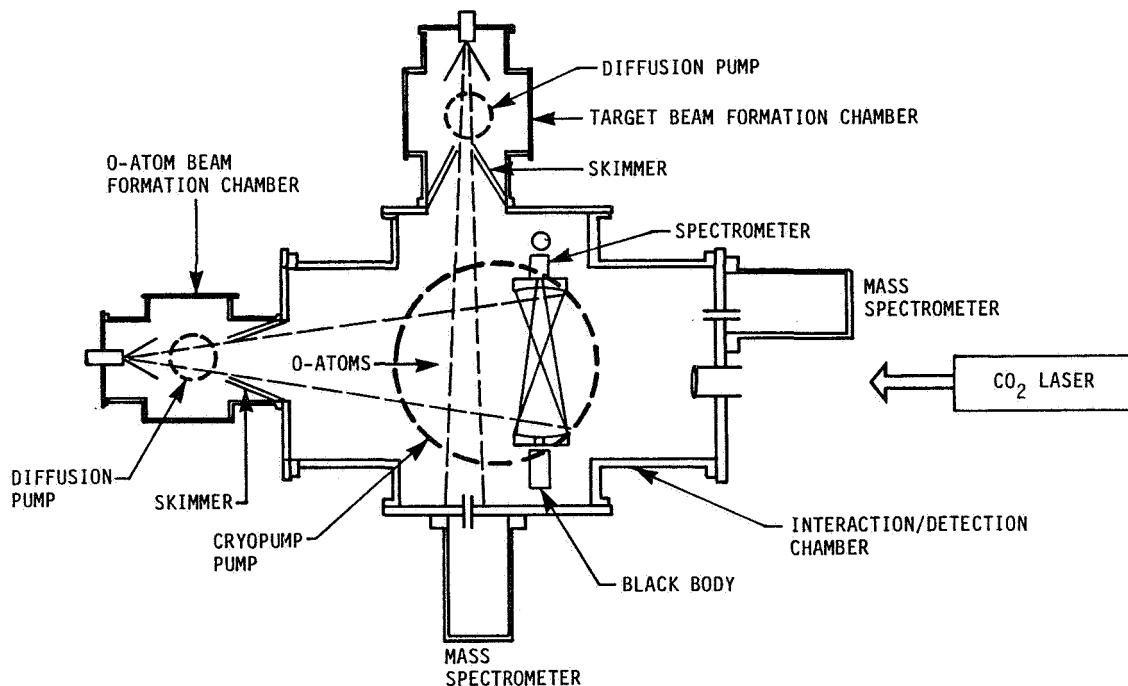

Fig. 2. Crossed beam system for excitation studies.

129

to experience only one collision in the interaction zone to ensure that the radiation is characteristic of fast atom impact. Similar techniques can be used to study visible excitation and chemical reaction in such systems.

The study of ionic reactions at interaction velocities of 8 km s^{-1} is straightforwardly performed using standard techniques. The data base for O$^+$ reactions with various contaminant species is limited at these energies, however, and the rate constants and products of such reactions should be evaluated. The evaluation of product energies is, perhaps, more stressing but also achievable.

Summary

A number of important quantities which must be evaluated in order to both understand and predict the contamination field about Space Station have been enumerated. It has been shown that the recent development of energetic oxygen atom sources enables the laboratory evaluation of the majority of these quantities. A number of potential measurement techniques have been briefly reviewed.

References

Caledonia, G.E. and R.H. Krech, Energetic oxygen atom material degradation studies, AIAA-87-0105, 25th Aerospace Sciences Meeting, January 1987, Reno, Nevada.

Caledonia, G.E., R.H. Krech, and B.D. Green, A high flux source of energetic oxygen atoms for material degradation studies, AIAA J., 25, 59, 1987 b.

Caledonia, G.E., J.C. Person, and D.E. Hastings, The interpretation of Space Shuttle measurements of ionic species, J. Geophys. Res., 92, 273, 1987 a.

Green, B.D., G.E. Caledonia, and T.D. Wilkerson, The Shuttle environment: gases, particulates, and glow, J. Spacecraft & Roc., 22, 500, 1985.

Green, B.D., W.T. Rawlins, and W.J. Marinelli, Chemiluminescent processes occurring above Shuttle surfaces, Planet. Space Sci., 34, 879, 1986.

Leger, L.J. and J.T. Visentine, A consideration of atomic oxygen interactions with the space station, J. Spacecraft & Roc., 23, 50, 1986.

Leger, L.J. and J.T. Visentine, unpublished results (1987).

Papadopoulos, K., On the Shuttle glow (the plasma alternative), Radio Sci., 19, 571, 1974.

Visentine, J.T. and L.J. Leger, Atomic oxygen effects experiments: current status and future directions, NASA TM, JSC (May 18, 1987).

CONTAMINATION OF THE SPACE STATION ENVIRONMENT BY VENTED CHEMICALS

Paul A. Bernhardt

Geophysical and Plasma Dynamics Branch
Naval Research Laboratory
Washington, D.C. 20375

Abstract. Gaseous materials vented from the Space Station may have noticeable effects on the optical or plasma environment. The magnitude of the effects depends on: (1) rarefied gas dynamics, (2) photochemical reactions, and (3) airglow excitation mechanisms. In general, the effects from atomic species can be mitigated, but the disturbances resulting from venting of molecules like SF_6, CO_2, and C_2H_2 can be significant. The interaction of molecules with the ambient plasma at orbital velocities should be studied with laboratory or space experiments.

Introduction

In this work, we will discuss the environmental effects from vapor substances vented during materials science and life science experiments on the Space Station. These effects can be transient or long-lived depending on the duration of the venting and the type of interaction. Both transport and chemical reactions of the released materials will disturb the neutral and plasma densities of the background atmosphere. The injected atoms may become collisionally or chemically excited to yield enhanced airglow. Procedures for estimating the magnitude of the airglow and density perturbations are described.

As a baseline, we are considering a Space Station orbit at 450 km altitude where, during solar maximum, the neutral density will be about 4 x 10^8 cm^{-3} and the neutral temperature may be as high as 2000° K. During solar minimum, the orbit altitude could be reduced to 320 km where neutral densities and temperatures are as low as 1.3 x 10^8 cm^{-3} and 705° K, respectively.

The materials considered in this study are listed in Table 1. The atomic species from the materials science experiments are released at rates of 10^{15} to 10^{17} atoms s^{-1} for several days. The life science experiments deposit atomic or molecular species in 1 to 500 g bursts.

Table 1. Space Station Vented Species.

Vapor	Molecular Weight	Release Amount
Atoms		
Helium	4	7.5×10^{25}[a]
Neon	20	3.0×10^{24}[a]
Argon	40	1.5×10^{24}[a]
Aluminum	27	10^{15} to 10^{17}[b]
Phosphorous	31	"
Manganese	54.9	"
Gallium	69.7	"
Arsenic	74.9	"
Cadmium	112.4	"
Indium	114.8	"
Tin	118.7	"
Tellurium	127.6	"
Mercury	200.7	"
Lead	207.2	"
Molecules		
Carbon monoxide	28	2.1×10^{22}[c]
Nitrogen	28	1.1×10^{25}[c]
Oxygen	32	9.4×10^{24}[c]
Carbon dioxide	44	1.4×10^{24}[c]
Acetylene	26	2.3×10^{22}[c]
Sulfur hexafluoride	146	4.0×10^{23}[c]

[a] atoms

[b] atoms s^{-1}

[c] molecules per run

The Space Station will be moving supersonically with respect to the ambient atmosphere. At 450 km altitude, the orbital velocity is 7.6 km s^{-1}. The exospheric neutral temperature range of 700 to 2000° K and an average molecular weight of 16.4 amu gives a sound speed of about 10^3 m s^{-1}. Moving at Mach 7 or greater, the mean times between collisions of a single particle will be dependent on the mean free path in the atmosphere, λ_a.

The type of flow for the vented gases will depend on the relationship between the gas cloud size (L), the mean free path inside the cloud (λ_c), and the atmospheric mean free path (λ_a). Figure 1 illustrates these relationships for self-continuum flow ($\lambda_c < L < \lambda_a$), collisionless flow (L $< \lambda_c < \lambda_a$), and diffusive flow ($\lambda_a < L < \lambda_c$). Each one of these phases occurs during the gas expansion process.
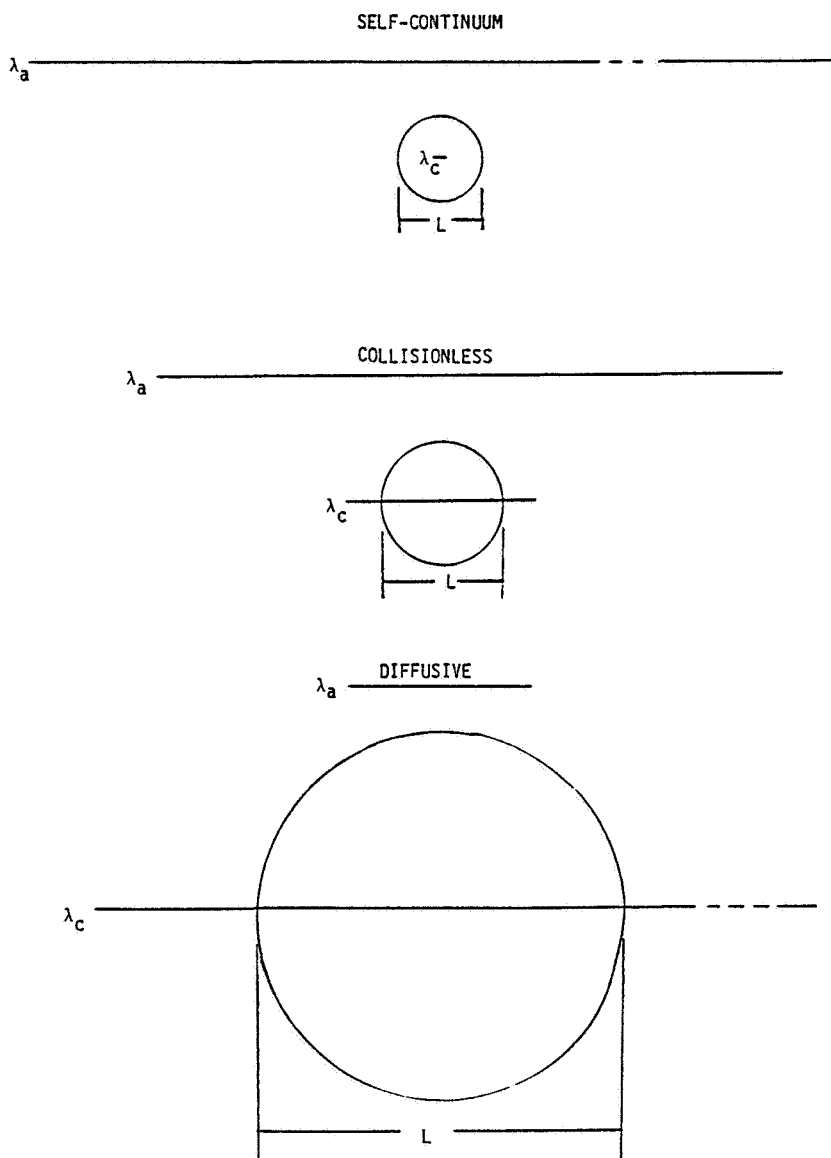
SELF-CONTINUUM

COLLISIONLESS

DIFFUSIVE

Fig. 1. Relationships between atmospheric mean-free-path, cloud diameter, and cloud mean-free-path for different flow descriptions.

133

A sample calculation for the self-continuum phase is illustrated in Figure 2. The motion of 0.1 kg of CO_2 released from a point moving at 4.7 km s^{-1} is simulated using the Los Alamos multi-fluid flow-model (Bernhardt et al., 1988). This type of interaction with the upper atmosphere is representative of venting from the life science experiments on the Space Station. The background atmosphere is assumed to be uniform with $m_a = 16.4$ amu, $T_a = 705°$ K, $n_a = 1.3 \times 10^8$ cm^{-3}, and $\gamma_a = 1.5$ based on a thermospheric model for a 317 km release altitude. The core of the injected material is heated to a few thousand Kelvin above ambient. The background atmosphere – ions, electrons, and neutrals – is swept up by the fast moving release.
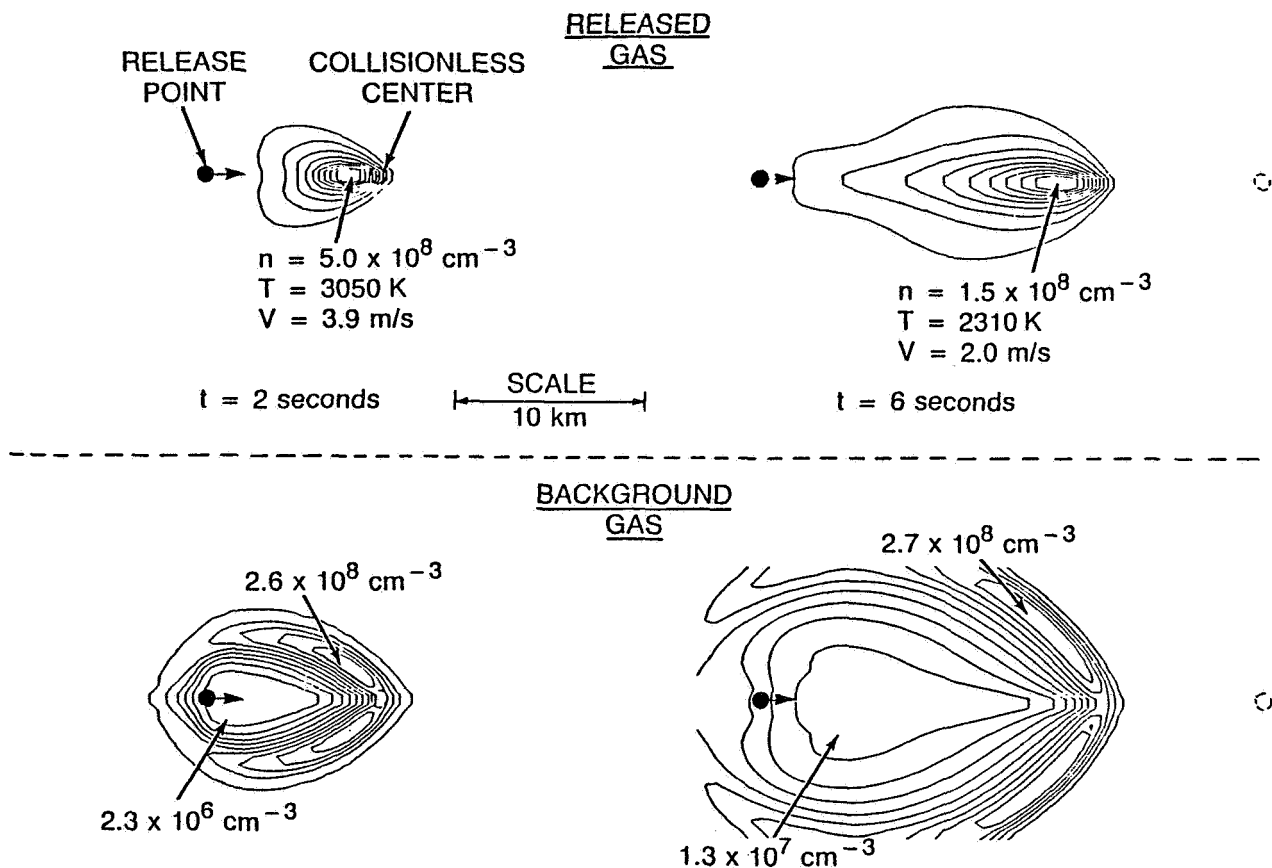
RELEASE POINT · COLLISIONLESS CENTER

RELEASED GAS

$n = 5.0 \times 10^8$ cm^{-3}
$T = 3050$ K
$V = 3.9$ m/s

$t = 2$ seconds

SCALE
10 km

$n = 1.5 \times 10^8$ cm^{-3}
$T = 2310$ K
$V = 2.0$ m/s

$t = 6$ seconds

BACKGROUND GAS

2.6×10^8 cm^{-3}

2.3×10^6 cm^{-3}

2.7×10^8 cm^{-3}

1.3×10^7 cm^{-3}

Fig. 2.   Neutral gas distribution form the release of 0.1 kg of vented CO_2 at 317 km altitude. The solid circle is the release location. The dashed circle shows the center of the release for collisionless motion. An elongated cavity is formed in the background.

134

The diffusive-expansion phase is shown in Figures 3 and 4. Molecules are released from a source moving horizontally at 7.6 km s^{-1}. The release rate is 10^{17} atoms s^{-1} lasting 150 s. The calculation uses the three-dimensional diffusion model described by Bernhardt (1979). The neutral scale height at the 400 km release altitude is 57 km. Relatively larger diffusion at higher altitudes causes the cloud to settle and to dissipate.
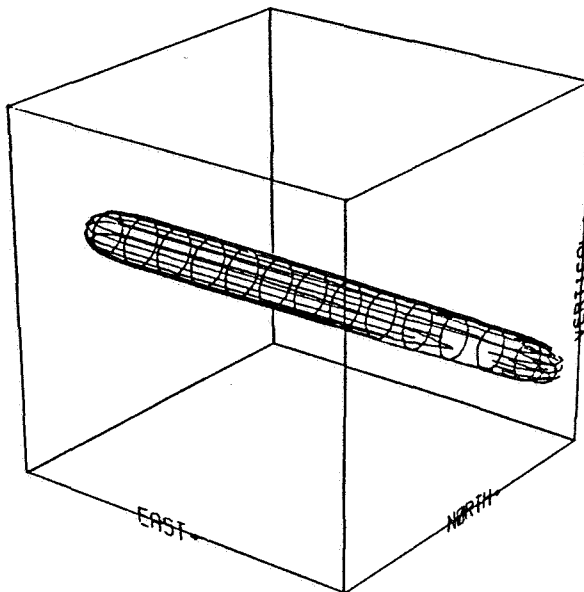
1638 km CUBE CENTERED AT 400.0 km ALTITUDE
TIME AFTER RELEASE: 25.8 sec
H$_2$O CONCENTRATION AT SURFACE: 5.7x10^4 m^{-3}

Fig. 3.   Cylindrical cloud of H$_2$O to illustrate molecular diffusion.

One half hour after the release, the maximum density of the cloud has been reduced by a factor of 11 and the peak has fallen to 220 km altitude. When the Space Station crosses a release point after one orbit of 1.5 hours, the original release will be dissipated. Recontamination does not seem to be a problem.
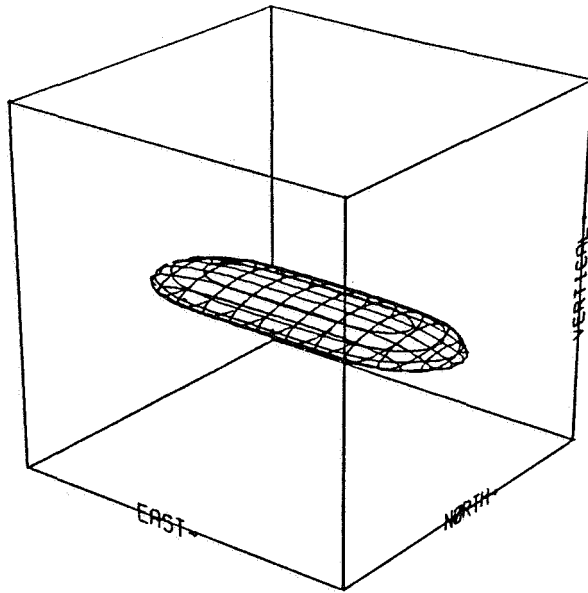
2560 km CUBE CENTERED AT 400.0 km ALTITUDE
TIME AFTER RELEASE: 1736.5 sec
H_2O CONCENTRATION AT SURFACE: 3.3×10^3 m^{-3}

Fig. 4.   Late-time, pancake distribution of the diffusing gas.


Chemistry of the Vented Species

Chemical reactions may determine the fate of the vented species. Should the vapors become ionized, they will become trapped in magnetic flux tubes and their dispersal will be limited by one-dimensional diffusion along $\underline{B}$. The materials may become ionized by photo-processes, collisional processes, charge exchange with ambient O^+ ions, or by electron attachment. Table 2 lists the ionization potentials of the vented atoms. All of the ionization potentials are less than their kinetic energy at orbital velocity. Consequently, collisional ionization or critical-velocity ionization may be important. Photoionization by single photon events takes about 10^6 s for substances like Al, Ga, and In which have ionization potentials near 6 eV.
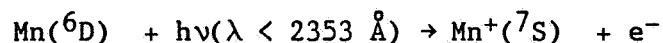
136

Table 2. Atomic Species Release.

Name	Symbol	IP (eV)	λ_0 (Å)
Helium	He	24.6	591
Neon	Ne	21.6	626
Aluminum	Al	6.0	3944
Argon	Ar	15.8	894
Phosphorous	P	10.5	1788
Manganese	Mn	7.4	4034
Gallium	Ga	6.0	4173
Arsenic	As	9.8	1973
Cadmium	Cd	9.0	3261
Indium	In	5.8	4513
Tin	Sn	7.3	3035
Tellurium	Te	9.0	--
Mercury	Hg	10.44	2536
Lead	Pb	7.42	3685

Atoms with metastable states may be ionized more rapidly by a two photon process. The first photon populates the metastable state and the second photon ionizes the material from this state. Consequently, lower-energy, more-abundant solar photons are used. Manganese may be a candidate for two photon ionization. The $Mn(^6D)$ level can be populated as follows
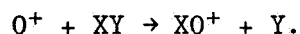
$$Mn(^6S) + h\nu(\lambda < 4033 \text{ Å}) \rightarrow Mn(^6P)$$

$$\rightarrow Mn(^6D) + h\nu(\lambda = 1.36 \text{ } \mu)$$
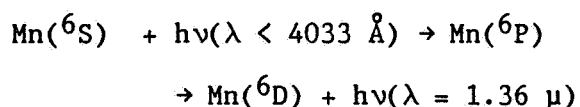
The ionization then only requires 5.27 eV.

$$Mn(^6D) + h\nu(\lambda < 2353 \text{ Å}) \rightarrow Mn^+(^7S) + e^-$$

the time constant for photoionization of Mn will be about 10^5 s.

Reactions with the ambient ionospheric constituents will ionize the vented species. In the ionosphere, most ion-molecule reactions have the form

$$O^+ + XY \rightarrow XO^+ + Y.$$

Thermal-energy rate constants for reactions between the vented molecules and ambient O^+ ions are given in Table 3. The rates and reaction products can be substantially different for orbital velocity interactions (Caledonia et al., 1987). Also listed in Table 3 is the electron attachment rate for SF_6 for the reactions

$$SF_6 + e^- \rightarrow SF_6^- \qquad (10\%)$$

$$\text{or} \rightarrow SF_5^- + F \qquad (90\%)$$
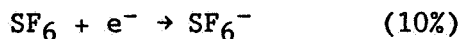
Subsequent chemical reactions of the newly created ions will deplete the ambient plasma and may leave the reaction products in excited states to produce airglow.

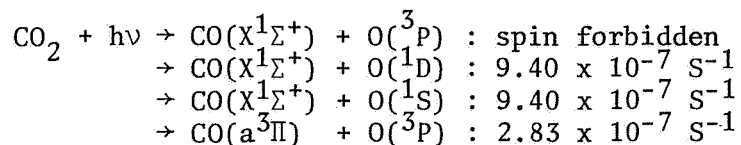Table 3. Molecular Species Releases.

NAME	IP(eV)	$t_I(10^6$ s)	D_0(eV)	$t_D(10^6$ s)	k_0^+(cm^3 s^{-1})	k_e^-(cm^3 s^{-1})
Carbon monoxide	14.014	3.2	11.09	3.6	5.0×10^{-13}	0.0
Nitrogen	15.581	2.9	9.76	1.5	1.2×10^{-12}	0.0
Oxygen	12.071	2.0	5.116	0.24	1.9×10^{-11}	0.0
Carbon dioxide	13.769	1.5	5.45 (CO-O)	0.82	9.4×10^{-10}	0.0
Acetylene	11.42	1.3	5.38 (C_2H-H)	0.03	10^{-9}	0.0
Sulfur hexafluoride	15	---	3.95	0.3	1.5×10^{-9}	2.2×10^{-7}

Airglow Production by the Vented Species

Airglow enhancements may be excited by solar photons or by chemical reactions. Resonance fluorescence occurs by absorption of a solar photon and subsequent re-radiation at the same wavelength in an arbitrary direction. Table 2 lists the wavelengths for ground state transitions of vented atoms. Emissions from these substances occur in the ultraviolet and visible spectrum. A radiometric standard for acceptable radiance (W sr^{-1} m^{-2}) should be established for line emissions.

Atomic species can react with neutrals to produce molecules which fluoresce in sunlight. Atomic aluminum reacts with oxygen (O_2) to produce AlO. Bands of AlO at 4842 (0,0), 5080 (0,1), 4648 (1,0), and 5337 (0,2) have been measured after releases between 80-140 km. Simultaneous releases of Al and O_2 at 450 km probably should be avoided to prevent production of the fluorescent aluminum monoxide.

Excited states are produced during photodissociation of molecular species. For example, Huebner and Carpenter (1979) list the following products for photolysis of CO_2 in sunlight:
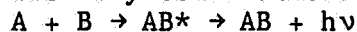
$$CO_2 + h\nu \rightarrow CO(X^1\Sigma^+) + O(^3P) \quad : \text{ spin forbidden}$$
$$\rightarrow CO(X^1\Sigma^+) + O(^1D) \quad : 9.40 \times 10^{-7} \text{ s}^{-1}$$
$$\rightarrow CO(X^1\Sigma^+) + O(^1S) \quad : 9.40 \times 10^{-7} \text{ s}^{-1}$$
$$\rightarrow CO(a^3\Pi) + O(^3P) \quad : 2.83 \times 10^{-7} \text{ s}^{-1}$$

where the rate constants are given. The excited states $O(^1D)$, $O(^1S)$, and $CO(a^3\Pi)$ radiate at 6300, 5577, and 2054 Å, respectively. The dissociative energies and rate constants for photolysis of the molecules are given in Table 3.

Excited states may be produced without sunlight by collisional or chemiluminescent processes. The types of chemiluminescent reactions which yield excited species are listed below.
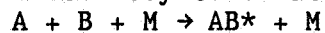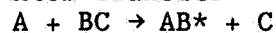
Direct Two-Body Combinations
$$O^+ + e^- \rightarrow O + h\nu$$
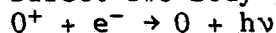
Two-Body Combinations with Preassociations
$$A + B \rightarrow AB^* \rightarrow AB + h\nu$$

Three-Body Combinations
$$A + B + M \rightarrow AB^* + M$$
$$AB^* \rightarrow AB + h\nu$$
$$AB^* + M \rightarrow AB + M$$

Atom Transfer
$$A + BC \rightarrow AB^* + C$$
$$A + BC \rightarrow AB + C^*$$

Mutual Neutralization
$$A^+ + B^- \rightarrow A^* + B^*$$
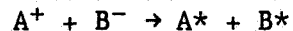
Dissociative Recombination
$$AB^+ + e^- \rightarrow A^* + B^*$$
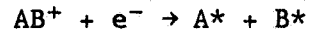
The excited CH and C_2 spectra from acetylene releases between 90 and 100 km altitude (Rosenberg, 1964) may be a result of photodissociation and atom transfer reactions with O_2.

The mutual neutralization and dissociative recombination reactions are known to yield excited atomic oxygen from SF_6 and CO_2 releases in the ionosphere (Bernhardt, 1987). The negative ions formed by electron attachment to SF_6 react with O^+ to give excited atoms.

$$SF_6^- + O^+ \rightarrow SF_6 + O^* \quad (12.81 \text{ eV})$$

$$SF_5^- + O^+ \rightarrow SF_5 + O^* \quad (9.91 \text{ eV})$$
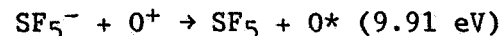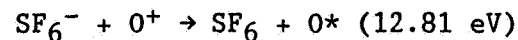
At thermal speeds, only the first reaction has enough energy to populate $O(3p^5P)$ and $O(3p^3P)$ states which radiate in the visible at 777.4 nm and 844.6 nm, respectively. The thermal, low-speed release of 7.4×10^{25} molecules of SF_6 into the ionosphere was estimated to produce 150 Rayleighs at 777.4 nm (Bernhardt et al., 1986). At orbital velocities, we calculate that the same SF_6 release would produce over 6000 Rayleighs.

Conclusions

In this note, we have tried to identify some upper atmosphere disturbances that are stimulated by the venting of vapors from the Space Station. These disturbances include neutral and plasma density perturbations and airglow enhancements. Modeling efforts should be considered for estimating:

(1) Transient behavior of the release, including gas dynamics, collisional airglow excitation, and chemical reactions.

(2) Long-term, global distribution of the material in neutral and ionized states.

Standards should be established for acceptable levels of line emissions. This would be in addition to the spectral irradiances (Watts m^{-2} sr^{-1} nm^{-1}) for particulate and molecular scattering given by the Space Station External Contamination Requirements (JSC 30426, November 19, 1986).

The atoms listed in Table 1 should present no hazard to the Space Station environment. All of the atomic species except helium, neon and argon, can be condensed and prevented from being released as a vapor. The other three atomic vapors (i.e., He, Ne, and Ar) are inert to photochemical process and should not be noticeable.

The molecules listed in Table 1 can be hazardous to both the optical and plasma environment. They are all gaseous at standard temperature and pressure and they all react with O^+ at orbital velocities. Sulfur hexafluoride seems to be the most harmful of these substances because it also interacts with the ambient plasma through dissociative or radiative attachment. The molecular species create excited states by dissociative recombination of positive ions and electrons and by mutual neutralization of negative ions and O^+. These states radiate line emissions which may interfere with low-light-level observations.

The primary uncertainty in predicting the effects of the vented species is the reactions of ambient O^+ with the high velocity molecules. At orbital velocity, O^+ has 5 eV energy and reaction products and rates are different than at thermal energies. These interactions should be measured with laboratory or space experiments. The Combined Release and Radiation Effects Satellite (CRRES) mission provides an excellent opportunity to measure the interaction of SF_6 and, possibly, CO_2 with O^+ at orbital velocities.

References

Bernhardt, P.A., Three-dimensional, time-dependent modeling of neutral gas diffusion in a nonuniform, chemically reactive atmosphere, J. Geophys. Res., 84, 793, 1979.

Bernhardt, P.A., A critical comparison of ionospheric depletion chemicals, J. Geophys. Res., 92, 4619, 1987.

Bernhardt, P.A., E.J. Weber, J.G. Moore, J. Baumgardner, and M. Mendillo, Excitation of oxygen permitted line emissions by SF_6 injection into the F-region, J. Geophys. Res., 91, 8937, 1986.

Bernhardt, P.A., B.A. Kashiwa, C.A. Tepley, and S.T. Noble, Spacelab 2 upper atmospheric modification experiment over Arecibo, 1, neutral gas dynamics, Astrophysical Lett. and Comm., in press, 1988.

Caledonia, G.E., J.C. Person, and D.E. Hastings, The interpretation of space shuttle measurements of ionic species, J. Geophys. Res., 92, 273, 1987.

Huebner, W.F. and C.W. Carpenter, Solar Rate Coefficients, Los Alamos Report LA-8085-MS, October 1979.

Rosenberg, N.W., Project Firefly 1962-1963, AFCRL-64-364, May 1964.

WORKSHOP PARTICIPANTS

M. R. Torr, Chairperson
Code ES51
NASA/Marshall Space Flight Center
Huntsville, AL 35812

F. O. von Bun, Sponsor
Code E
National Aeronautics and Space
    Administration
Washington, D.C. 20546

G. S. Arnold
Chemistry and Physics Laboratory
The Aerospace Corporation
P.O. Box 95957
Los Angeles, CA 90009

P. A. Bernhardt
Geophysical and Plasma Dynamics
    Branch
Naval Research Laboratory
Washington, D.C. 20375

G. E. Caledonia
Physical Sciences, Inc.
Dascomb Research Park
P.O. Box 3100
Andover, MA 01810

J. T. Dickinson
Department of Physics
Washington State University
Pullman, WA 99164-2814

B. D. Green
Physical Sciences, Inc.
Dascomb Research Park
P.O. Box 3100
Andover, MA 01810

D. F. Hall
Chemistry and Physics Laboratory
The Aerospace Corporation
P.O. Box 92957
Los Angeles, CA 90009

C. E. Keffer
Center for Space Plasma and Aeronomic
    Research
The University of Alabama in Huntsville
Huntsville, AL 35899

L. J. Leger
Code ES5
NASA/Johnson Space Center
Houston, TX 77058

E. R. Miller
Code ES61
NASA/Marshall Space Flight Center
Huntsville, AL 35812

G. B. Murphy
Department of Physics and Astronomy
The University of Iowa
Iowa City, IA 52242

R. O. Rantanen
Science and Engineering Associates, Inc.
6535 S. Dayton Street, Suite 2100
Englewood, CO 80111

W. R. Seebaugh
Science and Engineering Associates, Inc.
6535 S. Dayton Street
Englewood, CO 80111

N. Singh
Department of Electrical and Computer
    Engineering
The University of Alabama in Huntsville
Huntsville, AL 35899

J. F. Spann
Code ES55
NASA/Marshall Space Flight Center
Huntsville, AL 35812

D. G. Torr
Center for Space Plasma and Aeronomic
    Research
The University of Alabama in Huntsville
Huntsville, AL 35899

1. REPORT NO. NASA CP-3002	2. GOVERNMENT ACCESSION NO.	3. RECIPIENT'S CATALOG NO.
4. TITLE AND SUBTITLE A Study of Space Station Contamination Effects		5. REPORT DATE May 1988
		6. PERFORMING ORGANIZATION CODE ES51/ES55
7. AUTHOR(S) M. R. Torr, J. F. Spann, and T. W. Moorehead, Editors		8. PERFORMING ORGANIZATION REPORT #
9. PERFORMING ORGANIZATION NAME AND ADDRESS George C. Marshall Space Flight Center Marshall Space Flight Center, Alabama 35812		10. WORK UNIT NO. M-586
		11. CONTRACT OR GRANT NO.
12. SPONSORING AGENCY NAME AND ADDRESS National Aeronautics and Space Administration Washington, DC 20546		13. TYPE OF REPORT & PERIOD COVERED Conference Publication
		14. SPONSORING AGENCY CODE

15. SUPPLEMENTARY NOTES

Sponsored by the Office of Space Science and Applications, NASA Headquarters

16. ABSTRACT

This report contains results of a workshop held on October 29-30, 1987, at Hilton Head Island, South Carolina. The contents of this report are divided as follows:

- o Natural Environment
- o Plasma Electromagnetic Environment
- o Optical Environment
- o Particulate Environment
- o Spacecraft Contamination
- o Surface Physics Processes
- o Laboratory Experiments
- o Vented Chemicals/Contaminants

17. KEY WORDS Contamination Space Station Space Station Contamination	18. DISTRIBUTION STATEMENT Unclassified--Unlimited Subject Category: 88		
19. SECURITY CLASSIF. (of this report) Unclassified	20. SECURITY CLASSIF. (of this page) Unclassified	21. NO. OF PAGES 150	22. PRICE A08

National Aeronautics and
Space Administration
Code NTT-4

Washington, D.C.
20546-0001

NASA

POSTMASTER: If Undeliverable (Section 158
Postal Manual) Do Not Return